


**The Influence of Time-Dependent Material Behavior
on the Response of Sandwich Beams**

by

Lynda Lee Sensmeier Oleksuk

Thesis submitted to the Faculty of the
Virginia Polytechnic Institute and State University
in partial fulfillment of the requirements for the degree of
Master of Science
in
Engineering Mechanics

APPROVED:



M. W. Hyer, Chairman



D. A. Dillard



O. H. Griffin, Jr.

December 1990

Blacksburg, Virginia

c.2

LD
5655
V855
19.90
0545
C.2

**The Influence of Time-Dependent Material Behavior
on the Response of Sandwich Beams**

by

Lynda Lee Sensmeier Oleksuk

M. W. Hyer, Chairman

Engineering Mechanics

(ABSTRACT)

To study the influence of the time-dependent behavior of various materials being considered for use in orbiting precision segmented reflectors, simple sandwich beam models are developed. The beam models included layers representing face sheets, core and adhesive. The issue of time-dependency is essential because the expected life of a reflector is on the order of 20 years. Using the principle of stationary potential energy, the elastic response of three-layer and five-layer symmetric sandwich beams to mechanical and thermally-induced loads is studied. The sensitivity of the three-layer and five-layer sandwich beams to reductions of the material properties is studied. Using the correspondence principle of viscoelasticity, these elastic models are transformed to time-dependent models. Representative cases of time-dependent material properties are used to demonstrate the application of the correspondence principle and evaluate the time-dependent response of the reflector. To verify the viscoelastic models, and to obtain a better idea of the amount of time-dependency to expect from the materials, simple time-dependent experiments on candidate materials were performed. Candidate materials include a quartz-epoxy face sheet material and a glass-imide honeycomb core material. The percent increase in strain for a constant stress for the quartz-epoxy in tension and the honeycomb in shear were measured. For both, a four-parameter fluid model captured the essential characteristics of their behavior. These four-parameter fluid models were then used in the three-layer sandwich beam model to predict the time-dependent response of the beam to three-point bending. This predicted response was compared to experimental results of a sandwich beam subjected to three-point bending.

Acknowledgements

The research discussed in this thesis was supported by NASA-Langley Research Center through the NASA-Virginia Tech Composites Program, Grant NAG-1-343. David Bowles was the technical monitor. The author would like to express her gratitude to Dr. David Bowles, Dr. Steve Tompkins, Andre Lavoie and all of the other helpful folks at NASA-Langley Research Center for their insight and guidance. She is also grateful to Mara Knott, Bob Simonds, Danny Reed and Chuck Chandler at Virginia Tech for sharing their practical experience in experimentation and processing. The shop personnel at Virginia Tech, Robert Davis, William Shaver and Archie Montgomery have also been very helpful. A special thanks is due to Paula Davis for her help in making this thesis look like a thesis, and of course, the author would like to thank her advisor, M.W. Hyer, without whom none of this would have been possible. A note of thanks is also extended to her thesis committee, D.A. Dillard and O.H. Griffin, Jr.. On a more personal note, the author's husband and parents also deserve much of the credit for this work, as they provided encouragement and support throughout its development.

Table of Contents

Chapter 1 - Introduction and Background 1

Chapter 2 - Nomenclature and Procedure for the Development of the Models 8

Nomenclature and Geometry of the Models 8

 Three-Layer Sandwich Beam Model 11

 Five-Layer Sandwich Beam Model 11

Procedure for Development of Models 12

 The Correspondence Principle of Viscoelasticity 13

 The Development of the Models 20

Chapter 3 - Development of the Three-Layer Sandwich Beam Model 25

Displacement Field 25

Strain Field 27

Principle of Stationary Potential Energy 27

Solution of Euler Equations for Displacement Functions 34

 Solution for $u(x)$ 34

 Solution for $w(x)$, $\psi(x)$ and $\phi(x)$ 35

Application of Boundary Conditions	40
Chapter 4 - The Three-Layer Sandwich Beam Model: Numerical Results	45
Materials and Material Properties	46
Sensitivity Studies	47
Mechanical Load	48
Thermal Gradient	50
The Time-Dependent Three-Layer Tip-Loaded Cantilever Beam Model	53
Influence of Time-Dependent Face Sheet Shear Modulus (G_1) on Beam Response ...	56
Influence of Time-Dependent Core Shear Modulus (G_2) on Beam Response	61
Influence of Time-Dependent Face Sheet Modulus of Elasticity (E_1) on Beam Response	66
Quasi-Elastic Approach	74
Summary	76
 Chapter 5 - Development of the Five-Layer Sandwich Beam Model	 77
Displacement Field	77
Strain Field	79
Principle of Stationary Potential Energy	80
Solution of Euler Equations for Displacement Functions	87
Solution for $u(x)$	87
Solution for $w(x)$, $\alpha(x)$, $\beta(x)$ and $\gamma(x)$	87
Application of Boundary Conditions	94
Mechanical Load	94
Thermal Gradient	97
Combined Mechanical Load and Thermal Gradient	99
Summary	99
 Chapter 6 - The Five-Layer Sandwich Beam Model: Numerical Results	 101

Materials and Material Properties	101
Sensitivity Studies	102
Mechanical Load	103
Thermal Gradient	104
The Time-Dependent Five-Layer Beam Model	107
Mechanical Load	108
Influence of Time-Dependent Core Shear Modulus (G_3) on Beam Response	110
Influence of Time-Dependent Adhesive Shear Modulus (G_2) on Beam Response ..	113
Influence of Time-Dependent Face Sheet Shear Modulus (G_1) on Beam Response	115
Through-the-Thickness Linear Thermal Gradient	118
Influence of Time-Dependent Face Sheet Modulus of Elasticity (E_1) on Beam Re-	
sponse	119
Quasi-Elastic Approach	121
Summary	123
 Chapter 7 - Experimental Apparatus and Procedure	125
Time-Dependent Behavior of the Quasi-Isotropic Quartz-Epoxy Face Sheets	126
Time-Dependent Behavior of the Glass-Imide Honeycomb Core	127
Time-Dependent Behavior of the Sandwich Beam in Three-Point Bending	130
 Chapter 8 - Experimental Results and Viscoelastic Models	132
Time-Dependent Behavior of the Quasi-Isotropic Quartz-Epoxy Face Sheets	133
Time-Dependent Behavior of the Glass-Imide Honeycomb Core	140
Time-Dependent Behavior of the Sandwich Beam in Three-Point Bending	145
Summary	150
 Chapter 9 - Observations, Conclusions and Recommendations for Further Study	151

Appendix A. Coefficient of Thermal Expansion of Aluminum Honeycomb 154

Appendix B. Approximations: Three-Layer Sandwich Beam Model 158

Approximation for Equation 4.12 158

Approximation for Equation 4.32 159

Approximation for Equation 4.71 161

Appendix C. Approximations and Verifications: Five-Layer Sandwich Beam Model 165

Verification of Equations 5.41 and 5.47 165

Approximation for Equation 5.42 168

References 172

Vita 173

List of Illustrations

Figure 1. Artist's Rendition of Precision Segmented Reflector (as traced from NASA picture L-87-9643)	2
Figure 2. Detail of the Construction of a Single Segment	3
Figure 3. Three-Layer and Five-Layer Models	9
Figure 4. Simple Viscoelastic Models	15
Figure 5. Creep and Recovery of Four Simple Viscoelastic Models	18
Figure 6. Equivalence of Simply Supported Beam in Three-Point Bending and Tip-Loaded Cantilever Beam	23
Figure 7. Displacement Field of the Three-Layer Sandwich Beam Model	26
Figure 8. Percent Increase in Tip Deflection of Three-Layer Beam Model for $G_1(t)$	62
Figure 9. Percent Increase in Tip Deflection of Three-Layer Beam Model for $G_2(t)$	65
Figure 10. Percent Increase in Tip Deflection of Three-Layer Beam Model for $E_1(t)$	70
Figure 11. Percent Increase in Tip Deflection of Three-Layer Beam Model for $E_1(t)$ - Approximate	74
Figure 12. Displacement Field of the Five-Layer Sandwich Beam Model	78
Figure 13. Percent Increase in Tip Deflection of Five-Layer Beam Model for $G_3(t)$	113
Figure 14. Percent Increase in Tip Deflection of Five-Layer Beam Model for $G_2(t)$	116
Figure 15. Percent Increase in Tip Deflection of Five-Layer Beam Model for $G_1(t)$	118
Figure 16. Percent Increase in Tip Deflection of Five-Layer Beam Model for $E_1(t)$ - Thermal Gradient	122
Figure 17. Shear Fixture	128
Figure 18. Slider Mechanism	129
Figure 19. Three-Point Bending Fixture	131

Figure 20. Percent Increase in Strain of Quartz-Epoxy Face Sheets	134
Figure 21. Four-Parameter Fluid Model	135
Figure 22. Percent Increase in Strain of Quartz-Epoxy Face Sheets - Experimental and Model (First Approach)	138
Figure 23. Percent Increase in Strain of Quartz-Epoxy Face Sheets - Experimental and Model (Second Approach)	139
Figure 24. Percent Increase in Strain of Glass-Imide Honeycomb	141
Figure 25. Four-Parameter Fluid Model for Shear	142
Figure 26. Percent Increase in Strain of Glass-Imide Honeycomb - Experimental and Model (First Approach)	143
Figure 27. Percent Increase in Strain of Glass-Imide Honeycomb - Experimental and Model (Second Approach)	144
Figure 28. Percent Increase of Deflection of Sandwich Beam in Three-Point Bending ..	146
Figure 29. Percent Increase of Deflection of Sandwich Beam in Three-Point Bending - Experimental and Model	148
Figure A.1. Two Directions for Hexagonal Honeycomb Materials	155
Figure A.2. Single Hexagonal Cell of Honeycomb - Unexpanded and Expanded	157

List of Tables

Table 1.	Nominal Material Properties and Geometries for Three-Layer Model	47
Table 2.	Sensitivity of Three-Layer Aluminum Beam - Mechanical Load	50
Table 3.	Sensitivity of Three-Layer Composite Beam - Mechanical Load	51
Table 4.	Sensitivity of Three-Layer Aluminum Beam - Thermal Gradient	54
Table 5.	Sensitivity of Three-Layer Composite Beam - Thermal Gradient	55
Table 6.	Quasi-Elastic Tip Deflection of the Three-Layer Composite Tip-Loaded Cantilever Beam	76
Table 7.	Nominal Material Properties and Geometries for Five-Layer Beam Model	103
Table 8.	Sensitivity of Five-Layer Aluminum Beam - Mechanical Load	105
Table 9.	Sensitivity of Five-Layer Composite Beam - Mechanical Load	106
Table 10.	Sensitivity of Five-Layer Aluminum Beam - Thermal Gradient	108
Table 11.	Sensitivity of Five-Layer Composite Beam - Thermal Gradient	109
Table 12.	Quasi-Elastic Tip Deflection of the Five-Layer Composite Beam	123
Table B.1.	Approximation for Three-Layer Aluminum Beam - Thermal Gradient	160
Table B.2.	Approximation for Three-Layer Composite Beam - Thermal Gradient	161
Table B.3.	Approximation for Three-Layer Aluminum Beam - Mechanical Load	162
Table B.4.	Approximation for Three-Layer Composite Beam - Mechanical Load	162
Table B.5.	Approximation for Three-Layer Aluminum Beam ($E_2 = 0$) - Mechanical Load	163
Table B.6.	Approximation for Three-Layer Composite Beam ($E_2 = 0$) - Mechanical Load	164
Table C.1.	Approximation of Five-Layer Aluminum Beam - Mechanical Load	170
Table C.2.	Approximation of Five-Layer Composite Beam - Mechanical Load	171

Chapter 1 - Introduction and Background

Fiber-reinforced polymer-matrix composite materials are currently used in a variety of space applications, including communication and weather satellites, antennas and reflectors. The use of composite materials not only provides structures lighter than possible with more traditional engineering materials, but also provides the option of tailoring the material to meet design requirements. This tailoring is accomplished by changing the composition and orientation of fibers in the materials used.

One space application of composite materials currently under consideration is the precision segmented reflector, or PSR. The PSR is designed to be deployed in space for the purpose of deep space observation. The overall diameter of such a reflector is expected to be on the order of thirty meters. The tasks of manufacturing the reflector and of transporting it into space are simplified by its segmented construction. Currently, each segment is expected to be on the order of one meter in diameter and is hexagonal in planform. Once in space the segments can be assembled to form the surface of the reflector. An artist's rendition of a deployed precision segmented reflector can be seen in Figure 1. The surface of the reflector is to be protected from direct solar radiation by a sunshield, which in Figure 1 is being installed by two astronauts. As envisioned, the segments are to be constructed as symmetric sandwiches of composite face sheets and honeycomb core joined by adhesive layers. A detail

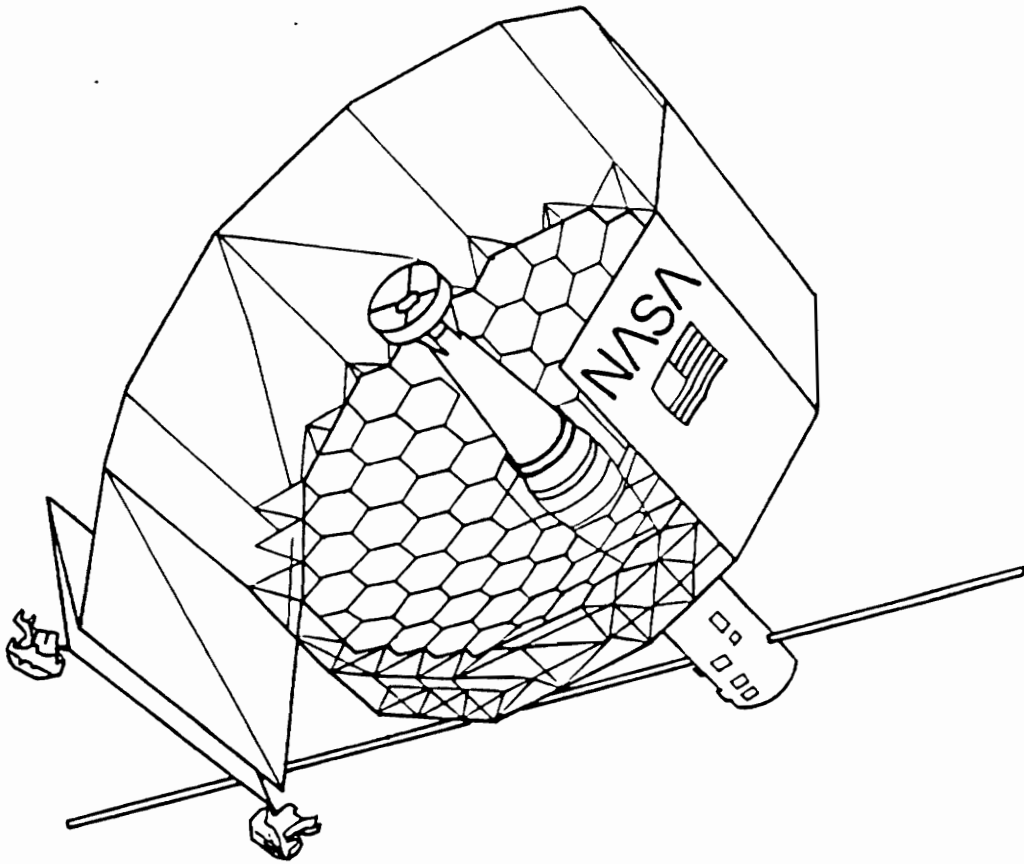


Figure 1. Artist's Rendition of Precision Segmented Reflector (as traced from NASA picture L-87-9643)

of the reflector construction is illustrated in Figure 2. Because of its intended use for deep space observation, the PSR has strict requirements on reflector surface smoothness and overall structural shape. Because the PSR will be protected from direct solar radiation and the associated high temperatures and high temperature gradients that spacecraft normally experience, the expected operating life is at least twenty years. During this time, despite the low operating temperatures, the polymer-based composite materials in the reflector segments may exhibit time-dependent material behavior. Because the stringent requirements on surface smoothness and overall shape must be maintained throughout the entire life of the re-

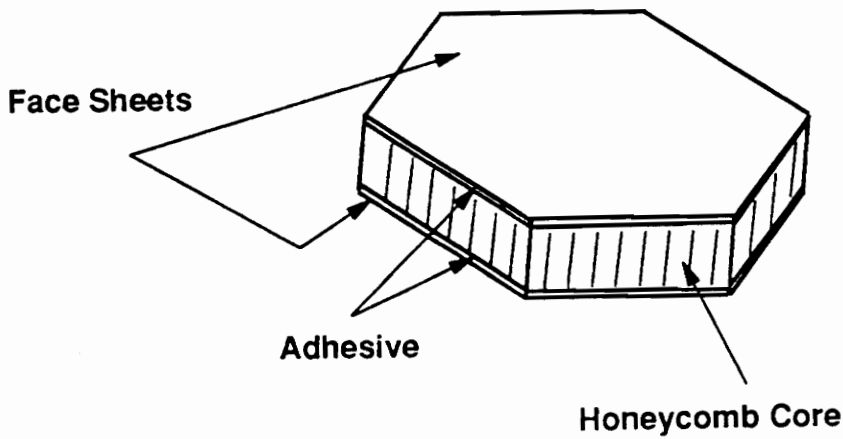


Figure 2. Detail of the Construction of a Single Segment

flector, the time-dependent behavior of its constituent materials may adversely affect its performance. Thus, the ability to quantify the amount of time-dependent behavior that a particular material exhibits, and to quantify the influence of that behavior on the reflector's performance, is a necessary design requirement. To meet this demand requires an analytical tool which properly models the important material properties, dimensions and construction features of a reflector segment. This tool, which can be used to predict the reflector's response to variances in the properties of all its constituent materials, can also be used to screen candidate materials for potential use in the reflector. To be used as design tools, these models should be simple and preferably would be found in closed-form rather than by numerical techniques.

Presented in this thesis is the development of analytical models which can be used to evaluate the influence of time-dependent material behavior on the performance of precision segmented reflectors. Empirical data on the time-dependent behavior of materials represen-

tative of reflector construction is also presented. Verification of the models is accomplished by using this empirical data. Because surface smoothness is influenced more by micromechanic material issues than by the macromechanic behavior of the materials, it will not be addressed within this thesis. The analysis and gathering of empirical data are directed more toward understanding the factors that influence changes in the overall dimensions and the shape of the segments. Although the analytical models do not represent the reflector segments as plates, they do incorporate the basic features of the symmetric sandwich construction. Thus, the models are able to predict the effect of time-dependent material behavior on the overall response of the reflector segment.

Specifically, the analytical models are three-layer and five-layer symmetric sandwich beam models. These beams represent strips of the hexagonal reflector segments. The five-layer sandwich beam model takes into account not only the face sheets and honeycomb core, but also the two layers of adhesive that bond them together. Although the five-layer model, by including all three constituent materials individually, is a more accurate and complete representation of the sandwich structure, the three-layer model is also important. The development of the three-layer model provides insight into the solution techniques necessary to develop the computationally more complicated five-layer model. Additionally, because of the difficulty in isolating the time-dependent behavior, and for that matter, the static behavior, of the honeycomb core from the adjacent adhesive layer, the three-layer model is a fair representation of the sandwich construction when the combined properties of honeycomb and adhesive are used as the core properties. Although in theory the reflector segments will experience very little mechanical loads, slight loads resulting from manufacturing processes and assembly may occur. Additionally, despite the relatively controlled thermal environment of the reflector structure, there may be small temperature gradients both in the plane of the reflector and through the thickness of the segment panels. Even though in practice the externally applied mechanical loads and thermally-induced loads may be small, the models will use these loads for the purpose of screening candidate materials for potential PSR use. A simple mechanical loading case, three-point bending, is used to compare the predictions of

the analytical models to the actual empirical data. Three-point bending of a beam is easily performed in a laboratory and also has relatively simple boundary conditions; thus, it is an ideal test case for the models and is potentially a good screening experiment for candidate construction materials. To simulate any thermal loadings, a linear temperature gradient through the thickness of the sandwich is considered.

The chapters that follow develop the tools necessary to study the time-dependent behavior of sandwich beams. As with any beam analysis, many of the stresses are zero; this simplifies the development of the models. The stresses which are zero are discussed in Chapter 2. Additionally, the nomenclature and conventions used for both the three-layer and five-layer beam models are introduced in Chapter 2. The steps used in developing the analytical models are also outlined in that chapter. The principle of stationary potential energy is used for both models rather than an equilibrium approach; thus, the governing equations **and** the associated boundary conditions are found for each model. The development begins with kinematic assumptions, specifically the assumed displacement field. Because honeycomb cores are quite soft in shear, and because the through-the-thickness shear modulus of fiber-reinforced composites is much lower than the in-plane extensional modulus, shear deformations are included in the displacement formulation. Once the displacement field has been introduced, the principle of stationary potential energy is used to obtain the governing differential equations, or Euler equations, and the boundary conditions. The Euler equations are then solved to yield the forms of the assumed displacements. The unknown constants in the displacement functions are next found by applying the boundary conditions. This, finally, is the static (elastic, as opposed to viscoelastic) solution. The next step in the development of the model is to incorporate the time-dependent behavior of the materials. This is done by using the correspondence principle of viscoelasticity. This principle is explained in greater detail later. Simple, representative cases of time-dependent behavior are used for demonstrative purposes.

The third and fourth chapters both deal with the three-layer beam model. The development of the three-layer model is outlined, step by step, in Chapter 3. Interesting numerical

studies based on this model are presented in Chapter 4. For example, the effects on the overall response of the beam due to varying material properties is shown. Comparisons of the effects due to different material properties changing by an order of magnitude are used to show to which material properties the model is most sensitive. This is important when screening candidate materials. For example, if a particular candidate material has an elastic property which is lower than in other candidate materials, or exhibits a high degree of time-dependent behavior, but the response of the beam model is not very sensitive to that material property, then the material may still be acceptable for use in the reflector structure. However, if a candidate material has a material property that is only moderately time-dependent, but the response of the beam is highly sensitive to that material property, then that material may not meet the design requirements. In Chapter 4, the properties which are most important for screening candidate materials, according to the three-layer model, are identified.

The purpose of Chapters 5 and 6 is similar to that of Chapters 3 and 4. In Chapters 5 and 6, the development of and some numerical results from the five-layer beam model are presented. The steps in the development are the same as for the three layer-model. However, for the three-layer model the results could be found in closed-form. The five-layer model, which is computationally more difficult, relies on a few intuitive steps to bring it to a form which is useful. These steps are based on the work of the three-layer model and are supported by computational evidence which is presented in Appendix C. Once again, the numerical results follow the development and are presented in Chapter 6. These numerical results identify the material properties that are most important when screening candidate materials according to the five-layer model.

Following the development of the models and their numerical results is an explanation of the experimental procedures in Chapter 7. Here the special apparatus that were designed for the tests are discussed. Not only were time-dependent three-point bending tests performed on the sandwich beams, but also time-dependent tests were performed to determine the time-dependent behavior of the independent constituent's material properties.

The results of the experimental work are discussed in Chapter 8. Simple time-dependent models are fit to the experimental data acquired from testing the separate materials, and these models are subsequently used with the three-layer analytical model to predict the overall response of a sandwich beam subjected to three-point bending. These predictions are compared to the experimental results of the sandwich beam in three-point bending. Finally, observations, conclusions and recommendations for further work are discussed in Chapter 9.

Chapter 2 - Nomenclature and Procedure for the Development of the Models

The purpose of this chapter is two-fold. First, the nomenclature and geometry for the three-layer and the five-layer sandwich beam models are introduced. Second, the analytical approach used to study the time-dependent behavior of the models is outlined.

Nomenclature and Geometry of the Models

Schematics of both the three-layer and the five-layer sandwich beam models are depicted in Figure 3. In both models, x is the coordinate coincident with the length of the beam. Also, the coordinate through the thickness of both beams is z ; in particular, the mid-thickness position of both beams is denoted by $z=0$. The width, or dimension in the y direction, for both models is unity. As with all beam theories, the primary stress is the extensional stress in the lengthwise direction, or σ_x . If shear deformations are considered important, as they are here, the through-the-thickness shear stress, τ_{xz} , must be included in the analysis. The other four

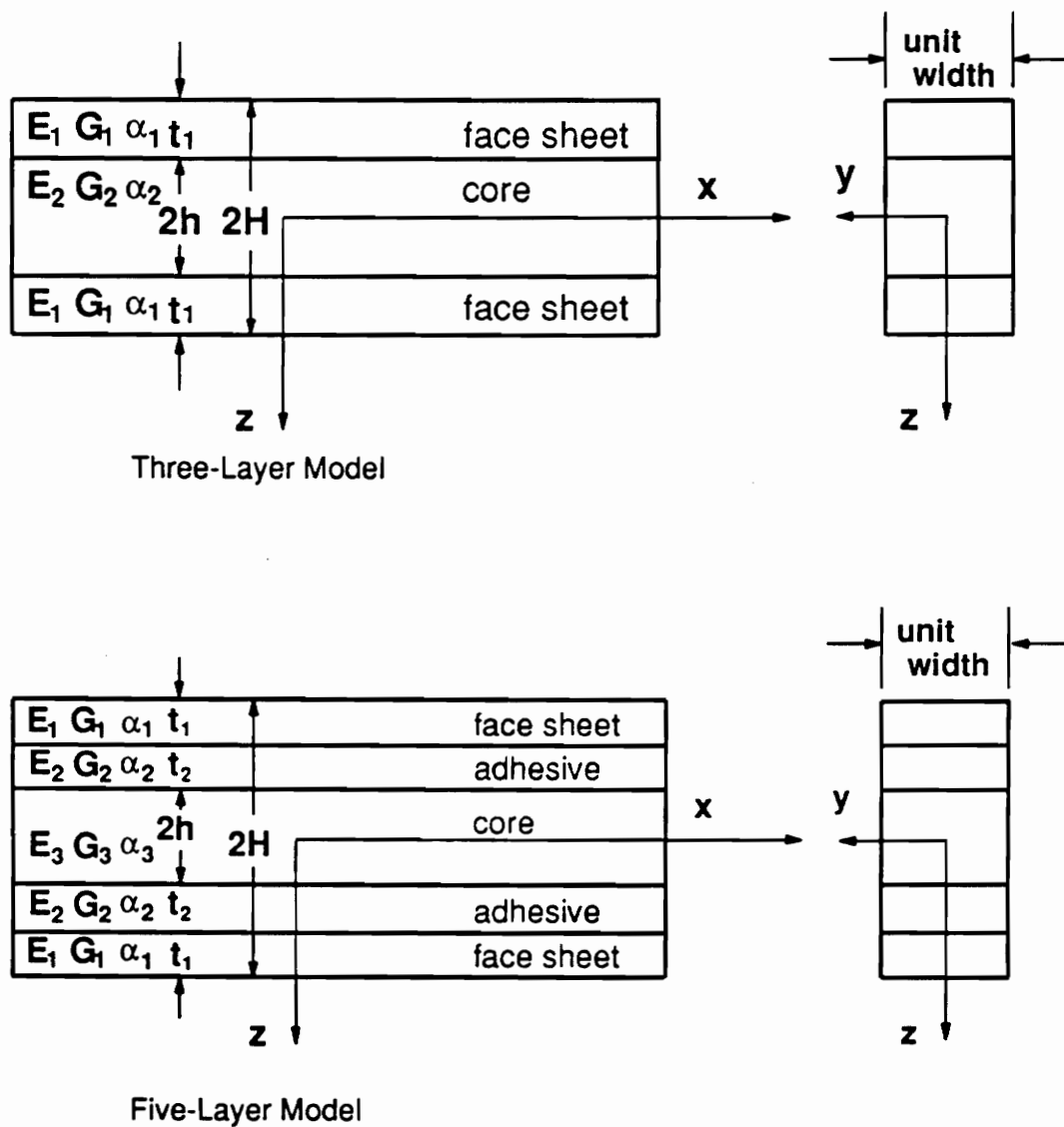


Figure 3. Three-Layer and Five-Layer Models

stress components, σ_y , σ_z , τ_{xy} and τ_{yz} , are considered negligible and are set to zero. In summary,

$$\sigma_x \neq 0 \quad \tau_{xz} \neq 0 \quad \sigma_y = \sigma_z = \tau_{xy} = \tau_{yz} = 0 . \quad (2.1)$$

As a result, Hooke's law reduces to

$$\sigma_x = E\epsilon_x \quad \tau_{xz} = G\gamma_{xz} . \quad (2.2)$$

where ϵ_x is the extensional strain in the x direction and γ_{xz} is the shear strain in the x-z plane, or the through-the-thickness shear strain. Also, E represents Young's modulus in the x direction and G is the shear modulus in the x-z plane. Although not explicitly shown in Equation 2.2, these material properties actually depend on z because they vary from layer to layer. If thermal expansion effects are important, Hooke's law becomes

$$\begin{aligned} \sigma_x &= E\epsilon_x - \sigma_x^T \\ \tau_{xz} &= G\gamma_{xz} \end{aligned} \quad (2.3)$$

where

$$\sigma_x^T = E\alpha_x\Delta T . \quad (2.4)$$

In the previous equation, α_x is the coefficient of thermal expansion of the material in the x direction and ΔT is the temperature rise relative to some arbitrary reference temperature. As before, these quantities depend on z; α_x varies from layer to layer, and ΔT could be any function of z. For this work, a linear function of z is considered.

In both the three-layer and the five-layer beam models, the outermost layers are the face sheets. These are, as currently envisioned, quasi-isotropic fiber-reinforced composite laminates. The face sheets are modelled as single layers, rather than modelling the eight or more layers that actually compose the face sheets.

Three-Layer Sandwich Beam Model

As shown in Figure 3, the three-layer beam model includes only the face sheets and core, not the adhesive layers which bond them together. The thickness of the adhesive layers can be included in the three-layer model, but only as part of the core or face sheets. Material properties which are actually the combined properties of the adhesive and the core, or the adhesive and the face sheets, can be used if the additional thickness of the adhesive layers is added to the thickness of the core, or face sheets. For the three-layer beam model, the subscript "1" is used to denote material properties of the face sheets. The modulus of elasticity in the x direction for the face sheets is E_1 , the shear modulus of the face sheets is G_1 , and the coefficient of thermal expansion is α_1 . (Unlike standard notation associated with mechanics of materials or mechanics of composite materials practice, the subscript "1" does not refer to principal direction or fiber direction, but rather that the material property is of the face sheet.) The thickness of each face sheet is represented by t_1 . The core properties are denoted by the subscript "2"; thus, the modulus of elasticity, shear modulus and the coefficient of thermal expansion of the core are, respectively, E_2 , G_2 and α_2 . The total thickness of the core is $2h$, and the total thickness of the beam is $2(h + t_1)$, or $2H$. The material properties and geometries are identified in Figure 3.

Five-Layer Sandwich Beam Model

The five-layer beam model, unlike the three-layer model, includes all three materials. Similar to the three-layer beam model, the subscript "1" is used to represent the material properties of the face sheets. Thus, E_1 , G_1 and α_1 are the modulus of elasticity, shear modulus and coefficient of thermal expansion of the face sheets, respectively. The thickness of each face sheets is t_1 . The properties of the adhesive layers are denoted by the subscript "2"; therefore,

the modulus of elasticity is E_2 , the shear modulus is G_2 and α_2 is the coefficient of thermal expansion of the adhesive layers. The thickness of one adhesive layer is t_2 . The honeycomb core has the properties E_3 , G_3 and α_3 , which are the modulus of elasticity, shear modulus and coefficient of thermal expansion, respectively. The total thickness of the core is $2h$, same as for the three-layer beam model, and the total thickness of the beam is $2(h + t_1 + t_2)$, or $2H$. These material properties and geometries can be seen in Figure 3. To make any meaningful comparison between the two models, the quantity $2H$ must be the same for both models. Thus, the thickness of the adhesive layers, which is modelled separately in the five-layer model, should be included in the thickness of the face sheets (t_1) or in the thickness of the core ($2h$) in the three-layer model.

Procedure for Development of Models

Now that the nomenclature and geometry for the two models have been introduced, the procedure for the development of the models is outlined. The procedure for both models is the same; only certain details vary. These details are covered in depth in Chapters 3 and 5. Generally, the Euler equations and boundary conditions that govern the beam's response to mechanical and thermal loads are found by using the principle of stationary potential energy. Then, these equations are solved and the boundary conditions applied to find the elastic solution. Finally, the correspondence principle of viscoelasticity is used to find the time-dependent response of the beam. Because the correspondence principle of viscoelasticity is so vital to the analytical models, it is discussed before the developmental procedure is outlined.

The Correspondence Principle of Viscoelasticity

Concisely stated, the correspondence principle of viscoelasticity is:

To find the stresses in and the deformation of a viscoelastic structure, replace E by $\frac{Q(s)}{P(s)}$, and the ensuing functions are the Laplace transforms of the solution of the viscoelastic function.[1]

The function $\frac{Q(s)}{P(s)}$ is the time-dependent modulus in Laplace domain. Although this statement considers only the case where the modulus of elasticity is time dependent, any of the elastic material properties can be time dependent. For example, the shear modulus may vary with time; the behavior of a fiber-reinforced polymer material in shear is polymer-dominated and therefore more expected to exhibit time-dependence than the fiber-dominated extensional behavior.

In general, to apply the correspondence principle, the solution to the elastic problem must first be known. Next, any time-dependent material properties in the elastic solution must be replaced by $\frac{Q(s)}{P(s)}$ and any time-dependent loads must be replaced by the load in Laplace domain. (A load that is applied initially and kept constant, or even eventually removed, is considered to be time-dependent and has the form of a step function.) The result is the solution to the viscoelastic problem in the Laplace domain. Performing the inverse transform function will yield the viscoelastic solution in the time domain. Because inversion must be performed, it is important to have the material properties appear explicitly in the elastic solution. If the material properties do not appear explicitly, or appear in a complicated fashion, performing the inverse transform may be prohibitively difficult. For example, consider the case where a displacement is given by the function

$$\delta = \frac{PL}{AE} \quad (2.5)$$

where P is a load applied at time zero, L is a characteristic length, A is a characteristic area and E is the modulus of the material. For simplicity, assume that the load P is applied at time

zero and remains constant at magnitude P_0 ; thus, its Laplace transform is P_0/s . [2] If E is a time-dependent quantity, then the time-dependent form of δ is

$$\delta(t) = \mathcal{L}^{-1} \left\{ \frac{P_0 L}{s A \frac{Q(s)}{P(s)}} \right\} , \quad (2.6)$$

which may in fact be relatively simple to find. However, if E is embedded deeply, as in the function

$$F = c \frac{P}{(\sqrt{E} + k)^{\frac{3}{2}}} , \quad (2.7)$$

where c and k are constants pertaining to the particular problem, then finding an explicit expression for the time dependent form $F(t)$,

$$F(t) = \mathcal{L}^{-1} \left\{ \frac{c P_0}{s \left(\sqrt{\frac{Q(s)}{P(s)}} + k \right)^{\frac{3}{2}}} \right\} , \quad (2.8)$$

can be difficult, if not impossible, even if $\frac{Q(s)}{P(s)}$ is a very simple function. In the formulation of the models, the elastic solution was developed with an eye towards the application of the correspondence principle without having to resort to numerical inversion techniques or numerically integrating time-dependent equations.

A common method of modelling the time dependent behavior of a material is to use different combinations of springs and dashpots to represent that behavior. Four simple viscoelastic models are shown in Figure 4. A spring alone, shown in part a of Figure 4, represents a perfectly elastic material. The strain of this spring is directly proportional to the stress applied, and a perfect spring returns to its original undeformed position when the load is removed. The behavior of a material symbolized by a spring can be written as

$$\sigma = E \varepsilon . \quad (2.9)$$

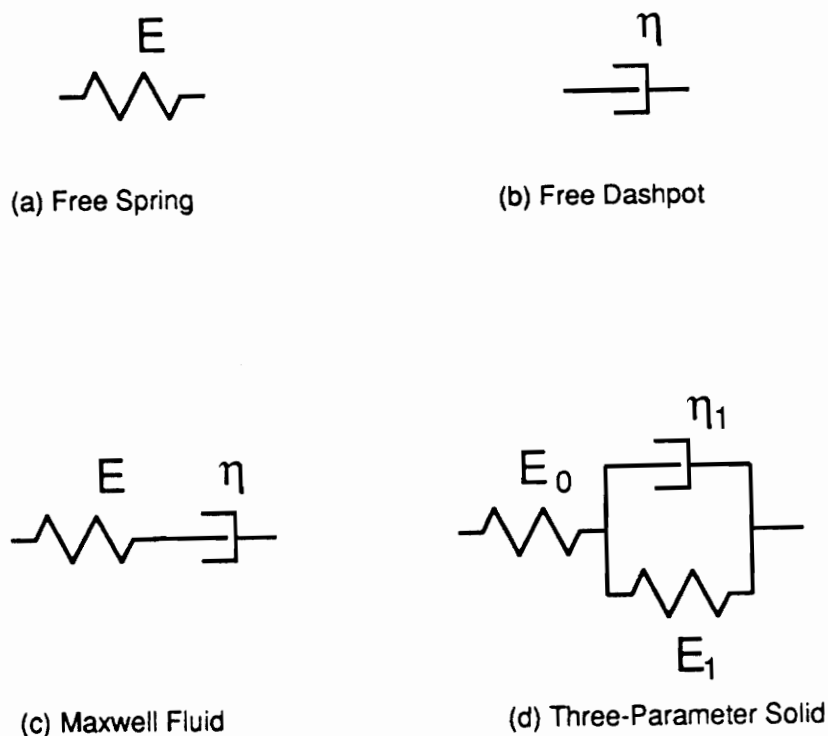


Figure 4. Simple Viscoelastic Models

where σ is the stress, ϵ is the strain and E is the extensional modulus of the material. If the stress and strain in question are shear stress and strain,

$$\tau = G\gamma \quad (2.10)$$

where τ is the shear stress, γ is the shear strain and G is the shear modulus of the material. For the remainder of the discussion of basic viscoelasticity, σ will represent either normal or shear stress and ϵ will represent the corresponding strain.

A dashpot alone, shown in part b of Figure 4, represents a viscous liquid. For a dashpot alone, the time derivative of the strain is directly proportional to the stress applied. The constitutive behavior of a material symbolized by a dashpot is

$$\sigma = \eta \dot{\epsilon} \quad (2.11)$$

However, a dashpot by itself is a poor representation of a solid; a dashpot can not respond instantaneously to an applied load. A more realistic model of a solid material is shown in part c of Figure 4. The spring and dashpot in series shown is sometimes called a Maxwell element or a Maxwell fluid. In this case, the word "fluid" refers to its viscoelastic behavior and not its elastic behavior. A Maxwell fluid is used to represent a material which responds instantaneously to an applied stress, like a solid, but then behaves like a liquid over time if the stress is not removed because it is unable to resist deformation caused by that stress. The constitutive equation for a material that behaves as a Maxwell fluid is

$$\sigma + \frac{\eta}{E} \dot{\sigma} = \eta \dot{\epsilon} \quad (2.12)$$

The Maxwell fluid is one of the simplest time-dependent models that can be used to represent a material. The spring in the Maxwell fluid model responds instantaneously to an applied stress, and the dashpot allows the strain of a Maxwell fluid to increase indefinitely as long as the stress is present. This is characteristic of any viscoelastic fluid; the strain continues to increase in the presence of a load. By contrast, the strain of a viscoelastic solid will, for a stress which is applied for a sufficient length of time, eventually stop increasing and reach some upper limit.

A spring and dashpot in parallel with each other is often referred to as a Kelvin element or a Kelvin solid; however, because it does not respond instantaneously to an applied stress, it is an unrealistic model of the behavior of a real solid material. The simplest realistic viscoelastic solid (except for a free spring, which has no time-dependent behavior) is the three-parameter solid. A three-parameter solid consists of a spring and dashpot in parallel, i.e. a Kelvin solid, in series with another spring. This model is shown in part d of Figure 4. The constitutive behavior of a three-parameter solid is governed by the following differential equation:

$$\sigma + \frac{\eta_1}{E_0 + E_1} \dot{\sigma} = \frac{E_0 E_1}{E_0 + E_1} \varepsilon + \frac{E_0 \eta_1}{E_0 + E_1} \dot{\varepsilon} \quad (2.13)$$

where E_0 is the modulus of the free spring, E_1 is the modulus of the spring in the Kelvin element and η_1 is the dashpot, or viscous, constant.

For the four models shown in Figure 4, the creep and recovery of each model is shown in Figure 5. To each model a stress is applied at time zero. The stress is held constant for a period of time and then removed. The time history of this stress is illustrated at the top right of Figure 5. Below that, the resulting strains as a function of time are shown for each of the four viscoelastic models represented. The free spring, shown in part a, has only a constant strain in response to the constant stress. This strain is completely recovered when the stress is removed. The free dashpot is shown in part b of Figure 5. It has no initial elastic response to the stress and no recovery when the stress is removed. The Maxwell fluid of part c combines the instantaneous elastic response of the spring with the linear creep of a dashpot. Additionally, the amount of recovery is only the initial elastic strain of the spring, ε_e . The creep and recovery behavior of a three-parameter solid, as shown in part d of Figure 5, is even more complicated. Once again, there is an initial elastic response to the applied stress, but now the transient, or time-dependent, strain is not linear with time. Once the load is removed, the initial elastic strain, ε_e , is recovered immediately, followed by a recovery period during which the model recovers completely.

The constitutive behavior of a general viscoelastic model is governed by an equation of the following form:

$$\sigma + p_1 \dot{\sigma} + p_2 \ddot{\sigma} + \dots + p_m \sigma^{(m)} = q_0 \varepsilon + q_1 \dot{\varepsilon} + q_2 \ddot{\varepsilon} + \dots + q_n \varepsilon^{(n)} \quad (2.14)$$

where $\sigma^{(m)}$ and $\varepsilon^{(n)}$ represent the m-th and n-th time-derivatives of σ and ε , respectively. There are certain physical limitations which restrict this equation. For example, the highest time-derivative of strain must always be of either the same order or one higher than time-derivative of the stress, that is,

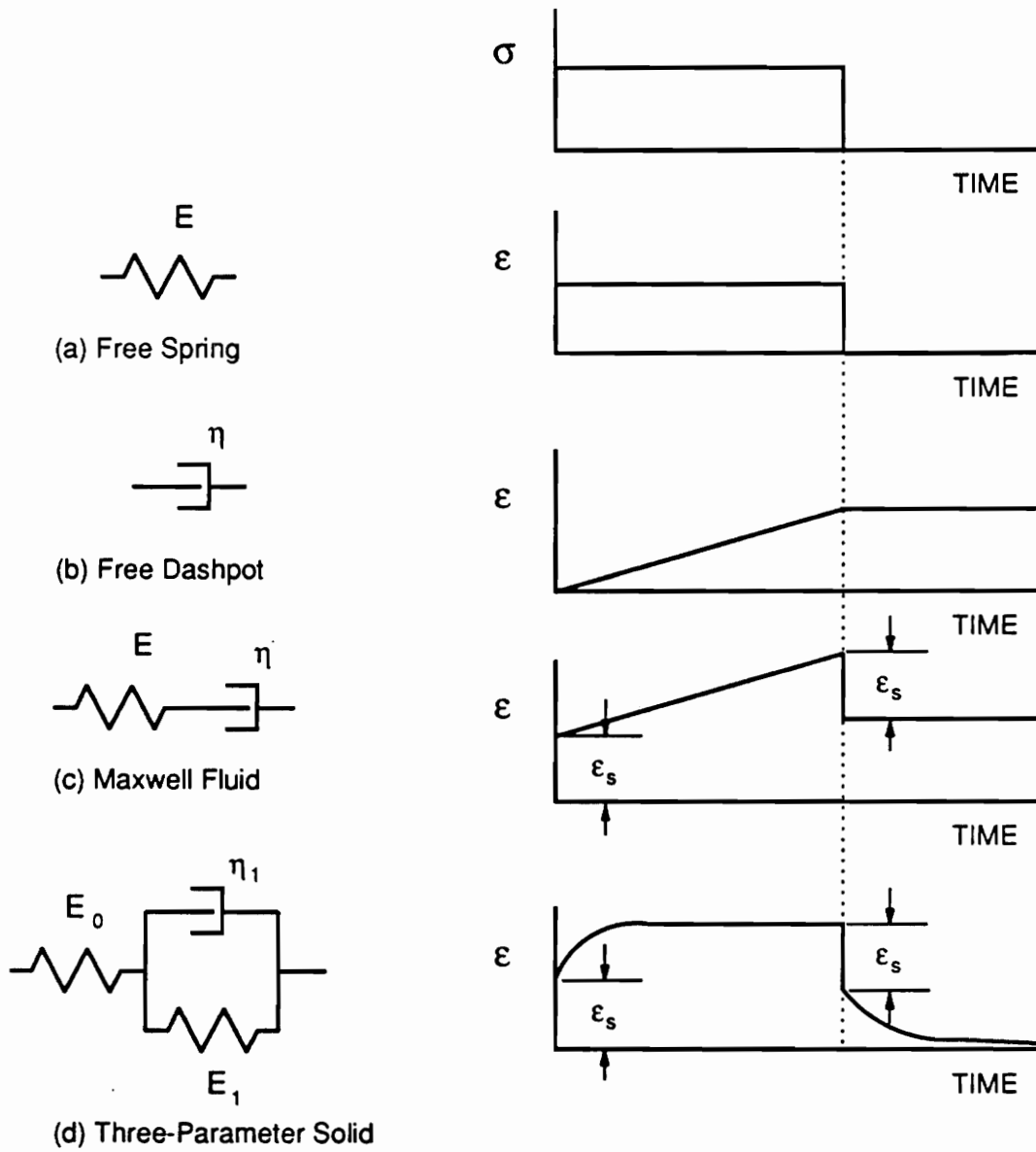


Figure 5. Creep and Recovery of Four Simple Viscoelastic Models

$$n = m \quad \text{or} \quad n = m + 1 \quad . \quad (2.15)$$

Also, information about the model can be gained by inspection of the constitutive equation. As an example, for the viscoelastic model to have instantaneous response to an applied stress, the highest derivatives of stress and strain must be of the same order, or

$$n = m \rightarrow \text{instantaneous response} \quad . \quad (2.16)$$

If the coefficient of the strain, q_0 , is zero, the model is a viscoelastic fluid; if q_0 is nonzero, the model is a viscoelastic solid:

$$\begin{aligned} q_0 = 0 &\rightarrow \text{fluid} \\ q_0 \neq 0 &\rightarrow \text{solid} \quad . \end{aligned} \quad (2.17)$$

The general constitutive equation of a viscoelastic model, Equation 2.14, can be transformed to the Laplace domain. In Laplace form, Equation 2.14 is

$$(1 + p_1 s + p_2 s^2 + \dots + p_m s^m) \bar{\sigma}(s) = (q_0 + q_1 s + \dots + q_n s^n) \bar{\epsilon}(s) \quad (2.18)$$

where $\bar{\sigma}(s)$ is the Laplace transformation of the stress as a function of time and $\bar{\epsilon}(s)$ is the Laplace transformation of the strain as a function of time. The polynomials which are the coefficients of these terms can be replaced by the notation $Q(s)$ and $P(s)$, respectively. These quantities are defined by the following:

$$P(s) = \sum_{i=0}^m p_i s^i \quad , \quad (2.19)$$

where p_0 is 1, and

$$Q(s) = \sum_{i=0}^n q_i s^i \quad (2.20)$$

The ratio of these polynomials appeared in the quotation of the correspondence principle of viscoelasticity; $\frac{Q(s)}{P(s)}$, is the viscoelastic modulus of a material in Laplace domain. Similarly, the ratio $\frac{P(s)}{Q(s)}$ is the viscoelastic compliance of a material in the Laplace domain.

The Development of the Models

The first step in the development of the three-layer and five-layer beam models is to assume an allowable displacement field for each model. The displacement fields must properly account for the deformation of each layer. Here each layer is assumed to have both extensional and shear deformations, and to shear independently of the other layers. To account for these deformations, lines in each layer that, when unloaded, are straight and normal to the midsurface of each layer remain straight within the layer upon loading. However, for the different layers these lines rotate through different angles. The nomenclature for the angles is different for the two models; thus, this is discussed in greater detail in the appropriate chapters. Also, each layer displaces uniformly downward in the z direction by the same amount, w . Specification of the displacement in the y direction, v , is not needed.

The second step in the development of the models is obtaining the strain fields. Once the important components of the displacement fields are known, finding the strain fields is a simple task. The pertinent strain-displacement relations are

$$\begin{aligned} \epsilon_x &= \frac{\partial u}{\partial x} \\ \gamma_{xz} &= \frac{\partial u}{\partial z} + \frac{\partial w}{\partial x} \end{aligned} \quad (2.21)$$

Inspection of the previous equations reveals that, indeed, it was not necessary to make any assumptions about the y direction displacement v as it does not appear in any of the needed strains. Again, because the strain field for the three-layer model is different than that of the five-layer model, each is presented in its appropriate chapter.

Third in the developmental procedure is to write the total potential energy, Π , of the beam for each model. For these models the total potential energy can be divided into two portions: Π_i , the internal strain energy; and Π^* , the potential energy caused by a load P^* which is applied at a point x^* along the length of the beam. Because of the interest in the three-point bending response, only point loads will be considered. The first of these, the internal strain energy, can be written as

$$\Pi_i = \frac{1}{2} \iiint_V [(\sigma_x - \sigma_x^T)\epsilon_x + (\sigma_y - \sigma_y^T)\epsilon_y + (\sigma_z - \sigma_z^T)\epsilon_z + \tau_{xz}\gamma_{xz} + \tau_{xy}\gamma_{xy} + \tau_{yz}\gamma_{yz}] dV \quad (2.22)$$

where V is the total volume of the beam.[2] This expression is simplified by the stress state, given in Equation 2.1, which exists in the beam. Also, because the width of the beam is assumed to be unity, the expression becomes

$$\Pi_i = \frac{1}{2} \int_{L^*} \int_{-H}^{+H} [(\sigma_x - \sigma_x^T)\epsilon_x + \tau_{xz}\gamma_{xz}] dz dx \quad (2.23)$$

where L^* refers to the total length of the beam, $2H$ is the total thickness of the beam and σ_x^T is given in Equation 2.4. If Hooke's law, Equation 2.3, is used and it is recognized that the material properties depend on z due to the layered nature of the beam, then Equation 2.23 becomes

$$\Pi_i = \frac{1}{2} \int_{L^*} \int_{-H}^{+H} [E(z)\epsilon_x^2 + G(z)\gamma_{xz}^2 - E(z)\alpha(z)\Delta T(z)\epsilon_x] dz dx \quad (2.24)$$

The second portion of the total potential energy of the beam is that caused by an externally applied point load P^* , or simply

$$\Pi^* = -P^*w|_{x=x^*} \quad (2.25)$$

where x^* is the point of application of P^* and w is the z -direction displacement at x^* .

Finally, the total potential energy of the beam, Π , can be written as the sum of its components, or

$$\Pi = \Pi_1 + \Pi^* \quad (2.26)$$

The final form for the total potential energy in the beam, as employed in Chapters 3 and 5, is

$$\Pi = \frac{1}{2} \int_{-L}^L \int_{-H}^{+H} [E(z)\epsilon_x^2 + G(z)\gamma_{xz}^2 - E(z)\alpha(z)\Delta T(z)\epsilon_x] dz dx - P^*w|_{x=x^*} \quad (2.27)$$

The next step in the development of the models is to apply the principle of stationary potential energy. Because the final forms for the potential energy for the two models are quite different, a general statement about the principle is made here and the details of application are left to the appropriate chapters. In general, if the first variation of the total potential energy, $\delta\Pi$, exists, then setting $\delta\Pi$ equal to zero is sufficient to ensure equilibrium. This step yields the Euler equations and boundary conditions which govern static equilibrium of the system.

Once the Euler equations have been found, the fifth step in the development of the models is to solve the Euler equations. Solution of the equations for the unknown displacement functions is covered in greater detail in Chapters 3 and 5. As an overview, the displacement functions are assumed to have the form $e^{i\lambda x}$; the eigenvalues λ_i are determined; and certain relations between the displacement functions are found which reduce the number of unknown constants to the number of available boundary conditions.

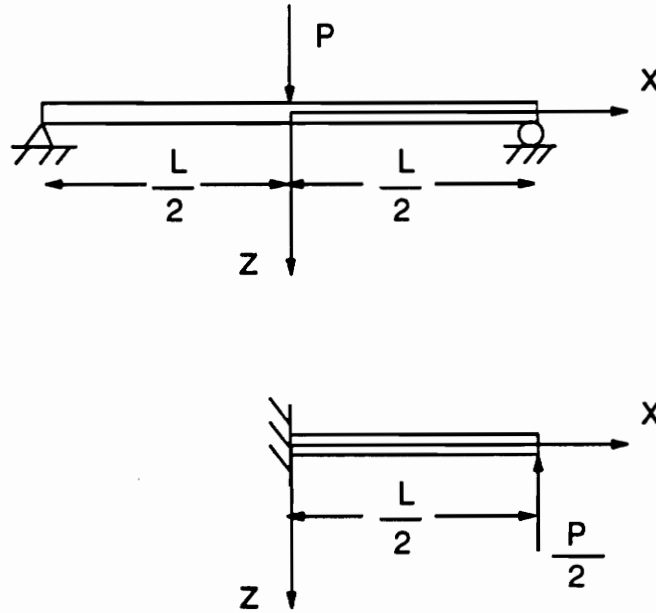


Figure 6. Equivalence of Simply Supported Beam in Three-Point Bending and Tip-Loaded Cantilever Beam

The sixth step is to apply the boundary conditions. As mentioned previously, a three-point bend test is considered a good candidate for a screening tool. It is simple to understand and can be performed in a laboratory. However, actually using the boundary conditions for three-point bending for the analytical model complicates the solution more than necessary. To represent three-point bending of a beam of length L which is loaded in the center by a point load P and simply supported at both ends, the boundary conditions used are actually those of a tip-loaded cantilever of length $L/2$ with load $P/2$. The equivalence of these two conditions are shown in Figure 6. The similarities between the two situations are evident upon inspection and henceforth, discussion will focus on the cantilever beam representation.

Once the boundary conditions are applied, all of the unknown constants in the displacement functions can be found. Some intuitive steps that are not needed in the computationally-simpler three-layer model are necessary in the five-layer model to make the form of the solution useful; these steps are supported by numerical evidence, and the need for the simpler form, to effect the inversion of the Laplace transform, was previously explained in the discussion of the correspondence principle of viscoelasticity. At this point, the elastic problem is completely solved. The next and final step is to incorporate the time-dependent material behavior into the response of the beam as predicted by the models. This final step is accomplished by applying the correspondence principle of viscoelasticity. Recall the earlier discussion of this principle; it was stated that the material properties must appear explicitly in the elastic solution to apply the correspondence principle in a simple fashion. As a result, simple functions for the time-dependence of the material properties are chosen in Chapters 4 and 6 to demonstrate the use of the correspondence principle and to provide information regarding the time-dependent behavior of the reflector segments. In Chapter 8, an attempt is made to select time functions which closely match the material behavior as found by the experiments.

In review, the steps for developing the three-layer and five-layer models are the same. First, a displacement field is assumed. Next, the strain field is found by applying the strain-displacement relations. Third, the total potential energy is written using these strains. Application of the principle of stationary potential energy is the fourth step; it yields the Euler equations and boundary conditions which govern the problem. Then, the fifth and sixth steps are to solve the Euler equations for the form of the displacement functions and to find the unknown constants in these functions by applying the boundary conditions. Finally, the correspondence principle of viscoelasticity is used to reveal the time-dependent solution.

The next chapter focuses on these steps for the three-layer beam model.

Chapter 3 - Development of the Three-Layer Sandwich Beam Model

Before the more complicated five-layer beam model was attempted, a three-layer beam model was studied. The computationally simpler three-layer model yielded insight into the solution and the solution techniques for the five-layer model. Also, because the adhesive layers on the actual structure are quite thin, the three layer model can be considered somewhat representative of the sandwich reflector segments. Additionally, because of the difficulty of measuring the material properties of only the honeycomb core, an argument can be made for using the effective or combined material properties of the honeycomb material and the adhesive as the material properties of the core.

Displacement Field

The displacement field for the three-layer model must properly account for the contribution that the face sheets and the honeycomb core make toward the overall response of the

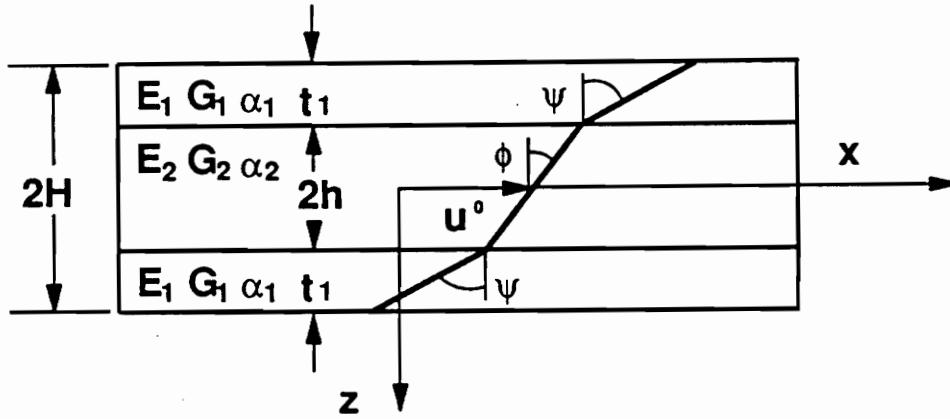


Figure 7. Displacement Field of the Three-Layer Sandwich Beam Model

sandwich beam. As explained in Chapter 2, each layer is assumed to have both extensional and shear deformations, and to shear independently of the other layers. Thus, each point in each layer displaces an amount $u^0(x)$ in the x direction due to the midsurface displacement $u^0(x)$ and an amount which depends on the rotation angle, either $\phi(x)$ for the core or $\psi(x)$ for the face sheets. Also, each layer displaces uniformly downward in the z direction an amount $w^0(x)$. Because the model is a beam, the displacements in the x and z directions are not dependent on y . The x -direction displacements, along with the geometry and material properties for each layer, are shown in Figure 7. Thus, the displacement field in the x - z plane is

$$u(x, z) = \begin{cases} u^0(x) + h\phi(x) - (z + h)\psi(x) & (-H \leq z \leq -h) \\ u^0(x) - z\phi(x) & (-h \leq z \leq +h) \\ u^0(x) - h\phi(x) - (z - h)\psi(x) & (+h \leq z \leq +H) \end{cases} \quad (3.1)$$

$$w(x, z) = w^0(x), \text{ all } z.$$

Because the z displacement, w , is only a function of x , the notation $w^o(x)$ will be replaced by $w(x)$ hereafter. Additionally, $u(x)$ will replace $u^o(x)$.

Strain Field

Applying the strain-displacement relations as given in Equation 2.21 to the assumed displacement field to find the strain components ϵ_x and γ_{xz} yields

$$\epsilon_x = \begin{cases} \frac{du}{dx} + h \frac{d\phi}{dx} - (z + h) \frac{d\psi}{dx} \\ \frac{du}{dx} - z \frac{d\phi}{dx} \\ \frac{du}{dx} - h \frac{d\phi}{dx} - (z - h) \frac{d\psi}{dx} \end{cases} \quad \gamma_{xz} = \begin{cases} -\psi + \frac{dw}{dx} & (-H \leq z \leq -h) \\ -\phi + \frac{dw}{dx} & (-h \leq z \leq +h) \\ -\psi + \frac{dw}{dx} & (+h \leq z \leq +H) \end{cases} \quad (3.2)$$

These strains are needed in the total potential energy expression.

Principle of Stationary Potential Energy

In general, to apply the principle of stationary potential energy, the first variation of the total potential energy is set equal to zero. The resulting equation or equations, called the Euler equations, and boundary conditions ensure equilibrium and govern the response of the system. For the three-layer beam model, there are four degrees of freedom: the displacements u , w , ϕ and ψ . Therefore, four equations and four sets of boundary conditions result from applying the principle. Specifically, for the three-layer beam model, the total potential energy must first be written as a functional of the functions $u(x)$, $\psi(x)$, $\phi(x)$ and $w(x)$. The first

variation of the total potential energy is taken and integration by parts is used. The governing conditions then follow.

The expression for the total potential energy of the beam is given by Equation 2.27, and is repeated here for convenience:

$$\Pi = \frac{1}{2} \int_{L^*} \int_{-H}^{+H} [E(z)\epsilon_x^2 + G(z)\gamma_{xz}^2 - E(z)\alpha(z)\Delta T(z)\epsilon_x] dz dx - P^* w|_{x=x^*} \quad (3.3)$$

The integral over the limits $z = -H$ to $z = +H$, through the thickness of the beam, can be logically separated into three integrals, one for each layer. Doing this, the material properties E , G and α become constant within each integral. Also, a thermal gradient which is linear in z will be considered; the gradient is assumed to have the form

$$\Delta T = a + bz, \quad (3.4)$$

where a and b are constants. With this formulation, the temperature of the geometric midplane of the beam is denoted by the constant a . The total potential energy can be rewritten, and is

$$\begin{aligned} \Pi = \frac{1}{2} \int_{L^*} \left\{ \int_{-h}^{-h} [E_1 \epsilon_x^2 + G_1 \gamma_{xz}^2 - E_1 \alpha_1 (a + bz) \epsilon_x] dz \right. \\ + \int_{-h}^{+h} [E_2 \epsilon_x^2 + G_2 \gamma_{xz}^2 - E_2 \alpha_2 (a + bz) \epsilon_x] dz \\ \left. + \int_{+h}^{+H} [E_1 \epsilon_x^2 + G_1 \gamma_{xz}^2 - E_1 \alpha_1 (a + bz) \epsilon_x] dz \right\} dx - P^* w|_{x=x^*} \quad (3.5) \end{aligned}$$

By substituting the appropriate expressions for the strains ϵ_x and γ_{xz} from Equation 3.2 and performing the z integration, the following expression for the total potential energy is obtained:

$$\begin{aligned}
\Pi = \int_{L^*} \left\{ \left(\frac{du}{dx} \right)^2 (E_1 t_1 + E_2 h) + \left(\frac{d\phi}{dx} \right)^2 \left[h^2 \left(E_1 t_1 + \frac{1}{3} E_2 h \right) \right] \right. \\
+ \left(\frac{d\psi}{dx} \right)^2 \left(\frac{1}{3} E_1 t_1^3 \right) + \left(\frac{dw}{dx} \right)^2 (G_1 t_1 + G_2 h) + \left(\frac{d\phi}{dx} \right) \left(\frac{d\psi}{dx} \right) (E_1 h t_1^2) \\
+ \phi^2 (G_2 h) + \psi^2 (G_1 t_1) + \psi \left(\frac{dw}{dx} \right) (-2G_1 t_1) + \phi \left(\frac{dw}{dx} \right) (-2G_2 h) \\
+ -a \left(\frac{du}{dx} \right) (E_1 \alpha_1 t_1 + E_2 \alpha_2 h) + b \left(\frac{d\psi}{dx} \right) \left[E_1 \alpha_1 \left(\frac{1}{2} h t_1^2 + \frac{1}{3} t_1^3 \right) \right] \\
\left. + b \left(\frac{d\phi}{dx} \right) \left[E_1 \alpha_1 \left(h^2 t_1 + \frac{1}{2} h t_1^2 \right) + E_2 \alpha_2 \left(\frac{1}{3} h^3 \right) \right] \right\} dx - P^* w|_{x=x^*} .
\end{aligned} \tag{3.6}$$

This expression for the total potential energy is in the functional form necessary for applying the principle of stationary potential energy.

To simplify the previous expression for potential energy, allow u' to represent the first derivative of u with respect to x , or $\frac{du}{dx}$, ϕ' to represent the first derivative of ϕ with respect to x and so on. The expression for the total potential energy can be rewritten as

$$\begin{aligned}
\Pi = \int_{L^*} \left[c_0 (u')^2 + c_1 (\phi')^2 + c_3 (\phi')(\psi') + c_6 (\psi')^2 + \frac{1}{2} (c_7 + c_9) (w')^2 \right. \\
+ \frac{1}{2} c_7 \psi^2 + \frac{1}{2} c_9 \phi^2 - c_7 \psi(w') - c_9 \phi(w') \\
\left. + N_u^T(u') + M_\psi^T(\psi') + M_\phi^T(\phi') \right] dx \\
- P^* w|_{x=x^*} .
\end{aligned} \tag{3.7}$$

where the constants c_i , $i=0,1,3,6,7,9$, and N_u^T , M_ψ^T and M_ϕ^T are as follows:

$$\begin{aligned}
c_0 &= E_1 t_1 + E_2 h \\
c_1 &= h^2 \left(E_1 t_1 + \frac{1}{3} E_2 h \right) \\
c_3 &= E_1 h t_1^2 \\
c_6 &= \frac{1}{3} E_1 t_1^3 \\
c_7 &= 2G_1 t_1 \\
c_9 &= 2G_2 h \\
N_U^T &= -a(E_1 \alpha_1 t_1 + E_2 \alpha_2 h) \\
M_\phi^T &= b \left[E_1 \alpha_1 t_1 \left(h^2 + \frac{1}{2} h t_1 \right) + E_2 \alpha_2 h \left(\frac{1}{3} h^2 \right) \right] \\
M_\psi^T &= b \left[E_1 \alpha_1 t_1 \left(\frac{1}{2} h t_1 + \frac{1}{3} t_1^2 \right) \right] .
\end{aligned} \tag{3.8}$$

The first variation of the total potential energy Π is of the form

$$\delta \Pi = \frac{\partial \Pi}{\partial u'} \delta u' + \frac{\partial \Pi}{\partial \phi'} \delta \phi' + \frac{\partial \Pi}{\partial \psi'} \delta \psi' + \frac{\partial \Pi}{\partial w'} \delta w' + \frac{\partial \Pi}{\partial \phi} \delta \phi + \frac{\partial \Pi}{\partial \psi} \delta \psi + \frac{\partial \Pi}{\partial w} \delta w . \tag{3.9}$$

Applying this form to the last expression for the total potential energy yields

$$\begin{aligned}
\delta \Pi &= \int_{L^*} \left\{ [2c_0(u') + N_U^T] \delta u' \right. \\
&\quad + [c_7(w' - \psi) + c_9(w' - \phi)] \delta w' \\
&\quad + [2c_1(\phi') + c_3(\psi') + M_\phi^T] \delta \phi' \\
&\quad + [c_3(\phi') + 2c_6(\psi') + M_\psi^T] \delta \psi' \\
&\quad + [c_7(\psi - w')] \delta \psi + [c_9(\phi - w')] \delta \phi \Big\} dx \\
&\quad - P^* \delta w|_{x=x^*} .
\end{aligned} \tag{3.10}$$

Portions of the integrand in this expression can be integrated by parts. Integration by parts has the general form

$$\int_A^B U dV = UV|_A^B - \int_A^B V dU . \quad (3.11)$$

As an example of the application of integration by parts, consider a portion of the previous integral,

$$\int_L \left[2c_0 \left(\frac{du}{dx} \right) + N_u^T \right] \delta \frac{du}{dx} dx . \quad (3.12)$$

Applying Equation 3.11 to this integral, where

$$\begin{aligned} U &= 2c_0 \left(\frac{du}{dx} \right) + N_u^T \\ dU &= 2c_0 \left(\frac{d^2u}{dx^2} \right) dx \\ V &= \delta u \\ \text{and} \\ dV &= \delta \frac{du}{dx} dx , \end{aligned} \quad (3.13)$$

yields

$$\begin{aligned} \int_L \left[2c_0 \left(\frac{du}{dx} \right) + N_u^T \right] \delta \frac{du}{dx} dx &= \left\{ \left[2c_0 \left(\frac{du}{dx} \right) + N_u^T \right] \delta u \right\} \Big|_{x=0}^{x=L/2} \\ &\quad - \int_L 2c_0 \left(\frac{d^2u}{dx^2} \right) \delta u dx . \end{aligned} \quad (3.14)$$

The first term on the right side of the previous equation reflects the fact that a cantilever beam with its root at $x=0$ and its free end at $x = L/2$ is being considered. This procedure can be repeated on the portions of the integrand that are products involving $\delta\phi'$, $\delta\psi'$ and $\delta w'$. Doing this, the previous expression for the first variation of potential energy becomes

$$\begin{aligned}
\delta \Pi = 0 = \int_{L^*} & \left\{ c_7 \left(\frac{d\psi}{dx} - \frac{d^2 w}{dx^2} \right) + c_9 \left(\frac{d\phi}{dx} - \frac{d^2 w}{dx^2} \right) \right\} \delta w - 2c_0 \left(\frac{d^2 u}{dx^2} \right) \delta u \\
& - \left[2c_1 \left(\frac{d^2 \phi}{dx^2} \right) + c_3 \left(\frac{d^2 \psi}{dx^2} \right) + c_9 \left(\frac{dw}{dx} - \phi \right) \right] \delta \phi \\
& - \left[c_3 \left(\frac{d^2 \phi}{dx^2} \right) + 2c_6 \left(\frac{d^2 \psi}{dx^2} \right) + c_7 \left(\frac{dw}{dx} - \psi \right) \right] \delta \psi \Big\} dx \\
& + \left\{ \left[2c_0 \left(\frac{du}{dx} \right) + N_u^T \right] \delta u \right\} \Big|_{x=0}^{x=\frac{L}{2}} \\
& + \left\{ \left[2c_1 \left(\frac{d\phi}{dx} \right) + c_3 \left(\frac{d\psi}{dx} \right) + M_\phi^T \right] \delta \phi \right\} \Big|_{x=0}^{x=\frac{L}{2}} \\
& + \left\{ \left[c_3 \left(\frac{d\phi}{dx} \right) + 2c_6 \left(\frac{d\psi}{dx} \right) + M_\psi^T \right] \delta \psi \right\} \Big|_{x=0}^{x=\frac{L}{2}} \\
& + \left\{ \left[c_7 \left(\frac{dw}{dx} - \psi \right) + c_9 \left(\frac{dw}{dx} - \phi \right) \right] \delta w \right\} \Big|_{x=0}^{x=\frac{L}{2}} - P^* \delta w \Big|_{x=x^*} .
\end{aligned} \tag{3.15}$$

Because the variation of each kinematic variable is independent of the others, for the entire expression $\delta \Pi$ to be zero, the individual coefficients of δu , $\delta \phi$, $\delta \psi$ and δw within the integral must each be equal to zero. These individual coefficients are the Euler equations for the three-layer beam model. They are:

$$\begin{aligned}
2c_0 \left(\frac{d^2 u}{dx^2} \right) &= 0 \\
2c_1 \left(\frac{d^2 \phi}{dx^2} \right) + c_3 \left(\frac{d^2 \psi}{dx^2} \right) + c_9 \left(\frac{dw}{dx} - \phi \right) &= 0 \\
c_3 \left(\frac{d^2 \phi}{dx^2} \right) + 2c_6 \left(\frac{d^2 \psi}{dx^2} \right) + c_7 \left(\frac{dw}{dx} - \psi \right) &= 0 \\
c_7 \left(\frac{d\psi}{dx} - \frac{d^2 w}{dx^2} \right) + c_9 \left(\frac{d\phi}{dx} - \frac{d^2 w}{dx^2} \right) &= 0 .
\end{aligned} \tag{3.16}$$

Also, each of the other expressions must be zero on an individual basis. These expressions are the boundary conditions for the three-layer beam model. Because of the interest in the

cantilever beam boundary conditions, the load P^* will be assumed to be applied at the free end of the beam. Thus P^* appears in the boundary conditions. For this situation, x^* is $L/2$. From this, the boundary conditions are

$$\begin{aligned}
 & \left[2c_0 \left(\frac{du}{dx} \right) + N_u^T \right] \delta u = 0 \\
 & \left[2c_1 \left(\frac{d\phi}{dx} \right) + c_3 \left(\frac{d\psi}{dx} \right) + M_\phi^T \right] \delta \phi = 0 \\
 & \left[c_3 \left(\frac{d\phi}{dx} \right) + 2c_6 \left(\frac{d\psi}{dx} \right) + M_\psi^T \right] \delta \psi = 0 \\
 & \left[(c_7 + c_9) \left(\frac{dw}{dx} \right) - c_7 \psi - c_9 \phi - P^* \right] \delta w = 0
 \end{aligned} \tag{3.17}$$

at both ends of the beam, except that in the last equation, it is understood that P^* is applied at the appropriate end of the beam and not both.

Notice that each boundary condition can be satisfied when **either** the first variation of the kinematic variables is zero (in other words, the value of the kinematic variable at the end in consideration is known or given), **or** the coefficient of the first variation of the kinematic variable (the bracketed term) is zero. Therefore, another way of expressing the boundary conditions is to say that at both ends of the beam,

$$\begin{aligned}
 & \text{either} \\
 & \quad 2c_0 \left(\frac{du}{dx} \right) + N_u^T = 0 \quad \text{or} \quad u = u^* \\
 & \text{and either} \\
 & \quad 2c_1 \left(\frac{d\phi}{dx} \right) + c_3 \left(\frac{d\psi}{dx} \right) + M_\phi^T = 0 \quad \text{or} \quad \phi = \phi^* \\
 & \text{and either} \\
 & \quad c_3 \left(\frac{d\phi}{dx} \right) + 2c_6 \left(\frac{d\psi}{dx} \right) + M_\psi^T = 0 \quad \text{or} \quad \psi = \psi^* \\
 & \text{and either} \\
 & \quad (c_7 + c_9) \left(\frac{dw}{dx} \right) - c_7 \psi - c_9 \phi = P^* \quad \text{or} \quad w = w^*
 \end{aligned} \tag{3.18}$$

The quantities u^* , ϕ^* , ψ^* and w^* are the known values of the displacement variables.

Solution of Euler Equations for Displacement Functions

To review briefly before proceeding, an assumed displacement field was used to find the strain field for the three-layer model. These strains, along with an externally applied load and linear thermal gradient, were used to find the total potential energy, Π , of the beam. The principle of stationary potential energy, when applied to Π , yielded four Euler equations and four boundary conditions for the model. Now, the four Euler equations, which are simply four coupled ordinary differential equations, will be solved for the displacement functions. These functions will still contain unknown constants which will later be determined by applying specific boundary conditions to the problem. First, the solution of the Euler equations will be presented.

Solution for $u(x)$

First, notice that the function $u(x)$ is decoupled from the rest of the problem because it appears alone in only one Euler equation and one boundary condition. The solution for $u(x)$ from its equation,

$$2c_0 \left(\frac{d^2 u}{dx^2} \right) = 0 \quad , \quad (3.19)$$

must necessarily be a linear function of x , specifically,

$$u(x) = u_1 x + u_0 \quad , \quad (3.20)$$

where u_1 and u_0 are constants of integration. Because the interest here will focus on studying the time-dependent out-of-plane response of the sandwich beams, $w(x)$, the solution to $u(x)$ will not be discussed further.

Solution for $w(x)$, $\psi(x)$ and $\phi(x)$

Referring to Equation 3.16, the solution for the remaining functions $w(x)$, $\phi(x)$ and $\psi(x)$ can be seen to involve only the last three equations, which are coupled. To find this portion of the beam's response, assume a solution of the form

$$\begin{aligned} w(x) &= we^{\lambda x} \\ \phi(x) &= fe^{\lambda x} \\ \psi(x) &= se^{\lambda x} \end{aligned} \quad (3.21)$$

where λ is unknown and f , s and w are constants which are yet to be determined. These assumed functions can be substituted into the three remaining Euler equations. Doing so yields

$$\begin{bmatrix} (2c_1\lambda^2 - c_9) & (c_3\lambda^2) & (c_9\lambda) \\ (c_3\lambda^2) & (2c_6\lambda^2 - c_7) & (c_7\lambda) \\ (c_9\lambda) & (c_7\lambda) & -\lambda^2(c_7 + c_9) \end{bmatrix} \begin{Bmatrix} fe^{\lambda x} \\ se^{\lambda x} \\ we^{\lambda x} \end{Bmatrix} = \begin{Bmatrix} 0 \\ 0 \\ 0 \end{Bmatrix} . \quad (3.22)$$

This set of equations has a non-trivial solution only when the determinant of the matrix has been forced to be zero, or

$$\begin{vmatrix} (2c_1\lambda^2 - c_9) & (c_3\lambda^2) & (c_9\lambda) \\ (c_3\lambda^2) & (2c_6\lambda^2 - c_7) & (c_7\lambda) \\ (c_9\lambda) & (c_7\lambda) & -\lambda^2(c_7 + c_9) \end{vmatrix} = 0 . \quad (3.23)$$

Finding the conditions under which the determinant is zero can be accomplished by finding the roots of the sixth order polynomial

$$\lambda^6(4c_1c_6 - c_3^2)(c_7 + c_9) - \lambda^4(2c_7c_9)(c_1 + c_3 + c_6) = 0 . \quad (3.24)$$

Equation 3.24 is satisfied when four of the roots are zero, or $\lambda_1 = \lambda_2 = \lambda_3 = \lambda_4 = 0$, and the remaining roots are

$$\lambda_5 = -\lambda_6 = \sqrt{\frac{2c_7c_9(c_1 + c_3 + c_6)}{(c_7 + c_9)(4c_1c_6 - c_3^2)}} \quad (3.25)$$

Henceforth, the symbol λ will represent

$$\lambda = \sqrt{\frac{2c_7c_9(c_1 + c_3 + c_6)}{(c_7 + c_9)(4c_1c_6 - c_3^2)}} \quad (3.26)$$

With six roots to Equation 3.24, the solution, previously shown in Equation 3.21, can be written as

$$\begin{aligned} w(x) &= w_3x^3 + w_2x^2 + w_1x + w_0 + w_5e^{\lambda x} + w_6e^{-\lambda x} \\ \phi(x) &= f_3x^3 + f_2x^2 + f_1x + f_0 + f_5e^{\lambda x} + f_6e^{-\lambda x} \\ \psi(x) &= s_3x^3 + s_2x^2 + s_1x + s_0 + s_5e^{\lambda x} + s_6e^{-\lambda x} \end{aligned} \quad (3.27)$$

Because the determinant of Equation 3.23 is zero, a relationship exists among the eighteen constants w_i , s_i and f_i . In particular, any two of the last three equations in Equation 3.16 can be used to find f_5 and f_6 , and s_5 and s_6 , in terms of w_5 and w_6 . Using the second and third portions of Equation 3.16, and defining

$$\begin{aligned} f_5 &= A_5w_5 & s_5 &= B_5w_5 \\ f_6 &= A_6w_6 & s_6 &= B_6w_6 \end{aligned} \quad (3.28)$$

the constants A_5 , A_6 , B_5 and B_6 can be found. They are

$$\begin{aligned} A_5 &= -A_6 = \frac{\lambda(c_3 + 2c_6)(c_7 + c_9)}{[c_7(2c_1 + c_3) - c_9(c_3 + 2c_6)]} \\ B_5 &= -B_6 = \frac{-\lambda(2c_1 + c_3)(c_7 + c_9)}{[c_7(2c_1 + c_3) - c_9(c_3 + 2c_6)]} \end{aligned} \quad (3.29)$$

For each repeated zero root, $\lambda_1 = \lambda_2 = \lambda_3 = \lambda_4 = 0$, a different approach must be used to find relationships between the f_i , s_i and w_i terms. That approach is detailed next.

Consider the portion of the solution which contains only the four repeated roots of zero. This portion of the solution can be expressed as

$$\begin{aligned}
w(x) &= w_3x^3 + w_2x^2 + w_1x + w_0 \\
\phi(x) &= f_3x^3 + f_2x^2 + f_1x + f_0 \\
\psi(x) &= s_3x^3 + s_2x^2 + s_1x + s_0
\end{aligned} \tag{3.30}$$

When these functions are substituted into the three Euler equations under consideration, given in Equation 3.16, the relationships between w_i , f_i and s_i can be found. Substitution leads to

$$\begin{aligned}
2c_1(6f_3x + 2f_2) + c_3(6s_3x + 2s_2) + c_9(3w_3x^2 + 2w_2x + w_1 - f_3x^3 - f_2x^2 - f_1x - f_0) &= 0 \\
c_3(6f_3x + 2f_2) + 2c_6(6s_3x + 2s_2) + c_7(3w_3x^2 + 2w_2x + w_1) \\
- c_7(s_3x^3 + s_2x^2 + s_1x + s_0) &= 0 \\
c_7(3s_3x^2 + 2s_2x + s_1) + c_9(3f_3x^2 + 2f_2x + f_1) - (c_7 + c_9)(6w_3x + 2w_2) &= 0
\end{aligned} \tag{3.31}$$

The first of these equations can be rewritten as

$$\begin{aligned}
x^3(-f_3) + x^2c_9(3w_3 - f_2) + x^1[12c_1f_3 + 6c_3s_3 + c_9(2w_2 - f_1)] \\
+ x^0[4c_1f_2 + 2c_3s_2 + c_9(w_1 - f_0)] &= 0
\end{aligned} \tag{3.32}$$

the second as

$$\begin{aligned}
x^3(-s_3) + x^2c_7(3w_3 - s_2) + x^1[6c_3f_3 + 12c_6s_3 + c_7(2w_2 - s_1)] \\
+ x^0[2c_3f_2 + 4c_6s_2 + c_7(w_1 - s_0)] &= 0
\end{aligned} \tag{3.33}$$

and the third as

$$\begin{aligned}
x^2[3(c_7s_3 + c_9f_3)] + x^1\{2[c_7s_2 + c_9f_2 - 3(c_7 + c_9)w_3]\} \\
+ x^0[c_7s_1 + c_9f_1 - 2w_2(c_7 + c_9)] &= 0
\end{aligned} \tag{3.34}$$

Because these three equations must be satisfied anywhere along the length of the beam, the choice of x is arbitrary. Thus, to ensure that each equation is identically equal to zero everywhere, the coefficient of each power of x in each equation must be zero. Inspection of the coefficients of the cubic terms in Equations 3.32 and 3.33 reveals that

$$f_3 = s_3 = 0 \quad . \quad (3.35)$$

Inspection of the coefficients of the x^2 terms in the same equations reveals that

$$w_3 = \frac{1}{3} f_2 = \frac{1}{3} s_2 \quad . \quad (3.36)$$

Substitution of these relationships into the coefficient of the linear x term in Equation 3.34 is sufficient to verify these relationships; this coefficient is identically equal to zero when these relationships are true. The same is true for the coefficient of x^2 in Equation 3.34; it is identically zero if both f_3 and s_3 are zero. Inspection of the coefficients of the linear x terms in Equations 3.32 and 3.33 reveal relationships similar to those given by Equation 3.35, namely

$$w_2 = \frac{1}{2} f_1 = \frac{1}{2} s_1 \quad . \quad (3.37)$$

Once again, these can be verified by substituting the relationships of Equation 3.37 into the constant (x^0) term in Equation 3.34; the result is simply zero. By substituting the relationships of Equation 3.36 for the terms in Equations 3.32 and 3.33 and by algebraically manipulating the results, the following relations can be found:

$$f_0 = w_1 + \frac{6(2c_1 + c_3)}{c_9} w_3 \quad (3.38)$$

and

$$s_0 = w_1 + \frac{6(c_3 + 2c_6)}{c_7} w_3 \quad . \quad (3.39)$$

Using the results given by Equations 3.35-39, the portion of the solution from the four repeated eigenvalues of zero, originally shown in Equation 3.30, can be rewritten as

$$\begin{aligned}
w(x) &= w_3x^3 + w_2x^2 + w_1x + w_0 \\
\phi(x) &= 3w_3x^2 + 2w_2x + \left[w_1 + \frac{6(2c_1 + c_3)}{c_9} w_3\right] \\
\psi(x) &= 3w_3x^2 + 2w_2x + \left[w_1 + \frac{6(c_3 + 2c_6)}{c_7} w_3\right]
\end{aligned} \tag{3.40}$$

Thus, the entire solution for $w(x)$, $\phi(x)$ and $\psi(x)$ can be written as a function of six unknown constants and is

$$\begin{aligned}
w(x) &= w_3x^3 + w_2x^2 + w_1x + w_0 + w_5e^{\lambda x} + w_6e^{-\lambda x} \\
\phi(x) &= 3w_3x^2 + 2w_2x + \left[w_1 + \frac{6(2c_1 + c_3)}{c_9} w_3\right] + w_5A_5e^{\lambda x} + w_6A_6e^{-\lambda x} \\
\psi(x) &= 3w_3x^2 + 2w_2x + \left[w_1 + \frac{6(c_3 + 2c_6)}{c_7} w_3\right] + w_5B_5e^{\lambda x} + w_6B_6e^{-\lambda x}
\end{aligned} \tag{3.41}$$

Notice that the $e^{\lambda x}$ and $e^{-\lambda x}$ terms in this solution can be combined to form hyperbolic sine and hyperbolic cosine terms using the following identities:

$$\begin{aligned}
\sinh(\lambda x) &= \frac{e^{\lambda x} - e^{-\lambda x}}{2} \\
\cosh(\lambda x) &= \frac{e^{\lambda x} + e^{-\lambda x}}{2}
\end{aligned} \tag{3.42}$$

Thus, the solution as shown in Equation 3.41 can be rewritten as

$$\begin{aligned}
w(x) &= w_3x^3 + w_2x^2 + w_1x + w_0 + w_5 \sinh(\lambda x) + w_6 \cosh(\lambda x) \\
\phi(x) &= 3w_3x^2 + 2w_2x + \left[w_1 + \frac{6(2c_1 + c_3)}{c_9} w_3\right] + w_5A_6 \cosh(\lambda x) + w_6A_6 \sinh(\lambda x) \\
\psi(x) &= 3w_3x^2 + 2w_2x + \left[w_1 + \frac{6(c_3 + 2c_6)}{c_7} w_3\right] + w_5B_6 \cosh(\lambda x) + w_6B_6 \sinh(\lambda x)
\end{aligned} \tag{3.43}$$

where w_5 and w_6 now represent different unknown quantities than they did in Equation 3.41.

Application of Boundary Conditions

All that remains is to find these six unknown constants by applying the boundary conditions. As previously discussed, a cantilever beam with its root at $x=0$ and its free end tip-loaded at $x=L/2$ is being considered. The load on the free end, previously denoted by P^* , is $P/2$. Thus, the boundary conditions for this beam are

$$\begin{array}{ll}
 \text{at } x = 0 : & \text{at } x = \frac{L}{2} : \\
 w = 0 & 2c_1\left(\frac{d\phi}{dx}\right) + c_3\left(\frac{d\psi}{dx}\right) + M_\phi^T = 0 \\
 \phi = 0 & c_3\left(\frac{d\phi}{dx}\right) + 2c_6\left(\frac{d\psi}{dx}\right) + M_\psi^T = 0 \\
 \psi = 0 & (c_7 + c_9)\left(\frac{dw}{dx}\right) - c_7\psi - c_9\phi = \frac{P}{2} .
 \end{array} \tag{3.44}$$

When the solution shown in Equation 3.43 is substituted into these boundary conditions, the result is a system of six equations and six unknowns. By examining the first and last boundary conditions independently, these can be reduced to a system of four equations and four unknowns. First, examine the last of the boundary conditions, or

$$\text{at } x = \frac{L}{2} : \quad (c_7 + c_9)\left(\frac{dw}{dx}\right) - c_7\psi - c_9\phi = \frac{P}{2} . \tag{3.45}$$

After substitution of Equation 3.43, this becomes

$$[\lambda(c_7 + c_9) - A_6c_9 - B_6c_7]\left(w_5 \cosh \frac{\lambda L}{2} + w_6 \sinh \frac{\lambda L}{2}\right) - 12(c_1 + c_3 + c_6)w_3 = \frac{P}{2} . \tag{3.46}$$

When the expressions for A_6 and B_6 as given in Equation 3.29 are substituted into Equation 3.46, it reduces to

$$-12(c_1 + c_3 + c_6)w_3 = \frac{P}{2} \quad (3.47)$$

The constant w_3 is therefore given by

$$w_3 = \frac{-P}{24(c_1 + c_3 + c_6)} \quad (3.48)$$

By examining the first boundary condition, or

$$\text{at } x = 0: \quad w = 0 \quad (3.49)$$

and substituting the expression for $w(x)$ from Equation 3.43, the identity

$$w_0 = -w_6 \quad (3.50)$$

becomes apparent. These results can be used in the remaining four boundary conditions to reduce the number of unknowns to four. Once the appropriate substitutions are made, those boundary conditions result in these four equations:

$$\begin{aligned} w_1 + w_5 A_6 &= \frac{P(2c_1 + c_3)}{4c_9(c_1 + c_3 + c_6)} \\ w_1 + w_5 B_6 &= \frac{P(c_3 + 2c_6)}{4c_7(c_1 + c_3 + c_6)} \\ 2w_2(2c_1 + c_3) + \lambda(w_5 \sinh \frac{\lambda L}{2} + w_6 \cosh \frac{\lambda L}{2})(2c_1 A_6 + c_3 B_6) &= -M_\phi^T + \frac{PL(2c_1 + c_3)}{8(c_1 + c_3 + c_6)} \\ 2w_2(c_3 + 2c_6) + \lambda(w_5 \sinh \frac{\lambda L}{2} + w_6 \cosh \frac{\lambda L}{2})(c_3 A_6 + 2c_6 B_6) &= -M_\psi^T + \frac{PL(c_3 + 2c_6)}{8(c_1 + c_3 + c_6)} \end{aligned} \quad (3.51)$$

These four equations can then be solved simultaneously to find the solutions to w_1 , w_2 , w_5 and w_6 . At this point, two more expressions are introduced to simplify the solution. They are

$$\begin{aligned} R_1 &= 2c_1 + c_3 \\ R_2 &= c_3 + 2c_6 \end{aligned} \quad (3.52)$$

Using these expressions, once the four equations in Equation 3.51 are solved, the constants w_0 , w_1 , w_2 , w_3 , w_5 and w_6 can be written as

$$\begin{aligned}
 w_3 &= \frac{-P}{12(R_1 + R_2)} \\
 w_2 &= \frac{PL}{8(R_1 + R_2)} - \frac{(M_\phi^T + M_\psi^T)}{2(R_1 + R_2)} \\
 w_1 &= \frac{P}{2(R_1 + R_2)^2} \left(\frac{R_1^2}{c_9} + \frac{R_2^2}{c_7} \right) \\
 w_5 &= \frac{-P(c_7 R_1 - c_9 R_2)^2}{2c_7 c_9 \lambda (c_7 + c_9)(R_1 + R_2)^2} \\
 w_6 &= -w_5 - \frac{(M_\psi^T R_1 - M_\phi^T R_2)(c_7 R_1 - c_9 R_2)}{c_7 c_9 \sinh \frac{\lambda L}{2} (R_1 + R_2)^2} \\
 w_0 &= -w_6
 \end{aligned} \tag{3.53}$$

Thus, the response of a three-layer shear-deformable sandwich beam to a mechanical load and through-the-thickness thermal gradient can be written as a third-order polynomial with additional hyperbolic sinusoidal terms.

A comparison of this model to the strength of materials solution for a tip-loaded cantilever is enlightening. Examine only the portion of the solution to the mechanical load $P/2$; in other words, let the thermal gradient be zero, or

$$M_\phi^T = M_\psi^T = 0 \quad . \tag{3.54}$$

Of particular interest are the cubic and quadratic terms in the model's expression for $w(x)$ as given by Equation 3.41. The strength of materials solution, $w_{som}(x)$, for a tip-loaded cantilever beam of length $L/2$ and load $P/2$ is

$$w_{som}(x) = \frac{-P}{12EI} \left(x^3 - \frac{3}{2} Lx^2 \right) \quad . \tag{3.55}$$

In strength of materials model for a sandwich beam, the quantity EI that appears in the previous equation is replaced by the effective EI for a sandwich beam. Using the same material

property and geometry nomenclature being used in the three-layer sandwich beam model, the effective EI for the sandwich beam is

$$EI_{\text{eff}} = E_1 t_1 \left(\frac{2t_1^2}{3} + 2ht_1 + 2h^2 \right) + E_2 h \left(\frac{2h^2}{3} \right) \quad (3.56)$$

Thus, the strength of materials solution for the deflection becomes

$$w_{\text{som}}(x) = \frac{-Px^3}{24 \left[E_1 t_1 \left(\frac{t_1^3}{3} + ht_1 + h^2 \right) + E_2 h \left(\frac{h^2}{3} \right) \right]} + \frac{PLx^2}{16 \left[E_1 t_1 \left(\frac{t_1^3}{3} + ht_1 + h^2 \right) + E_2 h \left(\frac{h^2}{3} \right) \right]} \quad (3.57)$$

Now examine the cubic and quadratic terms of the three-layer model developed in this chapter. The cubic and quadratic portion of the solution is

$$w_{\text{part}}(x) = \frac{-Px^3}{12(R_1 + R_2)} + \frac{PLx^2}{8(R_1 + R_2)} \quad (3.58)$$

By substituting the expressions that R_1 and R_2 represent in terms of the material properties (see Equations 3.8 and 3.52 for details), this partial solution becomes

$$w_{\text{part}}(x) = \frac{-Px^3}{24 \left[E_1 t_1 \left(\frac{t_1^3}{3} + ht_1 + h^2 \right) + E_2 h \left(\frac{h^2}{3} \right) \right]} + \frac{PLx^2}{16 \left[E_1 t_1 \left(\frac{t_1^3}{3} + ht_1 + h^2 \right) + E_2 h \left(\frac{h^2}{3} \right) \right]} \quad (3.59)$$

This is identical to the strength of materials solution. Recall from Equation 3.8 that the shear moduli G_1 and G_2 only appear in the constants c_7 and c_8 . Notice that these constants do not appear in the cubic or quadratic terms, but do appear in all of the remaining terms, or

w_0 , w_1 , w_5 and w_6 . Thus, the model developed in this chapter is the same as the strength of materials solution with additional terms which account for the shear deformations of the individual layers. Thus defining

$$w_{\text{shear}}(x) = w_1 x + w_0 + w_5 \sinh \lambda x + w_6 \cosh \lambda x \quad , \quad (3.60)$$

the three-layer sandwich beam model can be written as

$$w_{\text{model}}(x) = w_{\text{som}}(x) + w_{\text{shear}}(x) \quad . \quad (3.61)$$

Although the application of the correspondence principle of viscoelasticity was included in Chapter 2 as one of the steps in the development of the model, and should therefore be addressed here in Chapter 3, it is not be addressed until Chapter 4. In Chapter 4, values representative of actual candidate materials properties and geometries are used in the three-layer beam model. It is shown later that some terms in the solution (as given by Equations 3.43 and 3.53) are small enough in comparison to the other terms in the solution that they can be excluded. This makes the application of the correspondence principle more straightforward, which is a stated goal of this work.

The development of the three-layer model is now complete. The next chapter focuses on numerical results based on the model.

Chapter 4 - The Three-Layer Sandwich Beam

Model: Numerical Results

Before using the three-layer beam model with the correspondence principle to obtain a time-dependent beam model, the elastic beam model can be used to determine the sensitivity of the beam response to the different material properties. These sensitivity studies are used to determine how the reduction of the elastic moduli (both extensional and shear) of the face sheet and core influence increases in beam deflection. These results can be used then to estimate how sensitive the time-dependent behavior of the beam is to the time-dependent behavior of the constituents. Reducing the elastic moduli in the static elastic model should give a reasonable estimate of the magnitude of the effect of the time-dependent moduli reduction in the viscoelastic model. Substituting reduced material properties into the elastic model and claiming the result represents the viscoelastic response is wrong; however, the sensitivity of the response of the beam to various material properties is expected to be similar for the viscoelastic case and the elastic case. Material properties and geometries representative of candidate materials will be substituted into the model and the elastic sensitivity studies performed. First, an introduction to the candidate materials is in order.

Materials and Material Properties

Two different material systems are used for the representative material properties. First, a composite material system is considered. This consists of fiber-reinforced quasi-isotropic face sheets and composite honeycomb material for the core. Specifically, the face sheets are Astroquartz-155 (a fiber-reinforced polymer composite made by Hexcel) unidirectional laminae in a quasi-isotropic stacking sequence and the core is a glass-imide honeycomb produced by Hexcel, specifically HRH 327. The second system under consideration is an aluminum beam with the same thicknesses as the composite. The face sheets are aluminum and the core is an aluminum honeycomb. The purpose of using an aluminum beam is to give “baseline” values for comparison; aluminum is a fairly common engineering material and thus the numerical results may have greater intuitive meaning. The thickness of the aluminum face sheets and the honeycomb core are restricted to be the same thicknesses as the composite face sheets and the honeycomb core respectively. The material properties for both systems are presented in Table 1. The material properties of aluminum are widely available in standard engineering references. The extensional moduli of the aluminum and composite honeycomb cores is estimated based on the behavior of unreinforced honeycomb. The shear modulus of the aluminum honeycomb core is taken from published values, as is the shear modulus of the composite honeycomb.[3] The determination of the coefficient of thermal expansion of the aluminum honeycomb core is shown in Appendix A. The extensional modulus of the composite face sheet material is an average of experimentally determined and published values; the shear modulus is estimated by using the formula for calculating shear modulus of an isotropic material using 0.3 as Poisson’s ratio. The coefficient of thermal expansion of the quasi-isotropic quartz-epoxy face sheets is determined experimentally and the coefficient of thermal expansion of the composite honeycomb is an estimate. The thickness t_f of both models is the thickness of the composite face sheet, and the thickness h for both models is the half-thickness of the glass-imide honeycomb plus one layer of film adhesive.

(This allows direct comparison of the three-layer beam model to the five-layer beam model, which is to be developed in Chapter 5 and studied in Chapter 6.)

Table 1. Nominal Material Properties and Geometries for Three-Layer Model

Aluminum Beam	
Face Sheets	Honeycomb Core
$E_1 = 10\text{E}6 \text{ psi}$ $G_1 = 3.85\text{E}6 \text{ psi}$ $t = 0.04 \text{ in}$ $\alpha_1 = 13\text{E-}6 \frac{1}{^\circ\text{F}}$	$E_2 = 1\text{E}3 \text{ psi}$ $G_2 = 68\text{E}3 \text{ psi}$ $h = 0.255 \text{ in}$ $\alpha_2 = 13\text{E-}6 \frac{1}{^\circ\text{F}}$
Composite Beam	
Face Sheets	Honeycomb Core
$E_1 = 2.5\text{E}6 \text{ psi}$ $G_1 = 0.96\text{E}6 \text{ psi}$ $t = 0.04 \text{ in}$ $\alpha_1 = 5\text{E-}6 \frac{1}{^\circ\text{F}}$	$E_2 = 1\text{E}3 \text{ psi}$ $G_2 = 29\text{E}3 \text{ psi}$ $h = 0.255 \text{ in}$ $\alpha_2 = 1.5\text{E-}6 \frac{1}{^\circ\text{F}}$

Sensitivity Studies

In order to more completely understand which material properties have the greatest effect on the response of the three-layer beam model, the response to the mechanical load and the response to the thermal gradient are studied individually. The responses of both the aluminum material system and the composite material system beams are studied for both cases.

To study the sensitivity, a particular material property is decreased by a factor of ten relative to its nominal value. Thus, to study the sensitivity of the aluminum beam to the shear modulus of its face sheet, the value 3.85E5 (psi) is used for G , rather than the nominal value 3.85E6 (psi) as given in Table 1. Also, the sensitivity to reduced layer thicknesses is studied. Like the material property, the thickness of a given material is reduced by a factor of ten to determine the sensitivity of the response to that thickness.

The sensitivity of the response of the beam model to a particular material property being changed is normalized with respect to the response of a beam with the nominal material properties as given in Table 1. Specifically, tip-deflection is used to study the response of the beam. Thus, the sensitivity is

$$\text{Sensitivity} = \frac{w_{\text{tip}}}{w_{\text{tip}}^{\text{nominal}}} \quad (4.1)$$

For example, a number “two” reported for the sensitivity of the beam to a reduction in a given material property would signify that the tip deflection of a beam with the reduced material property is twice that of the tip deflection of a beam with the nominal material properties.

Mechanical Load

The response of the three-layer beam model to a mechanical load only can be extracted from Equations 3.43 and 3.53, and is

$$w(x) = w_3 x^3 + w_2 x^2 + w_1 x + w_0 + w_5 \sinh \lambda x + w_6 \cosh \lambda x \quad , \quad (4.2)$$

where

$$\begin{aligned}
w_3 &= \frac{-P}{12(R_1 + R_2)} \\
w_2 &= \frac{PL}{8(R_1 + R_2)} \\
w_1 &= \frac{P}{2(R_1 + R_2)^2} \left(\frac{R_1^2}{c_9} + \frac{R_2^2}{c_7} \right) \\
w_5 &= \frac{-P(c_7 R_1 - c_9 R_2)^2}{2c_7 c_9 \lambda (c_7 + c_9)(R_1 + R_2)^2} \\
w_6 &= -w_5 \\
w_0 &= w_5
\end{aligned} \tag{4.3}$$

The constants R_i and c_i are defined in Equation 3.52 and 3.8 respectively. To find the tip deflection, $x = \frac{L}{2}$ can be substituted into Equation 4.2. The tip deflection is

$$\begin{aligned}
w_{tip} = w\left(\frac{L}{2}\right) &= \frac{PL^3}{48(R_1 + R_2)} + \frac{PL}{4(R_1 + R_2)^2} \left(\frac{R_1^2}{c_9} + \frac{R_2^2}{c_7} \right) \\
&\quad - \frac{P(c_7 R_1 - c_9 R_2)^2}{2c_7 c_9 \lambda (c_7 + c_9)(R_1 + R_2)^2} \left(1 - e^{\frac{-\lambda L}{2}} \right)
\end{aligned} \tag{4.4}$$

The numerical results of the sensitivity studies for the mechanical load are reported in Table 2 and Table 3 for the aluminum beam and the composite beam respectively. The left column of each two-column table indicates which material property or thickness value is reduced by a factor of ten. The right column is the value of Equation 4.1 for that particular case.

The greatest sensitivity to a single reduction is, for both cases, when h , the half-thickness of the core, is reduced. This could be expected because of the nature of a sandwich beam; when the face sheets are close to each other, the sandwich beam is not as stiff as it would be were the face sheets further apart. Thus, there is a great sensitivity to the thickness h .

The next two greatest sensitivities to individual reductions for both cases are to the thickness of the face sheets, t , and the modulus of elasticity, E_1 , of the face sheets. This also is expected due to the nature of a sandwich beam; the face sheets provide the greatest resistance to bending. Reduce the stiffness or thickness of the face sheets and consequently the resistance to bending is reduced.

Table 2. Sensitivity of Three-Layer Aluminum Beam - Mechanical Load

Reduced Variable	Sensitivity
NONE	1.000
E_1	8.033
G_1	1.003
t_1	9.213
E_2	1.000
G_2	2.892
h	27.614
ALL	7848.78

The response of the beam is also sensitive to a reduction in the shear modulus of the core, G_2 . Like the web of an I-beam, the core of a sandwich beam should provide the primary resistance to shear loads. Thus, a reduction in the shear modulus would be expected to cause a substantial increase in deflection.

The response of the three-layer beam model seems virtually unaffected by reductions of the shear modulus of the face sheets, G_1 , and the modulus of elasticity of the core, E_2 . Thus, when the viscoelastic response of the beam is developed, the emphasis is on the response of the beam to the time-dependency of E_1 and G_2 .

Thermal Gradient

The response of the three-layer beam model to the thermal gradient in the absence of an applied mechanical load, i.e. $P=0$, can be extracted from Equations 3.43 and 3.53 and is

Table 3. Sensitivity of Three-Layer Composite Beam - Mechanical Load

Reduced Variable	Sensitivity
NONE	1.000
E_1	8.680
G_1	1.002
t_1	9.946
E_2	1.001
G_2	2.232
h	30.027
ALL	8609.04

$$w(x) = w_2 x^2 + w_0 + w_6 \cosh \lambda x , \quad (4.5)$$

where

$$\begin{aligned} w_2 &= - \frac{(M_\phi^T + M_\psi^T)}{2(R_1 + R_2)} \\ w_6 &= - \frac{(M_\psi^T R_1 - M_\phi^T R_2)(c_7 R_1 - c_9 R_2)}{c_7 c_9 \sinh \frac{\lambda L}{2} (R_1 + R_2)^2} \\ w_0 &= -w_6 \end{aligned} \quad (4.6)$$

The effective thermal moments M_ϕ^T and M_ψ^T are defined in Equation 3.8. The tip deflection is found by substituting $\frac{L}{2}$ for x in Equation 4.5, and is

$$w_{\text{tip}} = w\left(\frac{L}{2}\right) = - \frac{(M_\phi^T + M_\psi^T)L^2}{8(R_1 + R_2)} + \frac{(M_\psi^T R_1 - M_\phi^T R_2)(c_7 R_1 - c_9 R_2)}{c_7 c_9 \sinh \frac{\lambda L}{2} (R_1 + R_2)^2} \left(1 - \cosh \frac{\lambda L}{2}\right) . \quad (4.7)$$

Although Equation 4.7 is an explicit expression for the tip deflection, substituting the values of the material properties, thicknesses and length into it may now present a problem. For both the aluminum and the composite beams, the value of the expression $\frac{\lambda L}{2}$ is large enough that the value of $\cosh \frac{\lambda L}{2}$ and $\sinh \frac{\lambda L}{2}$ may exceed the ability of some computer systems. However, when the hyperbolic cosine and sine functions have large enough arguments, they can be replaced by the approximately equivalent exponential function, or

$$\cosh X \simeq \sinh X \simeq \frac{e^X}{2} \quad (4.8)$$

Thus, the tip deflection as given in Equation 4.7 can be rewritten as

$$w_{\text{tip}} = - \frac{(M_{\phi}^T + M_{\psi}^T)L^2}{8(R_1 + R_2)} + \frac{(M_{\psi}^T R_1 - M_{\phi}^T R_2)(c_7 R_1 - c_9 R_2)}{c_7 c_9 (R_1 + R_2)^2} \left(\frac{2}{e^{\frac{\lambda L}{2}}} - 1 \right) \quad (4.9)$$

However, because $e^{\frac{\lambda L}{2}}$ is very large for both cases, the approximation

$$\frac{1}{e^{\frac{\lambda L}{2}}} \simeq 0 \quad (4.10)$$

can be applied to further simplify the expression for the tip deflection. Therefore, a simpler expression for the tip deflection is

$$w_{\text{tip}} = - \frac{(M_{\phi}^T + M_{\psi}^T)L^2}{8(R_1 + R_2)} - \frac{(M_{\psi}^T R_1 - M_{\phi}^T R_2)(c_7 R_1 - c_9 R_2)}{c_7 c_9 (R_1 + R_2)^2} \quad (4.11)$$

The second term on the right hand side of Equation 4.11 is shown in Appendix B to be numerically much smaller than the first term, and so, to keep the expression for the tip deflection as simple as possible, the approximation

$$w_{\text{tip}} = - \frac{(M_{\phi}^T + M_{\psi}^T)L^2}{8(R_1 + R_2)} \quad (4.12)$$

is used to calculate the tip deflection for the thermal sensitivity study. When this approximation is used, the shear moduli G_1 and G_2 are no longer included in the expression for tip deflection. Therefore, the response of the beam should be insensitive to reductions in these material properties, as indeed it is. The numerical results of the sensitivity studies for the thermal gradients for the aluminum beam and the composite beam are reported in Table 4 and Table 5, respectively. Once again, the left column of these tables indicates which material property of thickness variable is reduced by an order of magnitude; the right column shows the value of Equation 4.1 for the case under consideration.

For both material systems, the response of the beam is almost totally insensitive to reductions of all the material properties with the single exception of the coefficient of thermal expansion of the face sheets, α_1 . When α_1 is reduced by a factor of ten, the deflection of the beam (for both material systems) is also reduced by approximately a factor of ten. Thus, the coefficient of thermal expansion of the face sheets controls the response of the three-layer sandwich beam to thermal gradients. However, this material property is not expected to behave viscoelastically. Therefore, as it is relatively insensitive to changes in material properties which may be viscoelastic, the response of the beam to thermal gradients will not be considered in the discussion of the influence of viscoelastic effects.

The Time-Dependent Three-Layer Tip-Loaded Cantilever Beam Model

Because the three-layer beam model is sensitive to reductions in the extensional modulus of the face sheets E_1 and the shear modulus of the core G_2 , these properties will now be allowed to vary with time, and the time-dependent response of the beam studied. Additionally, to verify that if the beam response is insensitive elastically to large reductions in a

Table 4. Sensitivity of Three-Layer Aluminum Beam - Thermal Gradient

Reduced Variable	Sensitivity
NONE	1.0000
E_1	0.9988
G_1	1.0000
t_1	0.9986
α_1	0.1000
E_2	1.0001
G_2	1.0000
h	1.0001
α_2	1.0000
ALL	0.1000

particular material property, then the response of the beam to time-dependent behavior of that material property is also small, another material property will be allowed to be time-dependent. Therefore, the shear modulus of the face sheets, G_1 , will be allowed to vary with time.

In order to consider the worst possible case, the material properties which are allowed to vary with time are assumed to behave as viscoelastic fluids. To maintain simplicity, the Maxwell fluid model is used in the analysis. Also, bracketing the actual behavior of the material in question is attempted by using two models, one which exhibits more time-dependent behavior than expected, and one which exhibits less. Because a linear theory of viscoelasticity is being used, it is possible to consider only one time-dependent material property at a time and then combine the viscoelastic effects by superposition. The influence of time-dependent material behavior is evaluated by studying the tip deflection. Here the tip

Table 5. Sensitivity of Three-Layer Composite Beam - Thermal Gradient

Reduced Variable	Sensitivity
NONE	1.0000
E ₁	0.9940
G ₁	1.0000
t ₁	0.9930
α ₁	0.1001
E ₂	1.0006
G ₂	1.0000
h	1.0006
α ₂	0.9999
ALL	0.1000

deflection that exceeds the static elastic tip deflection is considered a measure of the time-dependent response. Specifically, the percent increase in tip deflection is computed:

$$\text{Percent Increase in Tip Deflection} = \frac{w_{\text{tip}}(t) - w_{\text{tip}}}{w_{\text{tip}}} \times 100\% \quad (4.13)$$

In the previous equation, w_{tip} is the static elastic response.

Influence of Time-Dependent Face Sheet Shear Modulus (G_1) on Beam Response

Recall that the operational life of the precision segmented reflector is expected to be approximately 20 years. The two Maxwell fluid models used to bracket the expected behavior of the real face sheet material are one that under a constant shear stress allows the shear strain to double in 20 years and one that allows the shear strain to increase ten-fold in 20 years. The constitutive behavior of a Maxwell fluid is governed by Equation 2.12. This equation can be rewritten for shear and in its more general form (as in Equation 2.14) as

$$\tau + p_1 \dot{\tau} = q_1 \dot{\gamma} \quad , \quad (4.14)$$

where p_1 and q_1 are material constants given by

$$p_1 = \frac{\eta}{E} \quad \text{and} \quad q_1 = \eta \quad . \quad (4.15)$$

If the stress is applied at time zero, i.e. $t=0$, and remains constant,

$$\tau(t) = \hat{\tau} H(t) \quad , \quad (4.16)$$

where $\hat{\tau}$ is the amplitude of the stress and $H(t)$ is a step function, which is

$$H(t) = \begin{cases} 0 & t < 0 \\ 1 & t \geq 0 \end{cases} \quad . \quad (4.17)$$

The stress time history of Equation 4.16 can be transformed to the Laplace domain and is

$$\bar{\tau}(s) = \frac{\hat{\tau}}{s} \quad . \quad (4.18)$$

Also, Equation 4.14 can be transformed to Laplace domain. That transformation leads to

$$(1 + p_1 s) \bar{\tau}(s) = q_1 s \bar{\gamma}(s) , \quad (4.19)$$

which is in the form of Equation 2.18. From this it can be deduced that

$$\begin{aligned} \mathbb{P}(s) &= 1 + p_1 s \\ \mathbb{Q}(s) &= q_1 s \end{aligned} \quad (4.20)$$

These expressions are fundamental to the application of the correspondence principle. From Equation 4.19, $\bar{\gamma}(s)$ can be found as

$$\bar{\gamma}(s) = \bar{\tau}(s) \frac{(1 + p_1 s)}{q_1 s} \quad (4.21)$$

After substituting the Laplace transform of the applied stress, Equation 4.18, into Equation 4.21, the time-dependent strain can be found by performing the inverse Laplace transform; namely

$$\gamma(t) = \hat{\tau} \left(\frac{p_1}{q_1} + \frac{t}{q_1} \right) \quad (4.22)$$

From this expression for the material response, it is clear that the elastic shear modulus is $\frac{q_1}{p_1}$, while q_1 is associated with the time-dependent behavior. That is

$$\gamma(0) = \hat{\tau} \frac{p_1}{q_1} = \frac{\hat{\tau}}{G_1} , \quad (4.23)$$

so

$$\frac{p_1}{q_1} = \frac{1}{G_1} \quad (4.24)$$

To differentiate between the two Maxwell fluid models, a prime is now introduced for the model whose strain increases ten-fold in twenty years. However, both models have the same initial elastic response. This fact can be written as

$$\gamma(0) = \gamma'(0) \quad , \quad (4.25)$$

or,

$$\frac{p_1}{q_1} = \frac{p'_1}{q'_1} = \frac{1}{G_1} \quad . \quad (4.26)$$

The first model, which exhibits less time-dependent behavior, allows the strain to double in 20 years, or

$$\gamma(20) = \hat{\tau} \left(\frac{1}{G_1} + \frac{20}{q_1} \right) = 2\gamma(0) = 2 \frac{\hat{\tau}}{G_1} \quad . \quad (4.27)$$

As a result,

$$q_1 = 20G_1 \quad \text{and} \quad p_1 = 20 \quad . \quad (4.28)$$

For the other model, which allows the strain to increase ten-fold in twenty years,

$$\gamma(20) = \hat{\tau} \left(\frac{1}{G_1} + \frac{20}{q'_1} \right) = 10\gamma(0) = 10 \frac{\hat{\tau}}{G_1} \quad . \quad (4.29)$$

From this

$$q'_1 = \frac{20}{9} G_1 \quad \text{and} \quad p'_1 = \frac{20}{9} \quad . \quad (4.30)$$

Once the constants for the models have been found (Equations 4.28 and 4.30), the shear modulus G_1 can be replaced by $\frac{Q(s)}{P(s)}$ in the expression for the tip deflection, Equation 4.4. However, before that is done, the tip deflection can be further simplified by noting that one portion of the expression is always smaller than the others by several orders of magnitude, specifically,

$$\frac{P(c_7 R_1 - c_9 R_2)^2}{2c_7 c_9 \lambda (c_7 + c_9)(R_1 + R_2)^2} \left(1 - e^{\frac{-\lambda L}{2}}\right) \ll w_{\text{tip}} \quad (4.31)$$

The numerical proof for this is presented in Appendix B. Thus, a simplified expression for the elastic tip deflection,

$$w_{\text{tip}} = \frac{PL^3}{48(R_1 + R_2)} + \frac{PL}{4(R_1 + R_2)^2} \left(\frac{R_1^2}{c_9} + \frac{R_2^2}{c_7} \right) \quad (4.32)$$

is used to find the time-dependent behavior of the beam. The expression for the tip deflection in Equation 4.32 is rewritten, using Equation 3.8, to reveal the dependence on G_1 . That rewritten expression is

$$w_{\text{tip}} = \frac{PL^3}{48(R_1 + R_2)} + \frac{PL}{4(R_1 + R_2)^2} \left(\frac{R_1^2}{c_9} + \frac{R_2^2}{2G_1 t_1} \right) \quad (4.33)$$

Assuming P is a step function of the form shown in Equation 4.17, the Laplace transform of the time-dependent behavior of the tip deflection is given by

$$\bar{w}_{\text{tip}}(s) = \frac{P_o}{s} \left[\frac{L^3}{48(R_1 + R_2)} + \frac{L}{4(R_1 + R_2)^2} \left(\frac{R_1^2}{c_9} + \frac{R_2^2}{2 \frac{Q(s)}{P(s)} t_1} \right) \right] \quad (4.34)$$

where P_o is the magnitude of the load. By substituting the expressions for $P(s)$ and $Q(s)$ shown in Equation 4.20, the following expression is found:

$$\bar{w}_{\text{tip}}(s) = \frac{P_o}{s} \left[\frac{L^3}{48(R_1 + R_2)} + \frac{L}{4(R_1 + R_2)^2} \left(\frac{R_1^2}{c_9} + \frac{R_2^2}{2t_1} \left(\frac{1}{q_1 s} + \frac{p_1}{q_1} \right) \right) \right] \quad (4.35)$$

This can be rearranged to yield

$$\begin{aligned} \bar{w}_{tip}(s) = & \frac{P_o}{s} \left[\frac{L^3}{48(R_1 + R_2)} + \frac{L}{4(R_1 + R_2)^2} \left(\frac{R_1^2}{c_9} + \frac{R_2^2}{c_7} \right) \right] \\ & + \frac{P_o}{s^2} \left[\frac{R_2^2 L}{8(R_1 + R_2)^2 q_1 t_1} \right] \end{aligned} \quad (4.36)$$

The inverse Laplace transform is used to convert the previous expression, which is in Laplace domain, to a function in time domain:

$$w_{tip}(t) = w_{tip} + \frac{P_o L R_2^2}{4(R_1 + R_2)^2} \frac{t}{q_1} \quad (4.37)$$

where the first term to the right of the equal sign is the static elastic tip deflection as given by Equation 4.32. Notice that there is a linear dependence of the tip deflection on time.

For the case of less time-dependent behavior, q_1 is given in Equation 4.28. Using this, the time history of the tip deflection is

$$w_{tip}(t) = w_{tip} + \frac{P_o L R_2^2}{80(R_1 + R_2)^2 G_1} t \quad (4.38)$$

For the case of more time-dependent behavior as given in Equation 4.30, the time history is

$$w_{tip}(t) = w_{tip} + \frac{9P_o L R_2^2}{80(R_1 + R_2)^2 G_1} t \quad (4.39)$$

After 20 years, for the case of less and more time-dependent behavior respectively, the tip deflection is

$$w_{tip}(20) = w_{tip} + \frac{P_o L}{4(R_1 + R_2)^2} \left(\frac{R_2^2}{c_7} \right) \quad (4.40)$$

and

$$w_{\text{tip}}(20) = w_{\text{tip}} + \frac{9P_o L}{4(R_1 + R_2)^2} \left(\frac{R_2^2}{c_7} \right) \quad (4.41)$$

The percent increases of the tip deflection for the two cases of viscoelastic behavior are illustrated in Figure 8 as a function of time. The linear dependence of time is evident in this figure. After 20 years, due to the time-dependent behavior of the shear modulus of the face sheet, the tip deflection is predicted to increase by approximately 0.02% for the low level of time-dependent behavior and 0.16% for the higher level. These are small increases in tip deflection considering the long period of time. As will be shown later, these increases are small in comparison to the increases caused by other time-dependent material properties.

Influence of Time-Dependent Core Shear Modulus (G_2) on Beam

Response

Like the shear modulus of the face sheets, the time-dependent behavior of the core in shear will be bracketed by a two-fold and ten-fold increase in strain for a 20 year period. Maxwell fluid models are again used to represent these cases. Thus, the polynomials $\mathbb{P}(s)$ and $\mathbb{Q}(s)$ are the same as before, as shown in Equation 4.20. Like before, the time-dependent shear strain of the core material is

$$\gamma(t) = \hat{\tau} \left(\frac{p_1}{q_1} + \frac{t}{q_1} \right) \quad (4.41)$$

Again, the elastic shear modulus G_2 can be found by examining Equation 4.41 at time zero, or

$$\gamma(0) = \hat{\tau} \frac{p_1}{q_1} = \frac{\hat{\tau}}{G_2} \quad (4.42)$$

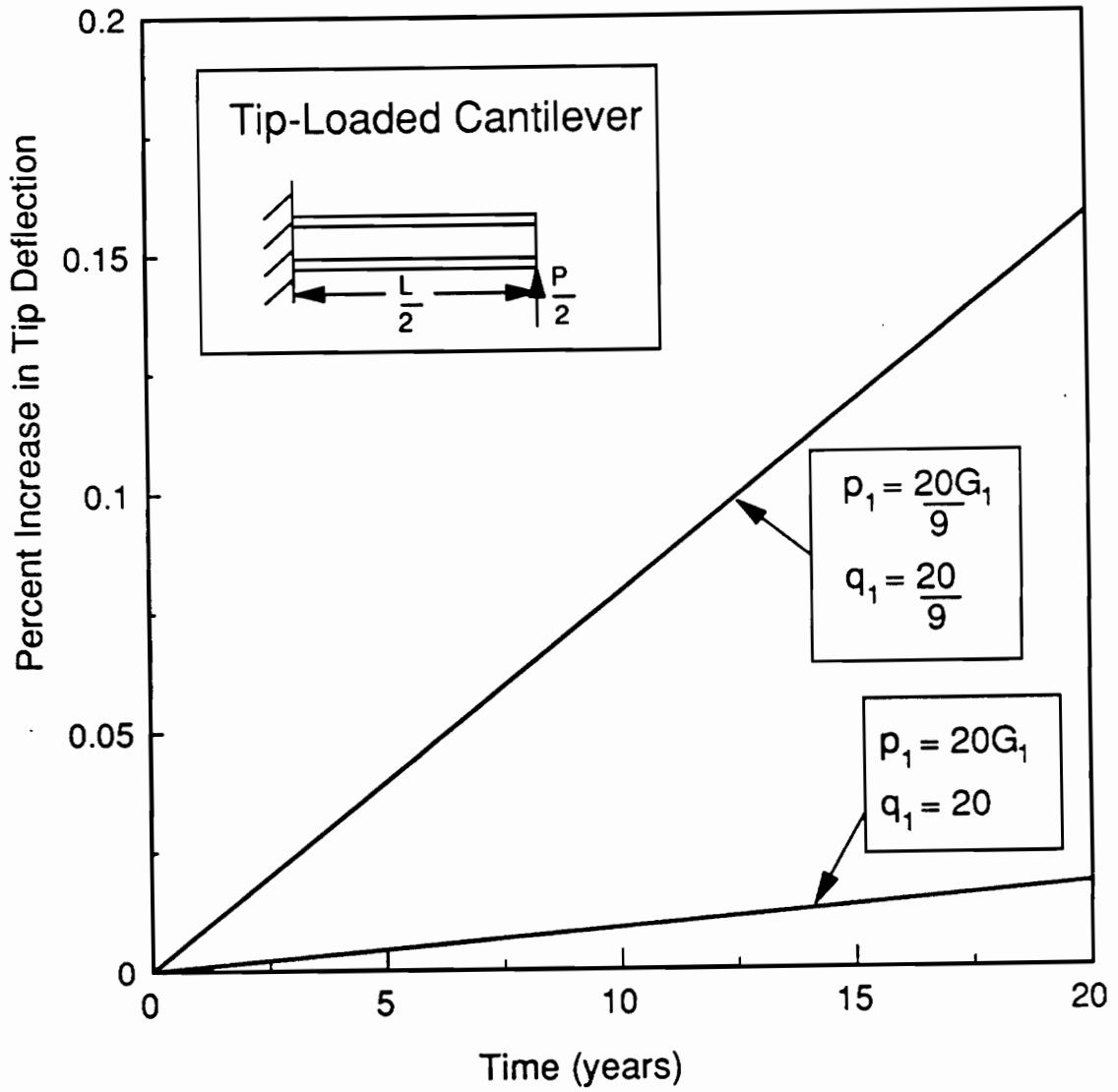


Figure 8. Percent Increase in Tip Deflection of Three-Layer Beam Model for $G_1(t)$

The elastic shear modulus is

$$\frac{p_1}{q_1} = \frac{1}{G_2} \quad (4.43)$$

As before, a prime is used to indicate the Maxwell fluid model whose strain increases ten-fold in 20 years. For the other model, the strain in 20 years is

$$\gamma(20) = \hat{\tau} \left(\frac{1}{G_2} + \frac{20}{q_1} \right) = 2\gamma(0) = 2 \frac{\hat{\tau}}{G_2} \quad (4.44)$$

so

$$q_1 = 20G_2 \text{ and } p_1 = 20 \quad (4.45)$$

For the Maxwell model which exhibits more time-dependent behavior, the shear strain in 20 years is

$$\gamma(20) = \hat{\tau} \left(\frac{1}{G_2} + \frac{20}{q'_1} \right) = 10\gamma(0) = 10 \frac{\hat{\tau}}{G_2} \quad (4.46)$$

so

$$q'_1 = \frac{20}{9} G_2 \text{ and } p'_1 = \frac{20}{9} \quad (4.47)$$

Now, the tip deflection as shown in Equation 4.32 can be rewritten using the definition of c_9 in Equation 3.8 to reveal the dependence on G_2 :

$$w_{\text{tip}} = \frac{PL^3}{48(R_1 + R_2)} + \frac{PL}{4(R_1 + R_2)^2} \left(\frac{R_1^2}{2G_2 h} + \frac{R_2^2}{c_7} \right) \quad (4.48)$$

Again, P is a step function with a magnitude of P_0 . In Equation 4.48, G_2 is replaced by the ratio of the polynomials $\frac{Q(s)}{P(s)}$:

$$\bar{w}_{\text{tip}}(s) = \frac{P_0}{s} \left[\frac{L^3}{48(R_1 + R_2)} + \frac{L}{4(R_1 + R_2)^2} \left(\frac{R_1^2}{2 \frac{Q(s)}{P(s)} h} + \frac{R_2^2}{c_7} \right) \right] \quad (4.49)$$

Using the Maxwell fluid model form of $Q(s)$ and $P(s)$ given in Equation 4.20 and rearranging, the following expression is obtained:

$$\begin{aligned} \bar{w}_{tip}(s) = & \frac{P_o}{s} \left[\frac{L^3}{48(R_1 + R_2)} + \frac{L}{4(R_1 + R_2)^2} \left(\frac{R_1^2}{c_9} + \frac{R_2^2}{c_7} \right) \right] \\ & + \frac{P_o}{s^2} \left[\frac{R_1^2 L}{8(R_1 + R_2)^2 q_1 h} \right] \end{aligned} \quad (4.50)$$

Performing the inverse Laplace transform of this expression yields the time-dependent tip deflection:

$$w_{tip}(t) = w_{tip} + \frac{P_o L R_1^2}{4(R_1 + R_2)^2} \frac{t}{q_1} \quad (4.51)$$

As before, the tip deflection is a linear function of time. Using the value of q_1 given in Equations 4.45 and 4.47, the tip deflection is, for the cases of less and more time-dependent behavior, respectively,

$$w_{tip}(t) = w_{tip} + \frac{P_o L R_1^2}{80(R_1 + R_2)^2 G_2} t \quad (4.52)$$

and

$$w_{tip}(t) = w_{tip} + \frac{9P_o L R_1^2}{80(R_1 + R_2)^2 G_2} t \quad (4.53)$$

The tip deflections in 20 years are, respectively,

$$w_{tip}(20) = w_{tip} + \frac{P_o L}{4(R_1 + R_2)^2} \left(\frac{R_1^2}{c_9} \right) \quad (4.54)$$

and

$$w_{tip}(20) = w_{tip} + \frac{9P_o L}{4(R_1 + R_2)^2} \left(\frac{R_1^2}{c_9} \right) \quad (4.55)$$

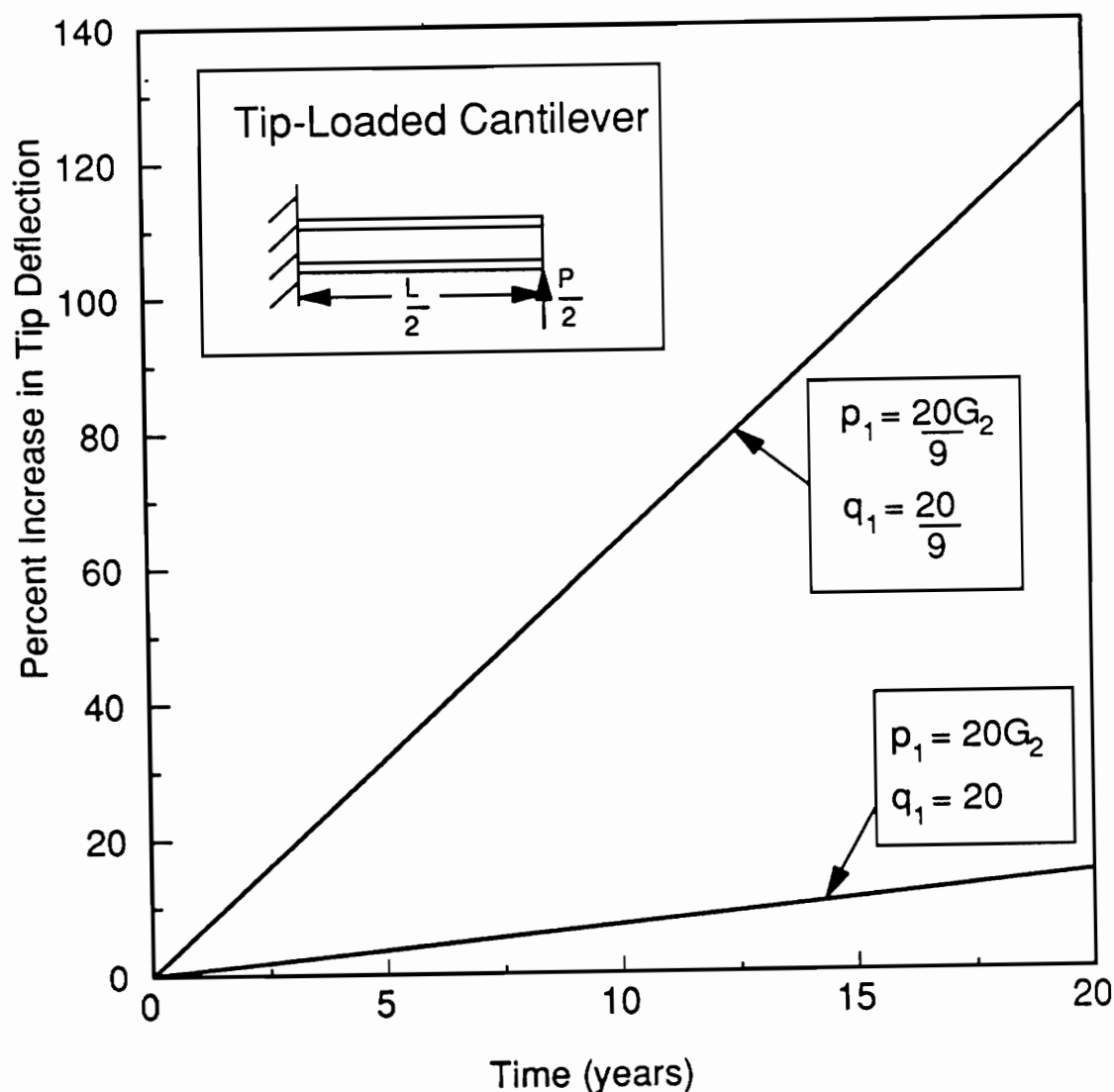


Figure 9. Percent Increase in Tip Deflection of Three-Layer Beam Model for $G_2(t)$

The percent increase of the tip deflection for these two cases of viscoelastic behavior is illustrated in Figure 9. In 20 years, the tip deflection increases approximately 14% for the case of less time-dependence and 127% for the case of more. Comparison of Figure 9 to Figure 8 reaffirms the sensitivity study of Table 3 on page 51. The static elastic response of the beam is much more sensitive to a reduction of the shear modulus of the core than to a reduction of the shear modulus of the face sheets; the viscoelastic response of the beam is

also much more sensitive to the time-dependent shear response of the core than the time-dependent shear response of the face sheets. In fact, the tip deflection of the beam more than doubles in twenty years when the shear response of the core is viscoelastic and corresponds to the higher of the two levels studied. This could lead to a serious problem in spacecraft, and should be considered in material selection.

Influence of Time-Dependent Face Sheet Modulus of Elasticity (E_1) on Beam Response

Elastically, the response of the beam is also quite sensitive to a reduction in the extensional modulus of the face sheets E_1 . Therefore, the time-dependent response of the beam to viscoelastic extensional behavior of the face sheets is expected to be important and is therefore studied. Unlike the shear behavior previously considered, this behavior is fiber-dominated. Therefore, it might be more realistic to bracket the expected behavior of the real material with a one percent and ten percent increase in strain, rather than the two- and ten-fold increases used for the shear behavior. A Maxwell fluid is again used to represent the behavior. The general form for the time-dependent behavior of a Maxwell fluid model was shown, for shear, in Equation 4.22. This form is repeated here for convenience using normal stress and normal strain:

$$\varepsilon(t) = \hat{\sigma} \left(\frac{p_1}{q_1} + \frac{t}{q_1} \right) . \quad (4.56)$$

Therefore, for the same initial elastic response,

$$\varepsilon(0) = \hat{\sigma} \left(\frac{p_1}{q_1} \right) = \hat{\sigma} \left(\frac{p'_1}{q'_1} \right) . \quad (4.57)$$

it is apparent that the elastic extensional modulus is given by $\frac{q_1}{p_1}$, or

$$\frac{p_1}{q_1} = \frac{1}{E_1} \quad (4.58)$$

For the model which exhibits less viscoelastic behavior, the strain increases in 20 years by one percent, or

$$\varepsilon(20) = 1.01\varepsilon(0) = \hat{\sigma} \left(\frac{1}{E_1} + \frac{20}{q_1} \right) \quad (4.59)$$

from which p_1 and q_1 are found:

$$p_1 = 2000 \text{ and } q_1 = 2000E_1 \quad (4.60)$$

The other model, which has a greater increase in strain, has a strain increase of ten percent in 20 years:

$$\varepsilon(20) = 1.10\varepsilon(0) = \hat{\sigma} \left(\frac{1}{E_1} + \frac{20}{q'_1} \right) \quad (4.61)$$

which leads to

$$p'_1 = 200 \text{ and } q'_1 = 200E_1 \quad (4.62)$$

As before, the next step in obtaining the time-dependent tip deflection is to substitute $\frac{Q(s)}{P(s)}$ for E_1 into the transformed form of Equation 4.29. However, this poses a problem for the extensional modulus which was not present for the shear moduli: the resulting expression is much more complicated and therefore it may be more difficult to perform the inverse Laplace transform in closed form. First, the tip deflection must be written to show the dependence on E_1 :

$$\begin{aligned}
 w_{\text{tip}} = & \frac{\left(\frac{PL^3}{96} \right)}{\left[E_1 t_1 (h^2 + ht_1 + \frac{1}{3} t_1^2) + E_2 h (\frac{1}{3} h^2) \right]} \\
 & + \left(\frac{PL}{16} \right) \frac{\left\{ \frac{\left[E_1 t_1 (2h^2 + ht_1) + E_2 h (\frac{2}{3} h^2) \right]^2}{c_9} + \frac{\left[E_1 t_1 (ht_1 + \frac{2}{3} t_1^2) \right]^2}{c_7} \right\}}{\left[E_1 t_1 (h^2 + ht_1 + \frac{1}{3} t_1^2) + E_2 h (\frac{1}{3} h^2) \right]^2} \quad (4.63)
 \end{aligned}$$

As before, the Laplace transform of the tip deflection can be performed and E_1 replaced by $\frac{Q(s)}{P(s)}$:

$$\begin{aligned}
 \bar{w}_{\text{tip}} = & \frac{\left(\frac{P_o L^3}{96} \right)}{\left[\frac{Q(s)}{P(s)} t_1 (h^2 + ht_1 + \frac{1}{3} t_1^2) + E_2 h (\frac{1}{3} h^2) \right]} \\
 & + \left(\frac{P_o L}{16} \right) \frac{\left\{ \frac{\left[\frac{Q(s)}{P(s)} t_1 (2h^2 + ht_1) + E_2 h (\frac{2}{3} h^2) \right]^2}{c_9} + \frac{\left[\frac{Q(s)}{P(s)} t_1 (ht_1 + \frac{2}{3} t_1^2) \right]^2}{c_7} \right\}}{\left[\frac{Q(s)}{P(s)} t_1 (h^2 + ht_1 + \frac{1}{3} t_1^2) + E_2 h (\frac{1}{3} h^2) \right]^2} \quad (4.64)
 \end{aligned}$$

When E_1 is modelled as a Maxwell fluid, this is

$$\begin{aligned}
 \bar{w}_{\text{tip}} = & \frac{\left(\frac{P_o L^3}{96} \right)}{\left[\left(\frac{q_1 s}{1 + p_1 s} \right) A + B \right]} \\
 & + \left(\frac{P_o L}{16} \right) \frac{\left\{ \frac{\left[\left(\frac{q_1 s}{1 + p_1 s} \right) C + D \right]^2}{c_9} + \frac{\left[\left(\frac{q_1 s}{1 + p_1 s} \right) F \right]^2}{c_7} \right\}}{\left[\left(\frac{q_1 s}{1 + p_1 s} \right) A + B \right]^2} \quad (4.65)
 \end{aligned}$$

where

$$\begin{aligned}
 A &= t_1(h^2 + ht_1 + \frac{1}{3}t_1^2) \\
 B &= E_2h(\frac{1}{3}h^2) \\
 C &= t_1(2h^2 + ht_1) \\
 D &= E_2h(\frac{2}{3}h^2) \\
 F &= t_1(ht_1 + \frac{2}{3}t_1^2) \\
 G &= Aq_1 + Bp_1 \\
 H &= Cq_1 + Dp_1
 \end{aligned} \tag{4.66}$$

Performing the inverse Laplace transform yields the time-dependent tip deflection, which is

$$\begin{aligned}
 w_{tip}(t) &= w_{tip} + \frac{P_o L^3}{96} \left(\frac{Aq_1}{BG} \right) \left(1 - e^{-\frac{Bt}{G}} \right) \\
 &+ \frac{P_o L}{16B^2} \left[\frac{1}{c_9} \left(D^2 - \frac{B^2 H^2}{G^2} \right) - \frac{1}{c_7} \left(\frac{B^2 F^2 q_1^2}{G^2} \right) \right] \left(1 - e^{-\frac{Bt}{G}} \right) \\
 &+ \frac{P_o L}{16BG} \left[\frac{1}{c_9} \left(D - \frac{BH}{G} \right)^2 + \frac{1}{c_7} \left(\frac{B^2 F^2 q_1^2}{G^2} \right) \right] t e^{-\frac{Bt}{G}}
 \end{aligned} \tag{4.66}$$

For the two levels of time-dependence given by Equations 4.60 and 4.62, the percent increases in tip deflection are shown in Figure 10 as a function of time. Despite the exponential form of Equation 4.67, the function is approximately linear in shape.

Although for a simple Maxwell fluid model it is possible to perform the inverse Laplace transform, the time-dependent tip deflection may be prohibitively difficult to find for more complicated functions. Thus, an approximate tip deflection will be used to find an approximate time-dependent tip deflection, and this will be compared to the exact time-dependent tip deflection just developed. The expression for the tip deflection given in Equation 4.63 can be rearranged as

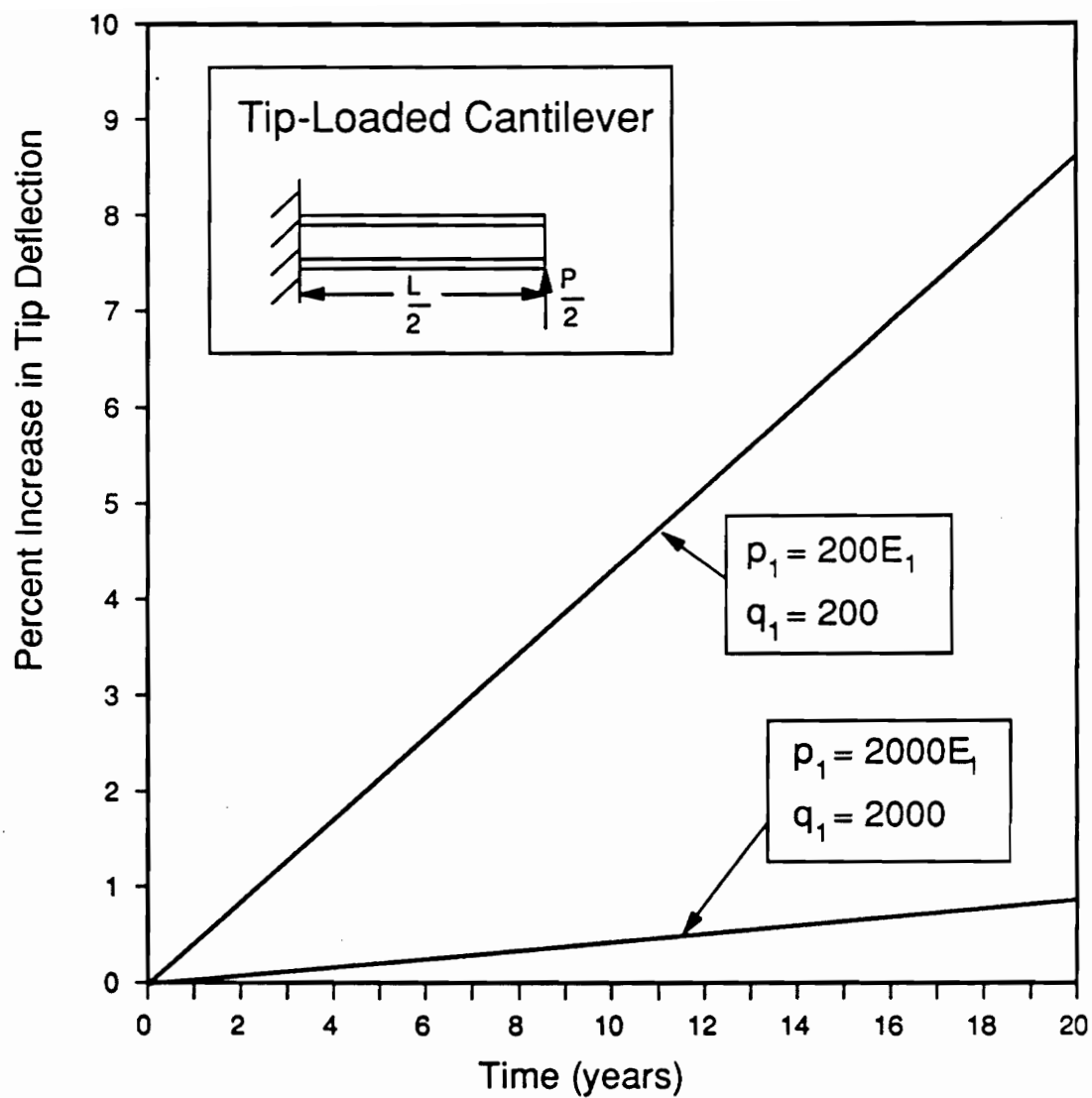


Figure 10. Percent Increase in Tip Deflection of Three-Layer Beam Model for $E_1(t)$

$$w_{tip} = \frac{\left(\frac{PL^3}{96E_1} \right)}{\left[t_1(h^2 + ht_1 + \frac{1}{3} t_1^2) + \frac{E_2}{E_1} h(\frac{1}{3} h^2) \right]} + \left(\frac{PL}{16} \right) \frac{\left\{ \frac{\left[t_1(2h^2 + ht_1) + \frac{E_2}{E_1} h(\frac{2}{3} h^2) \right]^2}{c_9} + \frac{t_1^2(ht_1 + \frac{2}{3} t_1^2)^2}{c_7} \right\}}{\left[t_1(h^2 + ht_1 + \frac{1}{3} t_1^2) + \frac{E_2}{E_1} h(\frac{1}{3} h^2) \right]^2} \quad (4.68)$$

This expression can be approximated by noting that E_2 is much smaller than E_1 , or

$$\frac{E_2}{E_1} \ll 1. \quad (4.69)$$

Thus, an approximation can be used for the ratio $\frac{E_2}{E_1}$:

$$\frac{E_2}{E_1} \approx 0. \quad (4.70)$$

Using this approximation, Equation 4.68 simplifies to

$$w_{tip} = \frac{PL^3}{96E_1 t_1(h^2 + ht_1 + \frac{1}{3} t_1^2)} + \frac{PL}{16(h^2 + ht_1 + \frac{1}{3} t_1^2)^2} \left[\frac{(2h^2 + ht_1)^2}{c_9} + \frac{(ht_1 + \frac{2}{3} t_1^2)^2}{c_7} \right]. \quad (4.71)$$

This expression is shown in Appendix B to be approximately equal to the expression for the tip deflection in Equation 4.32. In Equation 4.71, E_1 is replaced by $\frac{Q(s)}{P(s)}$ and the load P , a step function, is replaced by its Laplace transform $\frac{P_0}{s}$:

$$\begin{aligned}\bar{w}_{tip}(s) = & \frac{P_o L^3}{96s \frac{Q(s)}{P(s)} t_1(h^2 + ht_1 + \frac{1}{3} t_1^2)} \\ & + \frac{P_o L}{16s(h^2 + ht_1 + \frac{1}{3} t_1^2)^2} \left[\frac{(2h^2 + ht_1)^2}{c_9} + \frac{(ht_1 + \frac{2}{3} t_1^2)^2}{c_7} \right].\end{aligned}\quad (4.72)$$

Next, $Q(s)$ and $P(s)$ are replaced by the polynomials specific to a Maxwell fluid as shown in Equation 4.20:

$$\begin{aligned}\bar{w}_{tip}(s) = & \frac{P_o}{s^2} \left[\frac{L^3}{96q_1 t_1(h^2 + ht_1 + \frac{1}{3} t_1^2)} \right] \\ & + \frac{P_o}{s} \left\{ \frac{p_1 L^3}{96q_1 t_1(h^2 + ht_1 + \frac{1}{3} t_1^2)} + \frac{L}{16(h^2 + ht_1 + \frac{1}{3} t_1^2)^2} \left[\frac{(2h^2 + ht_1)^2}{c_9} + \frac{(ht_1 + \frac{2}{3} t_1^2)^2}{c_7} \right] \right\}\end{aligned}\quad (4.73)$$

The inverse Laplace transform of Equation 4.73 is the time history of the tip deflection, or

$$w_{tip}(t) = w_{tip} + \frac{P_o L^3}{96t_1(h^2 + ht_1 + \frac{1}{3} t_1^2)} \left(\frac{t}{q_1} \right), \quad (4.74)$$

where w_{tip} is the approximate elastic tip deflection of Equation 4.71. Thus, by using an approximation for the tip deflection which is based on the relatively small size of the extensional modulus of the core, a linear dependence on time is obtained for a Maxwell fluid representation of the viscoelastic extensional behavior of the face sheets. Thus, for the model whose strain increases one percent in 20 years, the tip deflection of the beam in 20 years can be found by using Equations 4.60 and 4.74:

$$w_{tip}(20) = w_{tip} + \frac{P_o L^3}{9600E_1 t_1(h^2 + ht_1 + \frac{1}{3} t_1^2)} \quad (4.75)$$

For the model with a ten percent increase in strain in 20 years, the tip deflection in 20 years is

$$w_{\text{tip}}(20) = w_{\text{tip}} + \frac{P_o L^3}{960E_1 t_1 (h^2 + ht_1 + \frac{1}{3} t_1^2)} \quad (4.76)$$

The percent increases in tip deflection as a function of time for the two bracketing time-dependent behaviors are shown in Figure 11. Also, the percent increases in tip deflection for the two exact cases are shown in this figure for comparison. The approximation is close to the exact solution for both cases. Both the approximate and exact time-dependent responses of the beam caused by the viscoelastic extensional behavior of the face sheet material are much less than the response caused by the viscoelastic behavior of the core in shear. This is not entirely unexpected because the bracketing conditions for the extensional behavior allow much less time-dependent response than the bracketing conditions for the shear behavior (e.g., a ten percent increase in strain as compared to a ten-fold increase). However, the tip deflection has a time-dependent increase of nearly one percent and ten percent in twenty years for both the approximate and exact cases, nearly the same amount of strain increase in the face sheets themselves. Thus, there is an almost one-to-one relationship between the time-dependent tip deflection and the time-dependent strain of the face sheets. As seen in Table 2 and Table 3, the elastic sensitivity of the tip deflection is much greater for reductions of E_1 than for the same reductions of G_1 . Therefore, the elastic sensitivity studies provide good indications of how sensitive the beam is to viscoelastic behavior of its constituents. Actually, the elastic sensitivity studies are similar in nature to the so-called quasi-elastic approach to studying viscoelastic effects.

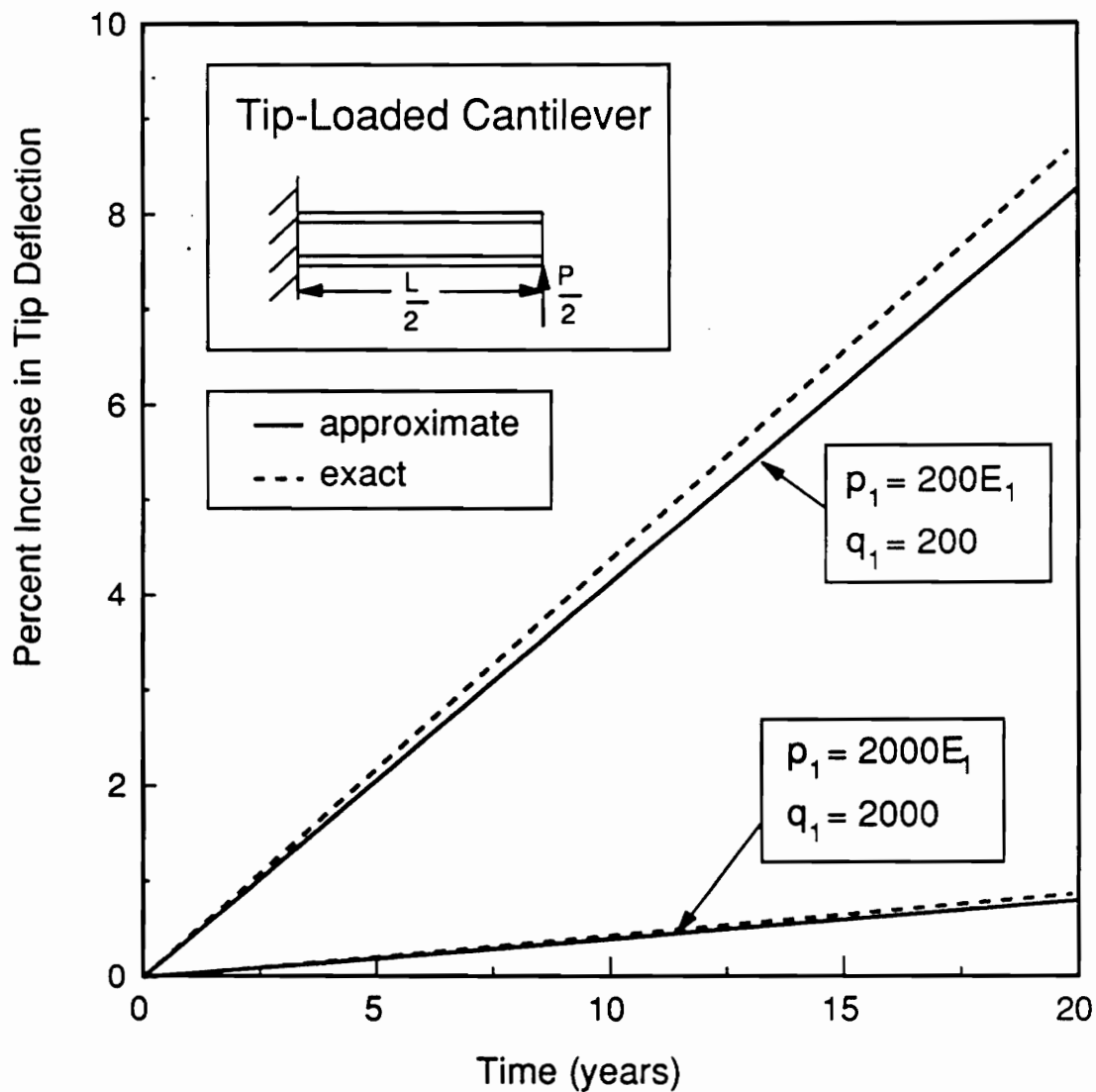


Figure 11. Percent Increase in Tip Deflection of Three-Layer Beam Model for $E_1(t)$ - Approximate

Quasi-Elastic Approach

A quasi-elastic approach can be used to estimate the viscoelastic response of a structure to the time-dependent behavior of its constituent material properties. With the quasi-elastic

approach, the compliance of a particular constituent is replaced by the compliance of the constituent evaluated at the time of interest, and an elastic analysis is performed. In particular, for the problem being considered here, the tip deflection of the tip-loaded cantilever beam in 20 years is found by increasing a specific compliance by a given factor. For example, for the case where the shear modulus of the face sheets, G_1 , is time-dependent, the compliance $\left(\frac{1}{G_1}\right)$ is replaced by $\frac{10}{G_1}$. This has exactly the same effect as replacing G_1 by $\frac{G_1}{10}$ as was done in the elastic sensitivity studies. To allow for direct comparison between the quasi-elastic and viscoelastic results, the compliances which correspond to the shear moduli (G_1 and G_2) are increased by a factor of ten and the compliance which corresponds to the modulus of elasticity of the face sheets (E_1) is increased by a factor of 1.1. Thus, the results of using the quasi-elastic approach which appear in Table 6 can be correlated with the results of the last three figures. In Table 6, the first column indicates the material property that is assumed to have a compliance increase and the second column presents the factor by which it is increased. The third column is the percent increase in tip deflection at twenty-years as computed by the quasi-elastic approach and normalized with respect to the elastic tip deflection, or

$$\frac{w_{\text{tip}}^{\text{quasi-elastic}} - w_{\text{tip}}}{w_{\text{tip}}} \times 100\% \quad . \quad (4.77)$$

The increase in tip deflection at 20 years as computed by the viscoelastic approach and normalized with respect to the elastic tip deflection, or

$$\frac{w_{\text{tip}}^{\text{viscoelastic}}(20) - w_{\text{tip}}}{w_{\text{tip}}} \times 100\% \quad , \quad (4.78)$$

is presented in the fourth column for comparison. The results from the quasi-elastic approach are nearly identical to the results from the viscoelastic approach for the three cases shown. There is only a minor difference in the two values for the case of the compliance corre-

sponding to G_2 , the shear modulus of the core. In this case, the quasi-elastic value is slightly less than the viscoelastic one.

Table 6. Quasi-Elastic Tip Deflection of the Three-Layer Composite Tip-Loaded Cantilever Beam

Material Property	Factor	Quasi-Elastic Result	Viscoelastic Result
E_1	1.1	8.6 %	8.6 %
G_1	10.0	0.2 %	0.2 %
G_2	10.0	123.2 %	126.8 %

Summary

This completes the numerical results based on the three-layer beam model. The results provide a glimpse of the effects of time-dependent behavior of various constituents on the overall response of the beam to both mechanical loads and a temperature gradient. The results are based on what might be considered simple representations of time-dependent material behavior. Nonetheless, the results are quite valuable. Additionally, if more complicated time-dependent material behavior models are to be considered, the equations and steps necessary to include these models are available in this chapter. The focus now shifts to the five-layer beam model. With this model, the importance of the adhesive layer to the overall response of the beam can be evaluated.

Chapter 5 - Development of the Five-Layer Sandwich Beam Model

Although the three-layer model is a valuable tool, the five-layer model accounts for separate adhesive layers. Because adhesives are generally polymer-based materials, the time-dependent behavior of the adhesive layers could be important to the response of the reflector segments. Thus, the analysis is not complete without studying the five-layer sandwich beam model. However, the importance of the three-layer model as a tool for simplifying the five-layer beam model will be revealed in the development of the five-layer model.

Displacement Field

Like that of the three-layer model, the displacement field of the five-layer sandwich beam model must account for the contribution that each layer makes toward the overall response of the beam. As was done in the three-layer model, each layer is assumed to have both extensional and shear deformations, and to shear independently of the other layers. The quan-

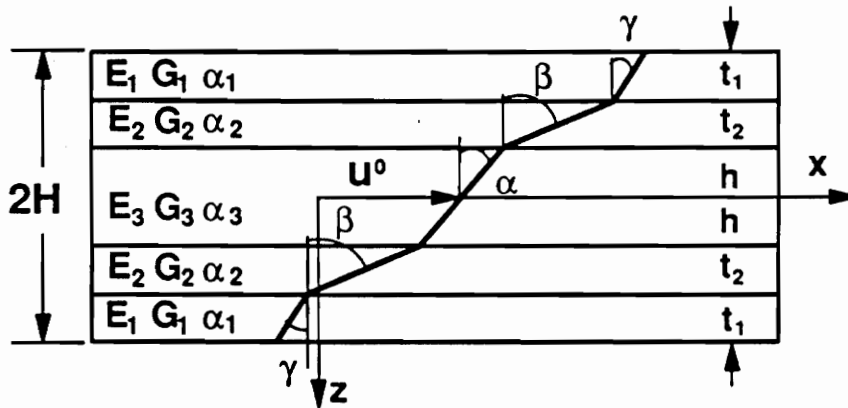


Figure 12. Displacement Field of the Five-Layer Sandwich Beam Model

tity u^0 again represents the midsurface x-direction displacement. An additional x-direction displacement is caused by the rotations of the different layers; the core has a rotational angle $\alpha(x)$, the adhesive layers $\beta(x)$ and the face sheets $\gamma(x)$. The displacement in the z direction is constant through the thickness. Because this is a beam model, the displacements are not dependent on the position through the width of the beam, y . Thus, the z-direction displacement is only a function of the position along the length of the beam, x . The y-direction displacement is not needed for the model; therefore, no assumptions are made about it. The displacement field for the five-layer beam model is

$$\begin{aligned}
 u(x,z) &= \begin{cases} u^0(x) + h\alpha(x) + t_2\beta(x) - (z + h + t_2)\gamma(x) & -H \leq z \leq -H + t_1 \\ u^0(x) + h\alpha(x) - (z + h)\beta(x) & -H + t_1 \leq z \leq -h \\ u^0(x) - z\alpha(x) & -h \leq z \leq h \\ u^0(x) - h\alpha(x) - (z - h)\beta(x) & h \leq z \leq H - t_1 \\ u^0(x) - h\alpha(x) - t_2\beta(x) - (z - h - t_2)\gamma(x) & H - t_1 \leq z \leq H \end{cases} \quad (5.1) \\
 w(x,z) &= w^0(x)
 \end{aligned}$$

The displacement field in the x direction and the geometry and nomenclature for the five-layer model are shown in Figure 12.

Strain Field

The strain-displacement relationships given in Equation 2.21 are applied to the displacement field to yield the strain field, which is

$$\varepsilon_x = \begin{cases} \frac{du}{dx} + h \frac{d\alpha}{dx} + t_2 \frac{d\beta}{dx} - (z + h + t_2) \frac{d\gamma}{dx} & -H \leq z \leq -H + t_1 \\ \frac{du}{dx} + h \frac{d\alpha}{dx} - (z + h) \frac{d\beta}{dx} & -H + t_1 \leq z \leq -h \\ \frac{du}{dx} - z \frac{d\alpha}{dx} & -h \leq z \leq h \\ \frac{du}{dx} - h \frac{d\alpha}{dx} - (z - h) \frac{d\beta}{dx} & h \leq z \leq H - t_1 \\ \frac{du}{dx} - h \frac{d\alpha}{dx} - t_2 \frac{d\beta}{dx} - (z - h - t_2) \frac{d\gamma}{dx} & H - t_1 \leq z \leq H \end{cases}$$

$$\gamma_{xz} = \begin{cases} -\gamma + \frac{dw}{dx} & -H \leq z \leq -H + t_1 \\ -\beta + \frac{dw}{dx} & -H + t_1 \leq z \leq -h \\ -\alpha + \frac{dw}{dx} & -h \leq z \leq h \\ -\beta + \frac{dw}{dx} & h \leq z \leq H - t_1 \\ -\gamma + \frac{dw}{dx} & H - t_1 \leq z \leq H \end{cases} \quad (5.2)$$

where the superscript "o" has been dropped from $u^o(x)$ and $w^o(x)$.

Principle of Stationary Potential Energy

For the five-layer beam model, five degrees of freedom have been assumed: the displacements u , w , α , β and γ . Therefore, application of the principle of stationary potential energy results in five Euler equations and five sets of boundary conditions.

First, the total potential energy of the beam must be written as a functional of the displacement functions. The total potential energy is given by Equation 2.27 and is

$$\Pi = \frac{1}{2} \int_{L^*} \int_{-H}^H [E(z)\varepsilon_x^2 + G(z)\gamma_{xz}^2 - E(z)\alpha(z)\Delta T(z)\varepsilon_x] dz dx - P^*w|_{x=x^*} \quad (5.3)$$

The thermal gradient considered is the same as for the three-layer case: a linear gradient through the thickness of the beam,

$$\Delta T = a + bz \quad . \quad (5.4)$$

If the integral over the thickness of the beam in Equation 5.3 is separated into five integrals, one for each layer, within each integral the material properties are no longer functions of z . Thus, the total potential energy is

$$\begin{aligned} \Pi = \frac{1}{2} \int_L \left\{ \int_{-H}^{-H+t_1} [E_1 \epsilon_x^2 + G_1 \gamma_{xz}^2 - E_1 \alpha_1 (a + bz) \epsilon_x] dz \right. \\ + \int_{-H+t_1}^{-h} [E_2 \epsilon_x^2 + G_2 \gamma_{xz}^2 - E_2 \alpha_2 (a + bz) \epsilon_x] dz \\ + \int_{-h}^h [E_3 \epsilon_x^2 + G_3 \gamma_{xz}^2 - E_3 \alpha_3 (a + bz) \epsilon_x] dz \\ + \int_h^{H-t_1} [E_2 \epsilon_x^2 + G_2 \gamma_{xz}^2 - E_2 \alpha_2 (a + bz) \epsilon_x] dz \\ \left. + \int_{H-t_1}^H [E_1 \epsilon_x^2 + G_1 \gamma_{xz}^2 - E_1 \alpha_1 (a + bz) \epsilon_x] dz \right\} dx \\ - P^* w|_{x=x^*} \quad , \end{aligned} \quad (5.5)$$

where the nomenclature for the material properties and geometry are shown in Figure 12. A set of constants similar to those used in Chapter 3 to represent combinations of material properties and geometry constants is introduced to simplify the development. These constants are

$$\begin{aligned}
c_0 &= E_1 t_1 + E_2 t_2 + E_3 h \\
c_1 &= h^2 (E_1 t_1 + E_2 t_2 + \frac{1}{3} E_3 h) \\
c_2 &= h t_2 (2 E_1 t_1 + E_2 t_2) \\
c_3 &= h t_1 (E_1 t_1) \\
c_4 &= t_2^2 (E_1 t_1 + \frac{1}{3} E_2 t_2) \\
c_5 &= t_1 t_2 (E_1 t_1) \\
c_6 &= t_1^2 (\frac{1}{3} E_1 t_1) \\
c_7 &= 2 G_1 t_1 \\
c_8 &= 2 G_2 t_2 \\
c_9 &= 2 G_3 h \\
N_u^T &= -a (E_1 \alpha_1 t_1 + E_2 \alpha_2 t_2 + E_3 \alpha_3 h) \\
M_\alpha^T &= b h [E_1 \alpha_1 t_1 (h + t_2 + \frac{1}{2} t_1) + E_2 \alpha_2 t_2 (h + \frac{1}{2} t_2) + E_3 \alpha_3 h (\frac{1}{3} h)] \\
M_\beta^T &= b t_2 [E_1 \alpha_1 t_1 (h + t_2 + \frac{1}{2} t_1) + E_2 \alpha_2 t_2 (\frac{1}{2} h + \frac{1}{3} t_2)] \\
M_\gamma^T &= b t_1 [E_1 \alpha_1 t_1 (\frac{1}{2} h + \frac{1}{2} t_2 + \frac{1}{3} t_1)] .
\end{aligned} \tag{5.6}$$

By substituting the appropriate expressions for the strains, as given by Equation 5.2, into Equation 5.5 and performing the integrations through the thickness of the layers, the following expression for the total potential energy is obtained:

$$\begin{aligned}
\Pi = \int_L \left[(c_0 u' + N_u^T) u' + (c_1 \alpha' + M_\alpha^T) \alpha' + c_2 \alpha' \beta' + c_3 \alpha' \gamma' + (c_4 \beta' + M_\beta^T) \beta' + (c_6 \gamma' + M_\gamma^T) \gamma' \right. \\
\left. + c_5 \beta' \gamma' + c_7 \gamma (\frac{\gamma}{2} - w') + c_8 \beta (\frac{\beta}{2} - w') + c_9 \alpha (\frac{\alpha}{2} - w') + \frac{(c_7 + c_8 + c_9)}{2} (w')^2 \right] dx \\
- P^* w|_{x=x^*} .
\end{aligned} \tag{5.7}$$

where the prime indicates a differentiation with respect to x ; for example, α' represents $\frac{d\alpha}{dx}$.

The next step in the application of the principle of stationary potential energy is to find the first variation of the total potential energy and equate it to zero. The previous expression for po-

tential energy is in the functional form necessary for this operation. The first variation of the total potential energy is found by using the following equation:

$$\begin{aligned} \delta\Pi = & \frac{\partial\Pi}{\partial u'} \delta u' + \frac{\partial\Pi}{\partial \alpha} \delta \alpha + \frac{\partial\Pi}{\partial \alpha'} \delta \alpha' + \frac{\partial\Pi}{\partial \beta} \delta \beta + \frac{\partial\Pi}{\partial \beta'} \delta \beta' \\ & + \frac{\partial\Pi}{\partial \gamma} \delta \gamma + \frac{\partial\Pi}{\partial \gamma'} \delta \gamma' + \frac{\partial\Pi}{\partial w} \delta w + \frac{\partial\Pi}{\partial w'} \delta w' . \end{aligned} \quad (5.8)$$

When Equation 5.8 is applied to the functional form of the potential energy in Equation 5.7, the result is

$$\begin{aligned} \delta\Pi = & \int_{L^*} \left\{ [2c_0 u' + N_U^T] \delta u' + [c_9(\alpha - w')] \delta \alpha + [2c_1 \alpha' + c_2 \beta' + c_3 \gamma' + M_\alpha^T] \delta \alpha' \right. \\ & + [c_8(\beta - w')] \delta \beta + [c_2 \alpha' + 2c_4 \beta' + c_5 \gamma' + M_\beta^T] \delta \beta' + [c_7(\gamma - w')] \delta \gamma \\ & + [c_3 \alpha' + c_5 \beta' + 2c_6 \gamma' + M_\gamma^T] \delta \gamma' + [c_7(w' - \gamma) + c_8(w' - \beta) + c_9(w' - \alpha)] \delta w' \left. \right\} dx \\ & - P^* \delta w \Big|_{x=x^*} . \end{aligned} \quad (5.9)$$

As in the three-layer model, integration by parts (Equation 3.11) is used to change the this form of the first variation of total potential energy to a more useful one. That form is:

$$\begin{aligned}
\delta \Pi = & \int_{L^*} \{ - [2c_0 u''] \delta u - [2c_1 \alpha'' + c_2 \beta'' + c_3 \gamma'' + c_9 (w' - \alpha)] \delta \alpha \\
& - [c_2 \alpha'' + 2c_4 \beta'' + c_5 \gamma'' + c_8 (w' - \beta)] \delta \beta \\
& - [c_3 \alpha'' + c_5 \beta'' + 2c_6 \gamma'' + c_7 (w' - \gamma)] \delta \gamma \\
& - [c_7 (w'' - \gamma') + c_8 (w'' - \beta') + c_9 (w'' - \alpha')] \delta w \} dx \\
& + \{ [2c_0 u' + N_u^T] \delta u \} \Big|_{x=0}^{x=\frac{L}{2}} \\
& + \{ [2c_1 \alpha' + c_2 \beta' + c_3 \gamma' + M_\alpha^T] \delta \alpha \} \Big|_{x=0}^{x=\frac{L}{2}} \\
& + \{ [c_2 \alpha' + 2c_4 \beta' + c_5 \gamma' + M_\beta^T] \delta \beta \} \Big|_{x=0}^{x=\frac{L}{2}} \\
& + \{ [c_3 \alpha' + c_5 \beta' + 2c_6 \gamma' + M_\gamma^T] \delta \gamma \} \Big|_{x=0}^{x=\frac{L}{2}} \\
& + \{ [c_7 (w' - \gamma) + c_8 (w' - \beta) + c_9 (w' - \alpha)] \delta w \} \Big|_{x=0}^{x=\frac{L}{2}} \\
& - \frac{P}{2} \delta w \Big|_{x=\frac{L}{2}} .
\end{aligned} \tag{5.10}$$

The second set of terms in Equation 5.10 are the boundary conditions. Again they reflect a tip-loaded cantilever beam with its fixed end at $x=0$ and its tip at $x=L/2$. The load on the tip is $P/2$. Because the variations δw , δu , $\delta \alpha$, $\delta \beta$ and $\delta \gamma$ are independent of one another, each of their coefficients must be zero in order for the first variation of the total potential energy to be identically zero. Equating to zero the expressions inside the integral over the length of the beam leads to the Euler equations for the five-layer beam model. They are

$$\begin{aligned}
2c_0 \left(\frac{d^2 u}{dx^2} \right) &= 0 \\
2c_1 \left(\frac{d^2 \alpha}{dx^2} \right) + c_2 \left(\frac{d^2 \beta}{dx^2} \right) + c_3 \left(\frac{d^2 \gamma}{dx^2} \right) + c_9 \left(\frac{dw}{dx} - \alpha \right) &= 0 \\
c_2 \left(\frac{d^2 \alpha}{dx^2} \right) + 2c_4 \left(\frac{d^2 \beta}{dx^2} \right) + c_5 \left(\frac{d^2 \gamma}{dx^2} \right) + c_8 \left(\frac{dw}{dx} - \beta \right) &= 0 \\
c_3 \left(\frac{d^2 \alpha}{dx^2} \right) + c_5 \left(\frac{d^2 \beta}{dx^2} \right) + 2c_6 \left(\frac{d^2 \gamma}{dx^2} \right) + c_7 \left(\frac{dw}{dx} - \gamma \right) &= 0 \\
c_7 \left(\frac{d\gamma}{dx} - \frac{d^2 w}{dx^2} \right) + c_8 \left(\frac{d\beta}{dx} - \frac{d^2 w}{dx^2} \right) + c_9 \left(\frac{d\alpha}{dx} - \frac{d^2 w}{dx^2} \right) &= 0
\end{aligned} \tag{5.11}$$

Equating to zero the remaining portions of Equation 5.10 lead to the boundary conditions. On both ends of the beam,

$$\begin{aligned}
[2c_0 u' + N_u^T] \delta u &= 0 \\
[2c_1 \alpha' + c_2 \beta' + c_3 \gamma' + M_x^T] \delta \alpha &= 0 \\
[c_2 \alpha' + 2c_4 \beta' + c_5 \gamma' + M_\beta^T] \delta \beta &= 0 \\
[c_3 \alpha' + c_5 \beta' + 2c_6 \gamma' + M_\gamma^T] \delta \gamma &= 0 \\
[(c_7 + c_8 + c_9)w' - c_7 \gamma - c_8 \beta - c_9 \alpha - \frac{P}{2}] \delta w &= 0
\end{aligned} \tag{5.12}$$

where in the last equation it is implied that the load $P/2$ applies only at $x=L/2$ and not $x=0$. The boundary conditions in Equation 5.12 are satisfied when, for each of the five expressions and on both ends of the beam, either the term in brackets is zero, or the kinematic variable is specified. The boundary conditions can be written as, at each end of the beam,

$$\begin{aligned}
& \text{either} \\
& 2c_0 \frac{du}{dx} + N_u^T = 0 \quad \text{or} \quad u = u^* \\
& \text{and either} \\
& 2c_1 \frac{d\alpha}{dx} + c_2 \frac{d\beta}{dx} + c_3 \frac{d\gamma}{dx} + M_\alpha^T = 0 \quad \text{or} \quad \alpha = \alpha^* \\
& \text{and either} \\
& c_2 \frac{d\alpha}{dx} + 2c_4 \frac{d\beta}{dx} + c_5 \frac{d\gamma}{dx} + M_\beta^T = 0 \quad \text{or} \quad \beta = \beta^* \\
& \text{and either} \\
& c_3 \frac{d\alpha}{dx} + c_5 \frac{d\beta}{dx} + 2c_6 \frac{d\gamma}{dx} + M_\gamma^T = 0 \quad \text{or} \quad \gamma = \gamma^* \\
& \text{and either} \\
& (c_7 + c_8 + c_9) \frac{dw}{dx} - c_7\gamma - c_8\beta - c_9\alpha = \frac{P}{2} \quad \text{or} \quad w = w^*
\end{aligned} \tag{5.13}$$

Therefore, for the tip-loaded cantilever beam under consideration which was shown in Figure 6 on page 23, the boundary conditions are

$$\begin{aligned}
& \text{at } x = 0: \quad \text{at } x = \frac{L}{2}: \\
& u = 0 \quad 2c_0 \left(\frac{du}{dx} \right) + N_u^T = 0 \\
& \alpha = 0 \quad 2c_1 \left(\frac{d\alpha}{dx} \right) + c_2 \left(\frac{d\beta}{dx} \right) + c_3 \left(\frac{d\gamma}{dx} \right) + M_\alpha^T = 0 \\
& \beta = 0 \quad c_2 \left(\frac{d\alpha}{dx} \right) + 2c_4 \left(\frac{d\beta}{dx} \right) + c_5 \left(\frac{d\gamma}{dx} \right) + M_\beta^T = 0 \\
& \gamma = 0 \quad c_3 \left(\frac{d\alpha}{dx} \right) + c_5 \left(\frac{d\beta}{dx} \right) + 2c_6 \left(\frac{d\gamma}{dx} \right) + M_\gamma^T = 0 \\
& w = 0 \quad (c_7 + c_8 + c_9) \left(\frac{dw}{dx} \right) - c_7\gamma - c_8\beta - c_9\alpha = \frac{P}{2} .
\end{aligned} \tag{5.14}$$

Solution of Euler Equations for Displacement Functions

Solution for $u(x)$

The displacement function $u(x)$ is, as it was in the three-layer sandwich beam model, completely decoupled from the rest of the displacement functions in the Euler equations. The Euler equation that governs $u(x)$ is .

$$2c_0 \left(\frac{d^2 u}{dx^2} \right) = 0 . \quad (5.15)$$

This is identical to Equation 3.19, the corresponding Euler equation for the three-layer beam model, except that the definition of c_0 now includes the extensional modulus and thickness of the adhesive. Therefore, the displacement function $u(x)$ must be the same as for the three-layer model, namely a linear function of x . Thus,

$$u(x) = u_1 x + u_0 . \quad (5.16)$$

Again, the focus of this work is the out-of-plane response of sandwich beams. No further discussion of $u(x)$ is necessary.

Solution for $w(x)$, $\alpha(x)$, $\beta(x)$ and $\gamma(x)$

The Euler equations for the remaining displacement functions are coupled ordinary differential equations. A solution of the form

$$\begin{aligned}
w(x) &= we^{\lambda x} \\
\alpha(x) &= ae^{\lambda x} \\
\beta(x) &= be^{\lambda x} \\
\gamma(x) &= me^{\lambda x}
\end{aligned} \tag{5.17}$$

is assumed, where λ is unknown and w , a , b and m are unknown constants. This assumed solution can be substituted into the four remaining Euler equations in Equation 5.11 to yield

$$\begin{bmatrix} (2c_1\lambda^2 - c_9) & c_2\lambda^2 & c_3\lambda^2 & c_9\lambda \\ c_2\lambda^2 & (2c_4\lambda^2 - c_8) & c_5\lambda^2 & c_8\lambda \\ c_3\lambda^2 & c_5\lambda^2 & (2c_6\lambda^2 - c_7) & c_7\lambda \\ c_9\lambda & c_8\lambda & c_7\lambda & -\lambda^2(c_7 + c_8 + c_9) \end{bmatrix} \begin{Bmatrix} ae^{\lambda x} \\ be^{\lambda x} \\ me^{\lambda x} \\ we^{\lambda x} \end{Bmatrix} = \begin{Bmatrix} 0 \\ 0 \\ 0 \\ 0 \end{Bmatrix}. \tag{5.18}$$

For the previous set of equations to have a non-trivial solution, the determinant of the matrix must be zero, or

$$\begin{vmatrix} (2c_1\lambda^2 - c_9) & c_2\lambda^2 & c_3\lambda^2 & c_9\lambda \\ c_2\lambda^2 & (2c_4\lambda^2 - c_8) & c_5\lambda^2 & c_8\lambda \\ c_3\lambda^2 & c_5\lambda^2 & (2c_6\lambda^2 - c_7) & c_7\lambda \\ c_9\lambda & c_8\lambda & c_7\lambda & -\lambda^2(c_7 + c_8 + c_9) \end{vmatrix} = 0. \tag{5.19}$$

The conditions under which the determinant is zero can be found by obtaining the roots of the eighth-order polynomial:

$$\begin{aligned}
& -\lambda^8(c_7 + c_8 + c_9)(8c_1c_4c_6 + 2c_2c_3c_5 - 2c_1c_5^2 - 2c_2^2c_6 - 2c_3^2c_4) \\
& + \lambda^6 \left\{ c_7c_8[4c_1(c_4 + c_5 + c_6) - (c_2 + c_3)^2] + c_8c_9[4c_6(c_1 + c_2 + c_3) - (c_3 + c_5)^2] \right. \\
& \quad \left. + c_7c_9[4c_4(c_1 + c_3 + c_6) - (c_2 + c_5)^2] \right\} \\
& - \lambda^4[2c_7c_8c_9(c_1 + c_2 + c_3 + c_4 + c_5 + c_6)] = 0.
\end{aligned} \tag{5.20}$$

As an interesting aside, the coefficient of λ^8 is actually a multiple of the determinant of another matrix, or

$$8c_1c_4c_6 + 2c_2c_3c_5 - 2c_1c_5^2 - 2c_2^2c_6 - 2c_3^2c_4 = \begin{vmatrix} 2c_1 & c_2 & c_3 \\ c_2 & 2c_4 & c_5 \\ c_3 & c_5 & 2c_6 \end{vmatrix} . \quad (5.21)$$

The analogous term in the three-layer beam model is the coefficient of λ^8 in Equation 3.24:

$$4c_1c_6 - c_3^2 = \begin{vmatrix} 2c_1 & c_3 \\ c_3 & 2c_6 \end{vmatrix} . \quad (5.22)$$

Thus, the coefficients of the highest power of λ for both models are similar in form; both are determinants of a matrix whose entries are the constants c_i , $i = 1-6$, (which are functions of the extensional moduli) multiplied by the sum of the remaining c_i (which are functions of the shear moduli). Also analogous are the coefficients of λ^4 . For both models, that coefficient is minus twice the sum of the constants which contain the extensional moduli (c_1 through c_6) multiplied by the constants which contain the shear moduli (c_7 through c_9), or for the three-layer model, that coefficient is

$$2c_7c_9(c_1 + c_3 + c_6) \quad (5.23)$$

while the same coefficient in the five-layer model is

$$2c_7c_8c_9(c_1 + c_2 + c_3 + c_4 + c_5 + c_6) . \quad (5.24)$$

The c_i of the three-layer model are defined in Equation 3.8 so that these similarities would be obvious under casual inspection. This explains why the constants c_2 , c_4 , c_5 and c_8 are not defined for the three-layer beam model.

Returning to the development of the five-layer beam model, the roots of Equation 5.20 are

$$\begin{aligned}
\lambda_1 &= \lambda_2 = \lambda_3 = \lambda_4 = 0 \\
\lambda_5 &= -\lambda_6 = \sqrt{\frac{-F_6 + \sqrt{F_6^2 - 4F_8F_4}}{2F_8}} \\
\lambda_7 &= -\lambda_8 = \sqrt{\frac{-F_6 - \sqrt{F_6^2 - 4F_8F_4}}{2F_8}}
\end{aligned} \tag{5.25}$$

where the constants F_4 , F_6 and F_8 are the coefficients of λ^4 , λ^6 and λ^8 , respectively, in Equation 5.20, or

$$\begin{aligned}
F_8 &= -(c_7 + c_8 + c_9)(8c_1c_4c_6 + 2c_2c_3c_5 - 2c_1c_5^2 - 2c_2^2c_6 - 2c_3^2c_4) \\
F_6 &= c_7c_8[4c_1(c_4 + c_5 + c_6) - (c_2 + c_3)^2] + c_8c_9[4c_6(c_1 + c_2 + c_3) - (c_3 + c_5)^2] \\
&\quad + c_7c_9[4c_4(c_1 + c_3 + c_6) - (c_2 + c_5)^2] \\
F_4 &= -2c_7c_8c_9(c_1 + c_2 + c_3 + c_4 + c_5 + c_6) .
\end{aligned} \tag{5.26}$$

As was done in the development of the three-layer beam model, the terms which contain $e^{\lambda_i x}$ and $e^{-\lambda_i x}$ can be combined and replaced by $\cosh \lambda_i x$ and $\sinh \lambda_i x$. Thus, the solution which was assumed in Equation 5.17 can be written as

$$\begin{aligned}
w(x) &= w_3x^3 + w_2x^2 + w_1x + w_0 + w_5 \cosh \lambda_5 x + w_6 \sinh \lambda_5 x \\
&\quad + w_7 \cosh \lambda_7 x + w_8 \sinh \lambda_7 x \\
\alpha(x) &= a_3x^3 + a_2x^2 + a_1x + a_0 + a_5 \sinh \lambda_5 x + a_6 \cosh \lambda_5 x \\
&\quad + a_7 \sinh \lambda_7 x + a_8 \cosh \lambda_7 x \\
\beta(x) &= b_3x^3 + b_2x^2 + b_1x + b_0 + b_5 \sinh \lambda_5 x + b_6 \cosh \lambda_5 x \\
&\quad + b_7 \sinh \lambda_7 x + b_8 \cosh \lambda_7 x \\
\gamma(x) &= m_3x^3 + m_2x^2 + m_1x + m_0 + m_5 \sinh \lambda_5 x + m_6 \cosh \lambda_5 x \\
&\quad + m_7 \sinh \lambda_7 x + m_8 \cosh \lambda_7 x .
\end{aligned} \tag{5.27}$$

Because the determinant in Equation 5.19 is zero, relationships exist between the 32 constants in Equation 5.27 that will reduce the number of unknowns to eight.

For the terms which contain nonzero values of λ_i , in other words w_i , a_i , b_i and m_i where $i=5,6,7,8$, these relationships can be expressed as

$$\begin{aligned}
a_5 &= A_5 w_5 & b_5 &= B_5 w_5 & m_5 &= M_5 w_5 \\
a_6 &= A_6 w_6 & b_6 &= B_6 w_6 & m_6 &= M_6 w_6 \\
a_7 &= A_7 w_7 & b_7 &= B_7 w_7 & m_7 &= M_7 w_7 \\
a_8 &= A_8 w_8 & b_8 &= B_8 w_8 & m_8 &= M_8 w_8
\end{aligned} \tag{5.28}$$

The expressions A_i , B_i and M_i where $i=5,6,7,8$ can be found by examining the second, third and fourth Euler equations from Equation 5.11. They are

$$\begin{aligned}
A_5 D_5 &= \lambda_5^4 (-4c_4 c_6 c_9 - c_2 c_5 c_7 - c_3 c_5 c_8 + 2c_3 c_4 c_7 + c_5^2 c_9 + 2c_2 c_6 c_8) \\
&\quad + \lambda_5^2 [2c_4 c_7 c_9 + 2c_6 c_8 c_9 - (c_2 + c_3) c_7 c_8] - c_7 c_8 c_9 \\
A_7 D_7 &= \lambda_7^4 (-4c_4 c_6 c_9 - c_2 c_5 c_7 - c_3 c_5 c_8 + 2c_3 c_4 c_7 + c_5^2 c_9 + 2c_2 c_6 c_8) \\
&\quad + \lambda_7^2 [2c_4 c_7 c_9 + 2c_6 c_8 c_9 - (c_2 + c_3) c_7 c_8] - c_7 c_8 c_9 \\
B_5 D_5 &= \lambda_5^4 (-4c_1 c_6 c_8 - c_3 c_5 c_9 - c_2 c_3 c_7 + 2c_1 c_5 c_7 + c_3^2 c_8 + 2c_2 c_6 c_9) \\
&\quad + \lambda_5^2 [2c_1 c_7 c_8 + 2c_6 c_8 c_9 - (c_2 + c_5) c_7 c_9] - c_7 c_8 c_9 \\
B_7 D_7 &= \lambda_7^4 (-4c_1 c_6 c_8 - c_3 c_5 c_9 - c_2 c_3 c_7 + 2c_1 c_5 c_7 + c_3^2 c_8 + 2c_2 c_6 c_9) \\
&\quad + \lambda_7^2 [2c_1 c_7 c_8 + 2c_6 c_8 c_9 - (c_2 + c_5) c_7 c_9] - c_7 c_8 c_9 \\
M_5 D_5 &= \lambda_5^4 (-4c_1 c_4 c_7 - c_2 c_3 c_8 - c_2 c_5 c_9 + 2c_3 c_4 c_9 + c_2^2 c_7 + 2c_1 c_5 c_8) \\
&\quad + \lambda_5^2 [2c_1 c_7 c_8 + 2c_4 c_7 c_9 - (c_3 + c_5) c_8 c_9] - c_7 c_8 c_9 \\
M_7 D_7 &= \lambda_7^4 (-4c_1 c_4 c_7 - c_2 c_3 c_8 - c_2 c_5 c_9 + 2c_3 c_4 c_9 + c_2^2 c_7 + 2c_1 c_5 c_8) \\
&\quad + \lambda_7^2 [2c_1 c_7 c_8 + 2c_4 c_7 c_9 - (c_3 + c_5) c_8 c_9] - c_7 c_8 c_9 \\
A_6 &= -A_5 \\
A_8 &= -A_7 \\
B_6 &= -B_5 \\
B_8 &= -B_7 \\
M_6 &= -M_5 \\
M_8 &= -M_7
\end{aligned} \tag{5.29}$$

where

$$\begin{aligned}
D_5 &= \lambda_5^6(8c_1c_4c_6 + 2c_2c_3c_5 - 2c_3^2c_4 - 2c_1c_5^2 - 2c_2^2c_6) \\
&\quad + \lambda_5^4[-4(c_4c_6c_9 + c_1c_6c_8 + c_1c_4c_7) + c_3^2c_8 + c_5^2c_9 + c_2^2c_7] \\
&\quad + \lambda_5^2[2(c_1c_7c_8 + c_4c_7c_9 + c_6c_8c_9)] - c_7c_8c_9 \\
D_7 &= \lambda_7^6(8c_1c_4c_6 + 2c_2c_3c_5 - 2c_3^2c_4 - 2c_1c_5^2 - 2c_2^2c_6) \\
&\quad + \lambda_7^4[-4(c_4c_6c_9 + c_1c_6c_8 + c_1c_4c_7) + c_3^2c_8 + c_5^2c_9 + c_2^2c_7] \\
&\quad + \lambda_7^2[2(c_1c_7c_8 + c_4c_7c_9 + c_6c_8c_9)] - c_7c_8c_9
\end{aligned} \tag{5.30}$$

For simplicity, the A_i , B_i and M_i where $i=5,6,7,8$, will be replaced by the following:

$$\begin{aligned}
A_1 &= A_5 = -A_6 & A_2 &= A_7 = -A_8 \\
B_1 &= B_5 = -B_6 & B_2 &= B_7 = -B_8 \\
M_1 &= M_5 = -M_6 & M_2 &= M_7 = -M_8
\end{aligned} \tag{5.31}$$

Next, consider only the portion of the solution that contains the four repeated zero roots,
or

$$\begin{aligned}
w(x) &= w_3x^3 + w_2x^2 + w_1x + w_0 \\
\alpha(x) &= a_3x^3 + a_2x^2 + a_1x + a_0 \\
\beta(x) &= b_3x^3 + b_2x^2 + b_1x + b_0 \\
\gamma(x) &= m_3x^3 + m_2x^2 + m_1x + m_0
\end{aligned} \tag{5.32}$$

When these functions are substituted into the last four Euler equations (Equation 5.11), relationships between the constants can be found. Three more constants which are functions of the material properties are introduced first:

$$\begin{aligned}
R_1 &= 2c_1 + c_2 + c_3 \\
R_2 &= c_2 + 2c_4 + c_5 \\
R_3 &= c_3 + c_5 + 2c_6
\end{aligned} \tag{5.33}$$

The details of finding the relationships between the unknown constants are omitted for brevity. The approach is identical as in the three-layer model; the powers of x are balanced in each of the four equations. For the five-layer beam model,

$$\begin{aligned}
a_3 &= 0 & a_1 &= 2w_2 \\
b_3 &= 0 & b_1 &= 2w_2 \\
m_3 &= 0 & m_1 &= 2w_2 \\
a_2 &= 3w_3 & a_0 &= w_1 + \frac{6R_1}{c_9} w_3 \\
b_2 &= 3w_3 & b_0 &= w_1 + \frac{6R_2}{c_8} w_3 \\
m_2 &= 3w_3 & m_0 &= w_1 + \frac{6R_3}{c_7} w_3
\end{aligned} \tag{5.34}$$

The assumed solution in Equation 5.27 was written as a function of 32 unknowns. That number has now been reduced to eight. The solution is

$$\begin{aligned}
w(x) &= w_3 x^3 + w_2 x^2 + w_1 x + w_0 + w_5 \cosh \lambda_5 x + w_6 \sinh \lambda_5 x + w_7 \cosh \lambda_7 x \\
&\quad + w_8 \sinh \lambda_7 x \\
\alpha(x) &= 3w_3 x^2 + 2w_2 x + \left(w_1 + \frac{6R_1}{c_9} w_3\right) + w_5 A_1 \sinh \lambda_5 x - w_6 A_1 \cosh \lambda_5 x \\
&\quad + w_7 A_2 \sinh \lambda_7 x - w_8 A_2 \cosh \lambda_7 x \\
\beta(x) &= 3w_3 x^2 + 2w_2 x + \left(w_1 + \frac{6R_2}{c_8} w_3\right) + w_5 B_1 \sinh \lambda_5 x - w_6 B_1 \cosh \lambda_5 x \\
&\quad + w_7 B_2 \sinh \lambda_7 x - w_8 B_2 \cosh \lambda_7 x \\
\gamma(x) &= 3w_3 x^2 + 2w_2 x + \left(w_1 + \frac{6R_3}{c_7} w_3\right) + w_5 M_1 \sinh \lambda_5 x - w_6 M_1 \cosh \lambda_5 x \\
&\quad + w_7 M_2 \sinh \lambda_7 x - w_8 M_2 \cosh \lambda_7 x .
\end{aligned} \tag{5.35}$$

The eight boundary conditions of Equation 5.14 which apply to these displacement functions can now be used to completely solve the static elastic problem.

Application of Boundary Conditions

To simplify the solution procedure, the boundary conditions for the beam's response to a mechanical load is considered separately from the response to a thermal gradient.

Mechanical Load

For no thermal gradient through-the-thickness of the beam, the constant b in Equation 5.4 is zero. Therefore, the constants M_{α}^T , M_{β}^T and M_{γ}^T , which are defined in Equation 5.6, are also zero. Thus, the boundary conditions in Equation 5.14 which contain these constants can be written as, at $x = \frac{L}{2}$:

$$\begin{bmatrix} 2c_1 & c_2 & c_3 \\ c_2 & 2c_4 & c_5 \\ c_3 & c_5 & 2c_6 \end{bmatrix} \begin{Bmatrix} \alpha' \\ \beta' \\ \gamma' \end{Bmatrix} = \begin{Bmatrix} 0 \\ 0 \\ 0 \end{Bmatrix} . \quad (5.36)$$

For these equations to have a non-trivial solution, the determinant of the matrix must be identically equal to zero. Substitution of the definitions of the c_i from Equation 5.6 shows that the determinant is not identically zero; therefore the quantities $\frac{d\alpha}{dx}$, $\frac{d\beta}{dx}$ and $\frac{d\gamma}{dx}$ each must be zero at $x = \frac{L}{2}$. The boundary conditions for the mechanical load are rewritten to reflect this fact:

$$\begin{aligned}
&\text{at } x = 0: & \text{at } x = \frac{L}{2}: \\
&\alpha = 0 & \frac{d\alpha}{dx} = 0 \\
&\beta = 0 & \frac{d\beta}{dx} = 0 \\
&\gamma = 0 & \frac{d\gamma}{dx} = 0 \\
&w = 0 & (c_7 + c_8 + c_9) \left(\frac{dw}{dx} \right) - c_7\gamma - c_8\beta - c_9\alpha = \frac{P}{2} .
\end{aligned} \tag{5.37}$$

When these boundary conditions are applied to the solution in Equation 5.35, a system of eight equations and eight unknowns results. These equations can be solved simultaneously to find the unknowns, which are

$$\begin{aligned}
w_3 &= \frac{-P}{12(R_1 + R_2 + R_3)} \\
w_2 &= \frac{PL}{8(R_1 + R_2 + R_3)} \\
w_1 &= \frac{P \left(\frac{R_1 BM}{c_9} + \frac{R_2 MA}{c_8} + \frac{R_3 AB}{c_7} \right)}{2(R_1 + R_2 + R_3)(AB + BM + MA)} \\
&\quad - P \left[\left(\frac{M_2 - A_2}{c_8 c_9} \right) (R_2 c_9 - R_1 c_8) - \left(\frac{B_2 - A_2}{c_7 c_9} \right) (R_3 c_9 - R_1 c_7) \right] \\
w_5 &= \frac{2(R_1 + R_2 + R_3)(AB + BM + MA)}{2(R_1 + R_2 + R_3)(AB + BM + MA)} \\
w_6 &= -w_5 \\
&\quad - P \left[\left(\frac{B_1 - A_1}{c_7 c_9} \right) (R_3 c_9 - R_1 c_7) - \left(\frac{M_1 - A_1}{c_8 c_9} \right) (R_2 c_9 - R_1 c_8) \right] \\
w_7 &= \frac{2(R_1 + R_2 + R_3)(AB + BM + MA)}{2(R_1 + R_2 + R_3)(AB + BM + MA)} \\
w_8 &= -w_7 \\
w_0 &= w_6 + w_8 ,
\end{aligned} \tag{5.38}$$

where

$$\begin{aligned}
AB &= A_1 B_2 - B_1 A_2 \\
BM &= B_1 M_2 - M_1 B_2 \\
MA &= M_1 A_2 - A_1 M_2 .
\end{aligned} \tag{5.39}$$

The expression for w_1 is much more complicated than in the three-layer sandwich beam model. Now, the three-layer solution is used to simplify the five-layer sandwich beam model. The expression for w_1 in the three-layer beam model is shown in Equation 3.53 and is repeated here for convenience:

$$w_1^{(3)} = \frac{P}{2(R_1 + R_2)^2} \left(\frac{R_1^2}{c_9} + \frac{R_2^2}{c_7} \right). \quad (5.40)$$

Assume a similar form for the five-layer model:

$$w_1^{(5)} = \frac{P}{2(R_1 + R_2 + R_3)^2} \left(\frac{R_1^2}{c_9} + \frac{R_2^2}{c_8} + \frac{R_3^2}{c_7} \right). \quad (5.41)$$

Although the algebra to prove that the previous expression is identical to w_1 in Equation 5.38 is prohibitively difficult, it has been proven computationally in Appendix C. Thus, the solution of the three-layer model is used to simplify the five-layer beam model when standard algebra techniques fail. The form of w_1 in Equation 5.41 is used hereafter.

Also presented in Appendix C is the proof that w_6 and w_8 are small compared to the tip deflection. Because of their relatively small size, they are approximately zero, or

$$\begin{aligned} w_5 &\simeq 0 \\ w_6 &\simeq 0 \\ w_7 &\simeq 0 \\ w_8 &\simeq 0 \\ w_0 &\simeq 0 \end{aligned} \quad (5.42)$$

A comparison of the five-layer sandwich beam model solution to a strength of materials solution for a five-layer tip-loaded cantilever sandwich beam again shows that the strength of materials solution is exactly

$$w_{\text{som}}(x) = w_3 x^3 + w_2 x^2. \quad (5.43)$$

Thus, the five-layer sandwich beam model is the sum of the strength of materials solution and additional terms which account for the shear deformation, just like the three-layer model.

Thermal Gradient

For a beam with no mechanical load, i.e. $P = 0$, the boundary conditions are

$$\begin{array}{ll}
 \text{at } x = 0: & \text{at } x = \frac{L}{2}: \\
 u = 0 & 2c_0\left(\frac{du}{dx}\right) + N_u^T = 0 \\
 \alpha = 0 & 2c_1\left(\frac{d\alpha}{dx}\right) + c_2\left(\frac{d\beta}{dx}\right) + c_3\left(\frac{d\gamma}{dx}\right) + M_x^T = 0 \\
 \beta = 0 & c_2\left(\frac{d\alpha}{dx}\right) + 2c_4\left(\frac{d\beta}{dx}\right) + c_5\left(\frac{d\gamma}{dx}\right) + M_\beta^T = 0 \\
 \gamma = 0 & c_3\left(\frac{d\alpha}{dx}\right) + c_5\left(\frac{d\beta}{dx}\right) + 2c_6\left(\frac{d\gamma}{dx}\right) + M_\gamma^T = 0 \\
 w = 0 & (c_7 + c_8 + c_9)\left(\frac{dw}{dx}\right) - c_7\gamma - c_8\beta - c_9\alpha = 0
 \end{array} \tag{5.44}$$

When the boundary conditions are applied to the solution in Equation 5.35, a system of eight equations and eight unknowns again is the result. Solved simultaneously, they yield

$$\begin{aligned}
w_3 &= w_1 = w_6 = w_8 = 0 \\
w_5 &\propto \frac{1}{\cosh \frac{\lambda_5 L}{2}} \simeq 0 \\
w_7 &\propto \frac{1}{\cosh \frac{\lambda_7 L}{2}} \simeq 0 \\
w_0 &= -w_5 - w_7 \simeq 0
\end{aligned} \tag{5.45}$$

$$\begin{aligned}
w_2 &= \frac{M_x^T [AB(c_2 c_5 - 2c_3 c_4) + BM(4c_4 c_6 - c_5^2) + MA(c_3 c_5 - 2c_2 c_6)]}{2(8c_1 c_4 c_6 + 2c_2 c_3 c_5 - 2c_1 c_5^2 - 2c_3^2 c_4 - 2c_2^2 c_6)(AB + BM + MA)} \\
&+ \frac{M_\beta^T [AB(c_2 c_3 - 2c_1 c_5) + BM(c_3 c_5 - 2c_2 c_6) + MA(4c_1 c_6 - c_3^2)]}{2(8c_1 c_4 c_6 + 2c_2 c_3 c_5 - 2c_1 c_5^2 - 2c_3^2 c_4 - 2c_2^2 c_6)(AB + BM + MA)} \\
&+ \frac{M_y^T [AB(4c_1 c_4 - c_2^2) + BM(c_2 c_5 - 2c_3 c_4) + MA(c_2 c_3 - 2c_1 c_5)]}{2(8c_1 c_4 c_6 + 2c_2 c_3 c_5 - 2c_1 c_5^2 - 2c_3^2 c_4 - 2c_2^2 c_6)(AB + BM + MA)}
\end{aligned}$$

The solution is similar to that of the three-layer beam subjected to a thermal gradient, the solution for which can be extracted from Equation 3.53. The actual expressions for w_5 and w_7 are incredibly complicated and, because they are inversely proportional to hyperbolic cosines of very large numbers, they are approximately zero anyway.

As was done in the solution for mechanical loads, the solution for the temperature-gradient problem can be simplified by using the three-layer model to make intuitive steps in the algebra that are substantiated by numerical computations. For the three-layer model, the coefficient w_2 resulting from the thermal gradient alone is (see Equation 3.53)

$$w_2^{(3)} = \frac{-(M_\phi^T + M_\psi^T)}{2(R_1 + R_2)} \tag{5.46}$$

The w_2 term in the five-layer model is assumed to have the same form, namely

$$w_2^{(5)} = \frac{-(M_\alpha^T + M_\beta^T + M_\gamma^T)}{2(R_1 + R_2 + R_3)} \tag{5.47}$$

Although the algebra necessary to move from the expression for w_2 in Equation 5.45 to w_2 in Equation 5.47 is prohibitively difficult, these expressions have been proven computationally to be equivalent in Appendix C. Thus, the three-layer model is used again to simplify the five-layer model.

Combined Mechanical Load and Thermal Gradient

The solution for the response of a tip-loaded cantilever beam with a through-the-thickness gradient is simply the sum of the two solutions, or, for the solution in Equation 5.35, the constants are

$$\begin{aligned}
 w_3 &= \frac{-P}{12(R_1 + R_2 + R_3)} \\
 w_2 &= \frac{PL}{8(R_1 + R_2 + R_3)} - \frac{(M_\alpha^T + M_\beta^T + M_\gamma^T)}{2(R_1 + R_2 + R_3)} \\
 w_1 &= \frac{P}{2(R_1 + R_2 + R_3)^2} \left(\frac{R_1^2}{c_9} + \frac{R_2^2}{c_8} + \frac{R_3^2}{c_7} \right) \\
 w_5 &\simeq 0 \\
 w_6 &\simeq 0 \\
 w_7 &\simeq 0 \\
 w_8 &\simeq 0 \\
 w_0 &\simeq 0
 \end{aligned} \tag{5.48}$$

Summary

The development of the five-layer beam model, a model considerably more complex than the three-layer beam model, is now complete. The three-layer beam model provided considerable guidance in the development of the five-layer model. It provided the motivation for

some of the simplifying approximations of the algebra and made it possible to see explicitly where the inclusion of the adhesive layer effected the model. The next chapter is devoted to numerical results obtained using the five-layer beam model.

Chapter 6 - The Five-Layer Sandwich Beam Model:

Numerical Results

Because the sensitivity studies using the static elastic solution did provide insight into the importance of the material properties for the three-layer model, the sensitivity calculations will be repeated for the five-layer model. Thus, the static elastic response of the five-layer beam is studied before the viscoelastic response is studied. Because the adhesive is a separate constituent in the five-layer model, its material properties must now be considered.

Materials and Material Properties

As with the three-layer beam model, the five-layer beam model is studied for two different material systems. The composite material system of the three-layer model is one of these. For the five-layer model, the thickness of the honeycomb (HRH 327) is now the value $2h$ and the thickness of the adhesive layers, t_2 , is a separate quantity. The elastic moduli of the honeycomb are the same as in the three-layer model. The adhesive under consideration is

FM73, a film adhesive produced by American Cyanamide. The extensional modulus E_2 is a typical value for adhesives, and G_2 was found by assuming that the adhesive is isotropic and has a Poisson's ratio of 0.3. The nominal thickness of FM73 is 0.005". The face sheets are the quasi-isotropic quartz-epoxy material used for the three-layer model composite beam. Also, the aluminum beam studied in Chapter 4 is considered. This aluminum beam is now assumed to have FM73 adhesive joining the aluminum face sheets of the three-layer model to the aluminum honeycomb core of the three-layer model. The material properties for both systems are presented in Table 7.

Sensitivity Studies

The sensitivities of the static elastic five-layer beam model to reductions in material properties and layer thicknesses are found separately for the mechanical load and the thermal gradient, as they were in the three-layer model. To study the sensitivity, a particular material property or layer thickness is reduced by an order of magnitude and the tip deflection is found using this reduced value. This tip deflection is normalized with respect to the tip deflection that is found when the nominal material properties are used, or

$$\text{Sensitivity} = \frac{w_{\text{tip}}}{w_{\text{tip}}^{\text{nominal}}} \quad (6.1)$$

This is identical to the approach used in Chapter 4 to study the elastic sensitivity of the three-layer model to the various material properties and thicknesses.

Table 7. Nominal Material Properties and Geometries for Five-Layer Beam Model

Aluminum Beam		
Face Sheets	Adhesive	Honeycomb Core
$E_1 = 10.0\text{E}6 \text{ psi}$ $G_1 = 3.85\text{E}6 \text{ psi}$ $t_1 = 0.040 \text{ in}$ $\alpha_1 = 13\text{E}-6 \frac{1}{^\circ\text{F}}$	$E_2 = 0.5\text{E}6 \text{ psi}$ $G_2 = 0.179\text{E}6 \text{ psi}$ $t_2 = 0.005 \text{ in}$ $\alpha_2 = 25\text{E}-6 \frac{1}{^\circ\text{F}}$	$E_3 = 1.0\text{E}3 \text{ psi}$ $G_3 = 68\text{E}3 \text{ psi}$ $h = 0.250 \text{ in}$ $\alpha_3 = 13\text{E}-6 \frac{1}{^\circ\text{F}}$
Composite Beam		
Face Sheets	Adhesive	Honeycomb Core
$E_1 = 2.5\text{E}6 \text{ psi}$ $G_1 = 0.96\text{E}6 \text{ psi}$ $t_1 = 0.040 \text{ in}$ $\alpha_1 = 5\text{E}-6 \frac{1}{^\circ\text{F}}$	$E_2 = 0.5\text{E}6 \text{ psi}$ $G_2 = 0.179\text{E}6 \text{ psi}$ $t_2 = 0.005 \text{ in}$ $\alpha_2 = 25\text{E}-6 \frac{1}{^\circ\text{F}}$	$E_3 = 1.0\text{E}3 \text{ psi}$ $G_3 = 29\text{E}3 \text{ psi}$ $h = 0.250 \text{ in}$ $\alpha_3 = 1.5\text{E}-6 \frac{1}{^\circ\text{F}}$

Mechanical Load

The bending response of the five-layer beam model to a mechanical load is shown in Equations 5.35, 5.38, 5.41 and 5.42. To find the tip deflection, $x = \frac{L}{2}$ is used:

$$w_{\text{tip}} = \frac{PL^3}{48(R_1 + R_2 + R_3)^2} + \frac{PL}{4(R_1 + R_2 + R_3)^2} \left(\frac{R_1^2}{c_9} + \frac{R_2^2}{c_8} + \frac{R_3^2}{c_7} \right) \quad (6.2)$$

The numerical results of the sensitivity studies for the mechanical load are reported in Table 8 and Table 9 for the aluminum beam and composite beam respectively. For both ta-

bles, the left column indicates which material property or thickness is reduced by a factor of ten. The right column is the value of Equation 6.1 for that case.

Inspection of these tables reveals little information that was not already determined from the sensitivity studies of the three-layer model. The sensitivities of the two material systems are similar. The beam response is most sensitive to a reduction of the thickness h . Reductions of the modulus of elasticity and thickness of the face sheet cause the next greatest increase in tip deflection. Also, the five-layer model is sensitive to a reduction of the shear modulus of the core, G_3 . Like the three-layer model, the five-layer model is insensitive to reductions of the shear modulus of the face sheets, G_1 , and the modulus of elasticity of the core, E_3 .

The major difference between the three- and five-layer models is the inclusion of separate adhesive layers in the five-layer model. However, it is apparent from Table 8 and Table 9 that the five-layer beam model is relatively insensitive to reductions of the elastic properties or thickness of the adhesive.

Thermal Gradient

The tip deflection for a five-layer beam subjected to a through-the-thickness thermal gradient with no mechanical loads is

$$w_{\text{tip}} = \frac{-L^2(M_x^T + M_y^T + M_z^T)}{8(R_1 + R_2 + R_3)} \quad (6.3)$$

Like the tip deflection of the three-layer beam subjected to a thermal gradient (Equation 4.12), this expression does not include any of the shear moduli; therefore, the tip deflection should be completely insensitive to reductions of the shear moduli.

The numerical results of these sensitivity studies are shown in Table 10 and Table 11 for the aluminum and composite beams, respectively. Again, the left column of these tables in-

Table 8. Sensitivity of Five-Layer Aluminum Beam - Mechanical Load

Reduced Variable	Sensitivity
NONE	1.000
E ₁	7.694
G ₁	1.002
t ₁	8.759
E ₂	1.004
G ₂	1.014
t ₂	1.036
E ₃	1.000
G ₃	2.869
h	23.260
ALL	7859.10

indicates which material property or thickness value was reduced by a factor of ten, and the right column is the value of Equation 6.1 for the case under consideration.

As was discovered for the mechanical load sensitivity study, the sensitivities of the five-layer beam differ little from those of the three-layer beam. Both material systems have similar sensitivities. The five-layer model, like the three-layer model, is relatively insensitive to reductions of nearly all the elastic properties and layer thickness values of the face sheets and core. The five-layer beam model is relatively insensitive to reductions of the elastic properties and thickness of the adhesive layers as well. One exception is the sensitivity to the coefficient of thermal expansion of the face sheets, α_1 ; however, the three-layer beam model was sensitive to α_1 too.

There is one unusual sensitivity that can only be found using the five-layer beam model. The five-layer composite beam subjected to a thermal gradient is more sensitive to reductions

Table 9. Sensitivity of Five-Layer Composite Beam - Mechanical Load

Reduced Variable	Sensitivity
NONE	1.000
E_1	7.353
G_1	1.002
t_1	8.219
E_2	1.016
G_2	1.004
t_2	1.049
E_3	1.001
G_3	2.235
h	25.460
ALL	8600.03

in the modulus of elasticity of the face sheets than the three-layer beam model (see Table 5 on page 55). Reducing E_1 by a factor of ten increases the thermally-induced deflection of the beam by 56% for the five-layer beam; however, it barely influences the deflection of the three-layer beam. The difference must be a result of the presence of the adhesive layer, but it also is only an issue for the composite beam. For both the aluminum and composite five-layer beams, the coefficient of thermal expansion of the face sheets, α_1 , has a strong influence on the thermally induced deflection. When the modulus of elasticity of the aluminum face sheets is reduced, it is still numerically larger than the modulus of elasticity of the adhesive. Therefore, control of the thermally-induced deflection still lies with the face sheets for the aluminum beam. However, when the modulus of elasticity of the composite face sheets is reduced, it is nearly one-half the modulus of elasticity of the adhesive layer. Thus, control of the thermally-influenced deflection of the five-layer composite beam with reduced E_1 lies with

the stiffer adhesive layer. Because the adhesive layer has a higher coefficient of thermal expansion than the composite face sheet, the thermally-influenced deflection is greater.

The Time-Dependent Five-Layer Beam Model

The sensitivity studies are a useful tool for determining which material properties influence the elastic response of the beam. They are not a substitute for a viscoelastic solution; rather, the elastic sensitivity studies complement the viscoelastic model. First, material properties which have a significant effect on the elastic tip deflection are determined from the sensitivity studies. Then, the viscoelastic tip deflection can be found by assuming these material properties are time-dependent. As was done in the three-layer viscoelastic model, Maxwell fluids are used to represent the behavior of the materials. Also, the cases of more and less time-dependent behavior are considered. The former case allows the shear strain in the material to increase by a factor of ten in 20 years, as it did previously, and the latter case allows it to double in 20 years. For the extensional material behavior, the higher level of time-dependent behavior allows a ten percent increase in normal strain in 20 years, and the lower level allows one percent. The material properties of the composite beam are used in the following studies. To measure the magnitude of the effect that time-dependent material behavior has on the beam response, the percent increase in tip deflection is again computed as

$$\text{Percent Increase in Tip Deflection} = \frac{w_{\text{tip}}(t) - w_{\text{tip}}}{w_{\text{tip}}} \times 100\% \quad (6.4)$$

Table 10. Sensitivity of Five-Layer Aluminum Beam - Thermal Gradient

Reduced Variable	Sensitivity
NONE	1.0000
E_1	1.0410
G_1	1.0000
t_1	1.0474
α_1	0.1092
E_2	0.9957
G_2	1.0000
t_2	0.9957
α_2	1.0000
E_3	1.0000
G_3	1.0000
h	0.9968
α_3	0.9998
ALL	0.1000

Mechanical Load

The five-layer model sensitivity studies reveal that, for the mechanically loaded case, the response of the beam is most sensitive to reductions in the extensional modulus of the face sheets, E_1 , and the shear modulus of the core, G_3 . The deflection is less sensitive to the reductions of the shear modulus of the face sheet, G_1 . This is identical to the information obtained from the sensitivity studies of the three-layer model.

Table 11. Sensitivity of Five-Layer Composite Beam - Thermal Gradient

Reduced Variable	Sensitivity
NONE	1.0000
E_1	1.5597
G_1	1.0000
t_1	1.6344
α_1	0.1858
E_2	0.9316
G_2	1.0000
t_2	0.9317
α_2	0.9143
E_3	1.0004
G_3	1.0000
h	0.9507
α_3	0.9998
ALL	0.1000

One goal of this work is to maintain simplicity and closed-form solutions. In the three-layer model, an approximation of the tip deflection based on the relative values of the extensional moduli of the core and face sheets (E_2 and E_1 respectively) is used to simplify the time-dependent model when E_1 is time dependent. Without this simplification, it has been shown that the time-dependent solution can be found but is not in a practical form. This simplification is not possible in the five-layer model. Therefore, because both the three-layer and five-layer models have similar sensitivities to elastic reductions of the modulus of elasticity of the face sheets, and because the five-layer time-dependent model for $E_1(t)$ is prohibitively complicated, a time-dependent E_1 is not considered here. Two material proper-

ties to which the five-layer model is not sensitive elastically are allowed to be time-dependent for this discussion. The shear modulus of the adhesive layers, G_2 , does not appear separately in the three-layer model; therefore, the effect of any possible time-dependence of G_2 has not previously been discussed. Also, the shear modulus of the face sheets, G_1 , is allowed to vary with time in order to compare the three-layer and five-layer viscoelastic models.

To study the influence of the shear moduli on the problem, the elastic tip deflection of the five-layer beam can be written to reveal the dependence on the three shear moduli using Equations 5.6 and 6.2:

$$w_{\text{tip}} = \frac{PL^3}{48(R_1 + R_2 + R_3)} + \frac{PL}{4(R_1 + R_2 + R_3)^2} \left(\frac{R_1^2}{2G_3h} + \frac{R_2^2}{2G_2t_2} + \frac{R_3^2}{2G_1t_1} \right) . \quad (6.5)$$

For the time-dependent tip deflection, the load P is a step function whose magnitude is P_0 .

Influence of Time-Dependent Core Shear Modulus (G_3) on Beam Response

In Chapter 4, the constitutive equation which governs the behavior of a Maxwell fluid model appeared in Equation 4.14 and is repeated here for convenience:

$$\tau + p_1 \dot{\tau} = q_1 \dot{\gamma} . \quad (6.6)$$

The strain as a function of time can be found for the case where the stress is a step function of magnitude $\hat{\tau}$:

$$\gamma(t) = \hat{\tau} \left(\frac{p_1}{q_1} + \frac{t}{q_1} \right) . \quad (6.7)$$

For time zero, the elastic case, it is apparent from

$$\gamma(0) = \hat{\tau} \left(\frac{p_1}{q_1} \right) = \hat{\tau} \left(\frac{1}{G_3} \right) , \quad (6.8)$$

that the elastic shear modulus of the core is $\frac{q_1}{p_1}$, or

$$G_3 = \frac{q_1}{p_1} \quad (6.9)$$

For the case where the shear strain of the core doubles in 20 years,

$$\gamma(20) = \hat{\tau} \left(\frac{1}{G_3} + \frac{20}{q_1} \right) = 2\gamma(0) = 2\hat{\tau} \frac{1}{G_3} \quad (6.10)$$

and the constants p_1 and q_1 are

$$p_1 = 20 \quad \text{and} \quad q_1 = 20G_3 \quad (6.11)$$

For the case of greater time-dependent behavior, the strain increases by a factor of ten in 20 years, or

$$\gamma(20) = \hat{\tau} \left(\frac{1}{G_3} + \frac{20}{q'_1} \right) = 10\gamma(0) = 10\hat{\tau} \frac{1}{G_3} \quad (6.12)$$

which leads to

$$p'_1 = \frac{20}{9} \quad \text{and} \quad q'_1 = \frac{20}{9} G_3 \quad (6.13)$$

To find the time-dependent tip deflection, the Laplace transform of the elastic tip deflection, Equation 6.5, is performed and G_3 is replaced by $\frac{Q(s)}{P(s)}$:

$$\begin{aligned} \bar{w}_{\text{tip}}(s) = & \frac{P_o}{s} \left[\frac{L^3}{48(R_1 + R_2 + R_3)} \right] \\ & + \frac{P_o}{s} \left[\frac{L}{4(R_1 + R_2 + R_3)^2} \right] \left(\frac{R_1^2}{2h \frac{Q(s)}{P(s)}} + \frac{R_2^2}{2G_2 t_2} + \frac{R_3^2}{2G_1 t_1} \right) \end{aligned} \quad (6.14)$$

For a Maxwell fluid, the ratio $\frac{Q(s)}{P(s)}$ is

$$\frac{Q(s)}{P(s)} = \frac{q_1 s}{1 + p_1 s} \quad (6.15)$$

Therefore, the tip deflection in Laplace domain is

$$\begin{aligned} \bar{w}_{tip}(s) = & \frac{P_o}{s} \left[\frac{L^3}{48(R_1 + R_2 + R_3)} \right] \\ & + \frac{P_o}{s} \left[\frac{L}{4(R_1 + R_2 + R_3)^2} \right] \left[\frac{R_1^2}{2h} \left(\frac{1 + p_1 s}{q_1 s} \right) + \frac{R_2^2}{2G_2 t_2} + \frac{R_3^2}{2G_1 t_1} \right] \end{aligned} \quad (6.16)$$

The inverse Laplace transform converts this to the time-dependent tip deflection, which is

$$w_{tip}(t) = w_{tip} + \frac{P_o L}{4(R_1 + R_2 + R_3)^2} \left(\frac{R_1^2}{2h} \right) \left(\frac{t}{q_1} \right) \quad (6.17)$$

Thus, for the model which allows for less time-dependent behavior, the tip deflection in 20 years is found using Equations 6.11 and 6.17. It is

$$w_{tip}(t) = w_{tip} + \frac{P_o L}{4(R_1 + R_2 + R_3)^2} \left(\frac{R_1^2}{2G_3 h} \right) \quad (6.18)$$

For the greater strain case, q'_1 is found in Equation 6.13. The tip deflection in 20 years is

$$w_{tip}(t) = w_{tip} + \frac{9P_o L}{4(R_1 + R_2 + R_3)^2} \left(\frac{R_1^2}{2G_3 h} \right) \quad (6.19)$$

These results are shown as a function of time in Figure 13 and can be directly compared to Figure 9. The three-layer and five-layer models have almost identical increases in tip deflection for time-dependent shear behavior of the core. Likewise, from Table 3 on page 51 and Table 9, the elastic sensitivities for both models are also nearly identical for reductions of the shear modulus of the core.

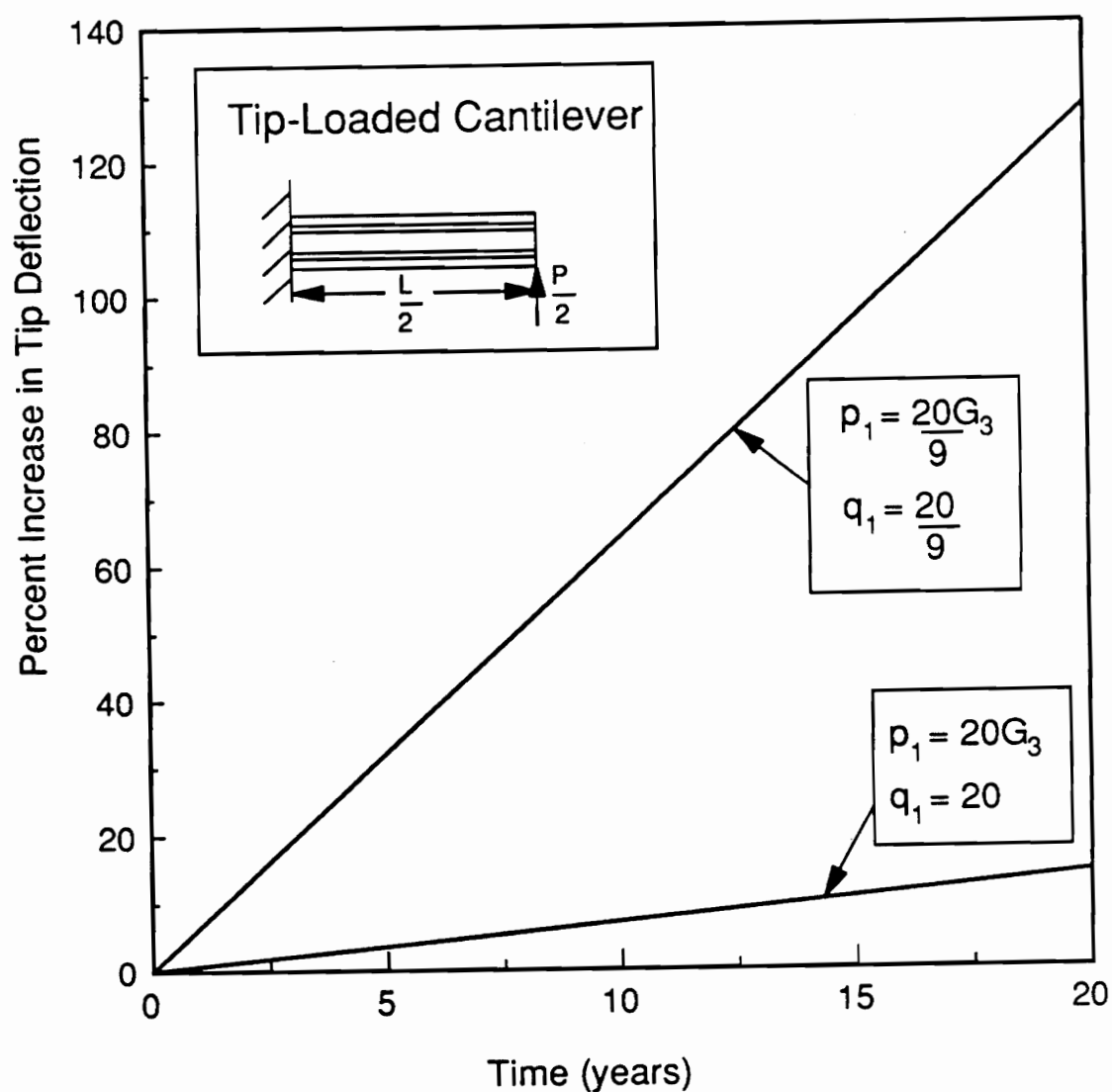


Figure 13. Percent Increase In Tip Deflection of Five-Layer Beam Model for $G_3(t)$

Influence of Time-Dependent Adhesive Shear Modulus (G_2) on Beam Response

Like the shear modulus of the core, the time-dependent behavior of the adhesive shear modulus G_2 is modelled by a Maxwell fluid and is bracketed by the cases where the strain

increases by a factor of two and a factor of ten in 20 years. In the previous work, the relationship between the shear modulus and p_1 and q_1 was found. That relationship is the same for this case and is, like Equation 6.9,

$$G_2 = \frac{q_1}{p_1} \quad (6.20)$$

Also, for the case where the strain doubles in 20 years, p_1 and q_1 are

$$q_1 = 20G_2 \quad \text{and} \quad p_1 = 20 \quad (6.21)$$

For the other case, that of the strain increasing ten-fold in 20 years,

$$q'_1 = \frac{20}{9} G_2 \quad \text{and} \quad p'_1 = \frac{20}{9} \quad (6.22)$$

As before, $\frac{Q(s)}{P(s)}$ replaces the shear modulus in the Laplace-transformed form of Equation 6.5:

$$\begin{aligned} \bar{w}_{tip}(s) = & \frac{P_o}{s} \left[\frac{L^3}{48(R_1 + R_2 + R_3)} \right] \\ & + \frac{P_o}{s} \left[\frac{L}{4(R_1 + R_2 + R_3)^2} \right] \left(\frac{R_1^2}{2G_3h} + \frac{R_2^2}{2t_2 \frac{Q(s)}{P(s)}} + \frac{R_3^2}{2G_1t_1} \right) \end{aligned} \quad (6.23)$$

In particular, the tip deflection in Laplace domain when G_2 is modelled as a Maxwell fluid is

$$\begin{aligned} \bar{w}_{tip}(s) = & \frac{P_o}{s} \left[\frac{L^3}{48(R_1 + R_2 + R_3)} \right] \\ & + \frac{P_o}{s} \left[\frac{L}{4(R_1 + R_2 + R_3)^2} \right] \left[\frac{R_1^2}{2G_3h} + \frac{R_2^2}{2t_2} \left(\frac{1 + p_1s}{q_1s} \right) + \frac{R_3^2}{2G_1t_1} \right] \end{aligned} \quad (6.24)$$

and the tip deflection as a function of time is

$$w_{tip}(t) = w_{tip} + \frac{P_o L}{4(R_1 + R_2 + R_3)^2} \left(\frac{R_2^2}{2t_2} \right) \left(\frac{t}{q_1} \right) \quad (6.25)$$

Thus, for the model whose strain doubles in 20 years, the tip deflection in 20 years is

$$w_{\text{tip}}(t) = w_{\text{tip}} + \frac{P_o L}{4(R_1 + R_2 + R_3)^2} \left(\frac{R_2^2}{2G_2 t_2} \right) \quad (6.26)$$

For the other case, the tip deflection in 20 years is

$$w_{\text{tip}}(t) = w_{\text{tip}} + \frac{9P_o L}{4(R_1 + R_2 + R_3)^2} \left(\frac{R_2^2}{2G_2 t_2} \right) \quad (6.27)$$

The tip deflection as a function of time is shown in Figure 14. The elastic sensitivity studies indicate that a reduction of G_2 has little effect on the tip deflection; the response of the beam changes only slightly for time-dependent shear behavior of the adhesive layers for both levels of time-dependence. The significance of the elastic sensitivity studies is again reaffirmed.

Influence of Time-Dependent Face Sheet Shear Modulus (G_1) on Beam Response

Again, two Maxwell fluid models are used to represent the time-dependent shear behavior of the face sheets. The relationship between p_1 and q_1 and the shear modulus is the same as in Equations 6.9 and 6.20:

$$G_1 = \frac{q_1}{p_1} \quad (6.28)$$

As before, the behavior is bracketed by a two-fold and ten-fold increase in strain in 20 years. For the first case, a two-fold increase,

$$q_1 = 20G_1 \text{ and } p_1 = 20 \quad (6.29)$$

For the ten-fold increase in strain,

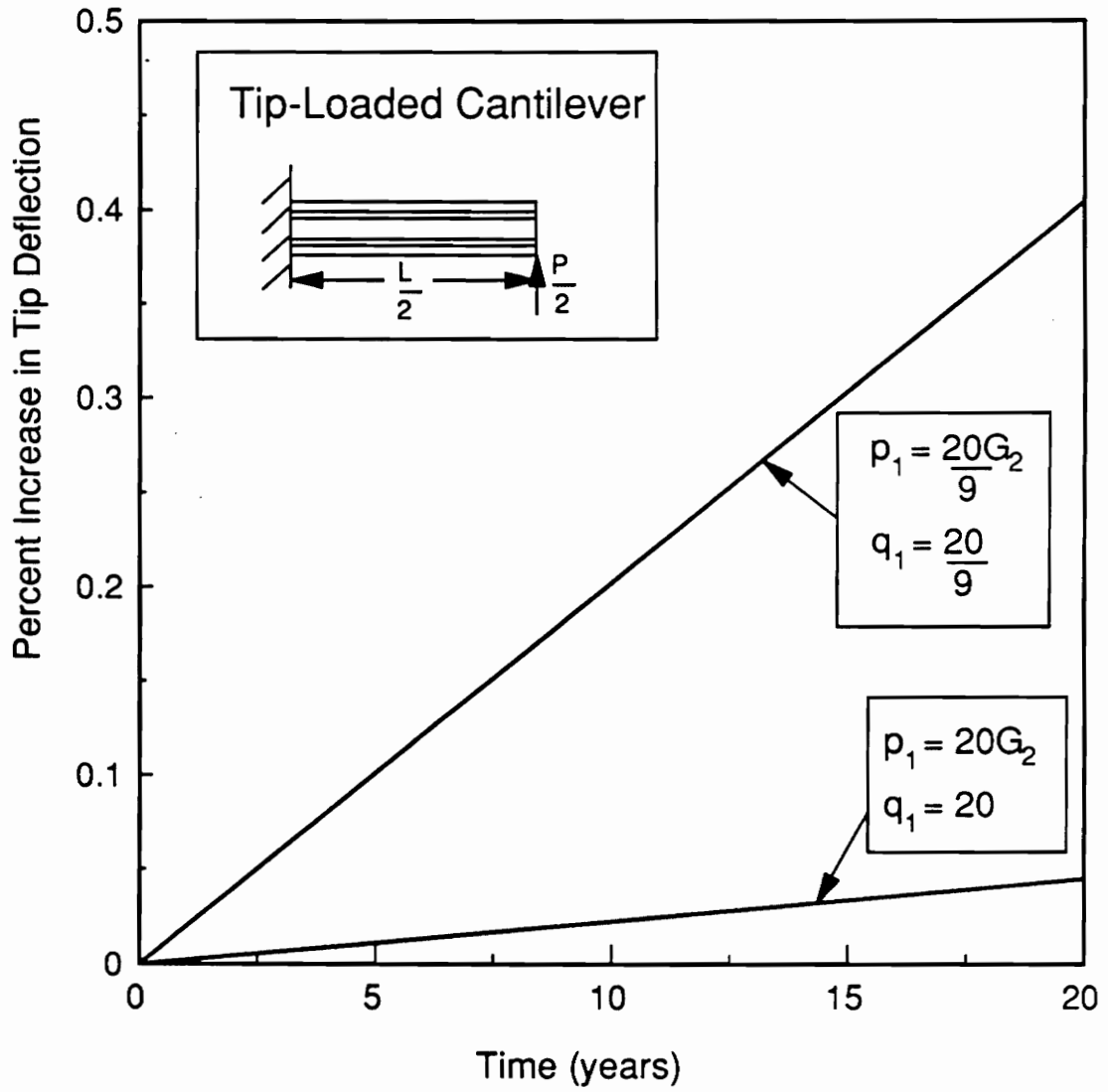


Figure 14. Percent Increase in Tip Deflection of Five-Layer Beam Model for $G_2(t)$

$$q'_1 = \frac{20}{9} G_1 \text{ and } p'_1 = \frac{20}{9} \quad (6.30)$$

To apply the correspondence principle to the tip deflection, G_1 is replaced by $\frac{Q(s)}{P(s)}$ in the transformed form of Equation 6.5:

$$\begin{aligned}\bar{w}_{tip}(s) = & \frac{P_o}{s} \left[\frac{L^3}{48(R_1 + R_2 + R_3)} \right] \\ & + \frac{P_o}{s} \left[\frac{L}{4(R_1 + R_2 + R_3)^2} \right] \left(\frac{R_1^2}{2G_3h} + \frac{R_2^2}{2G_2t_2} + \frac{R_3^2}{2 \frac{Q(s)}{P(s)} t_1} \right) .\end{aligned}\quad (6.31)$$

For the Maxwell fluid model, this is

$$\begin{aligned}\bar{w}_{tip}(s) = & \frac{P_o}{s} \left[\frac{L^3}{48(R_1 + R_2 + R_3)} \right] \\ & + \frac{P_o}{s} \left[\frac{L}{4(R_1 + R_2 + R_3)^2} \right] \left[\frac{R_1^2}{2G_3h} + \frac{R_2^2}{2G_2t_2} + \frac{R_3^2}{2t_1} \left(\frac{1 + p_1s}{q_1s} \right) \right] .\end{aligned}\quad (6.32)$$

Therefore, the time-dependent tip deflection is the inverse Laplace transform of Equation 6.32:

$$w_{tip}(t) = w_{tip} + \frac{P_o L}{4(R_1 + R_2 + R_3)^2} \left(\frac{R_3^2}{2t_1} \right) \left(\frac{t}{q_1} \right) .\quad (6.33)$$

For the Maxwell fluid model which allows less time-dependent behavior, the tip deflection in 20 years is

$$w_{tip}(t) = w_{tip} + \frac{P_o L}{4(R_1 + R_2 + R_3)^2} \left(\frac{R_3^2}{2G_1 t_1} \right) ,\quad (6.34)$$

and for the Maxwell fluid model which allows for more time-dependent behavior, it is

$$w_{tip}(t) = w_{tip} + \frac{9P_o L}{4(R_1 + R_2 + R_3)^2} \left(\frac{R_3^2}{2G_1 t_1} \right) .\quad (6.35)$$

Again, the tip deflection is linearly dependent on time and is shown as a function of time in Figure 15. As the elastic sensitivities imply, a time-dependent reduction of G_1 has even less effect on the tip deflection, than a time-dependent G_2 , Figure 14.

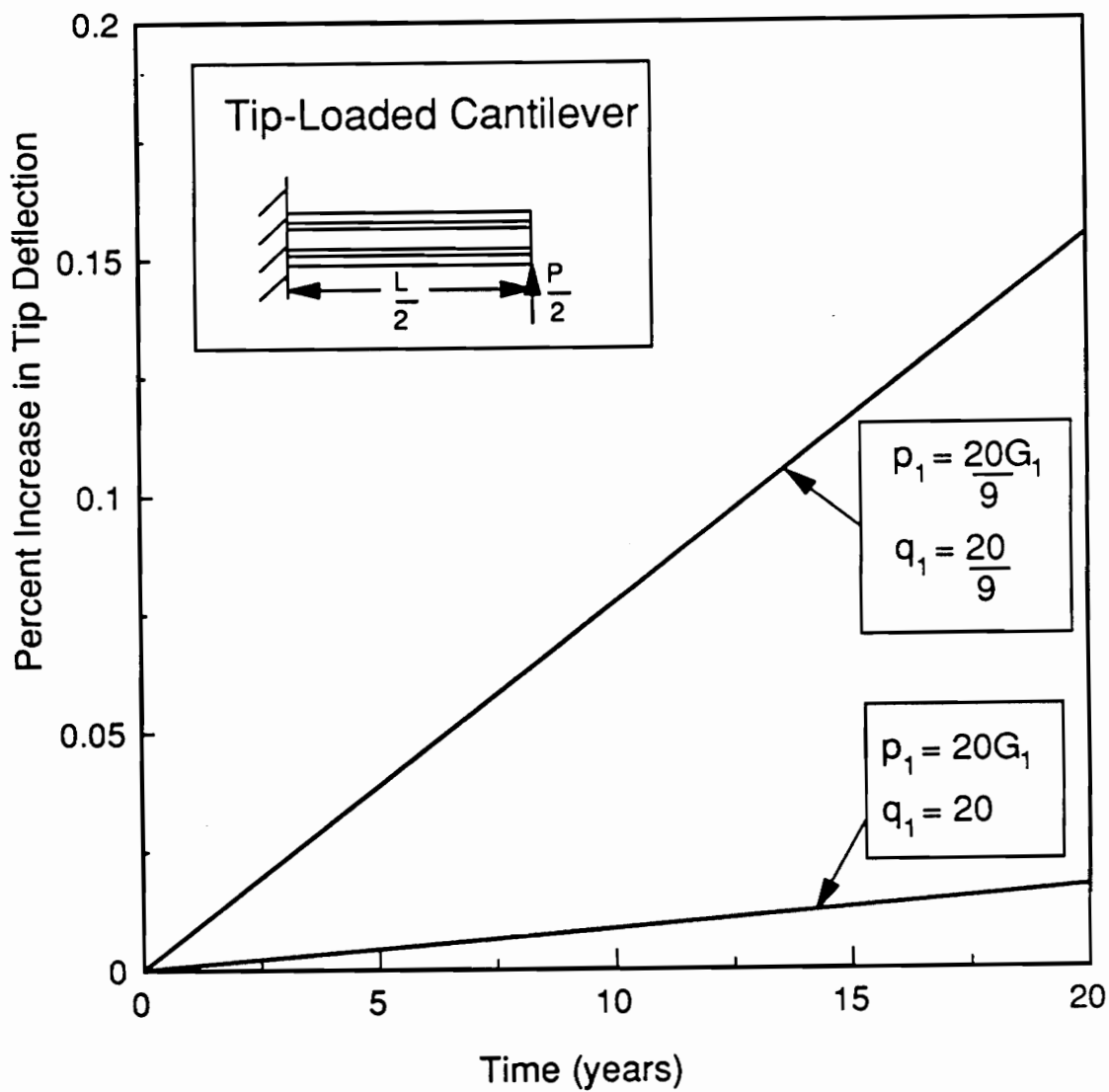


Figure 15. Percent Increase in Tip Deflection of Five-Layer Beam Model for $G_1(t)$

Through-the-Thickness Linear Thermal Gradient

The elastic sensitivity studies for the five-layer beam model subjected to a thermal gradient revealed that only a reduction of the modulus of elasticity of the composite face sheet

significantly increases the tip deflection. Therefore, the viscoelastic response of the beam to time-dependent extensional behavior of the face sheets is studied.

Influence of Time-Dependent Face Sheet Modulus of Elasticity (E_1) on Beam Response

Two Maxwell fluid models are used to bracket the expected behavior of the face sheets. One model allows the strain to increase by one percent in 20 years; the other allows a ten percent increase in 20 years. Because these models are identical to those used in Chapter 4, the constants p_1 and q_1 as found in Chapter 4 are used here. For the model which allows a one percent increase in strain, from Equation 4.60,

$$q_1 = 2000E_1 \text{ and } p_1 = 2000 \quad . \quad (6.36)$$

For the model which allows a ten percent increase in strain, from Equation 4.61,

$$q'_1 = 200E_1 \text{ and } p'_1 = 200 \quad . \quad (6.37)$$

The definitions in Equations 5.6 and 5.33 are substituted into the elastic tip deflection of a cantilever beam subjected to a linear through-the-thickness thermal gradient to reveal the dependence on E_1 :

$$w_{\text{tip}} = \frac{-bL^2}{16} \times \frac{\left\{ E_1 \alpha_1 t_1 \left[\left(h + t_2 + \frac{t_1}{2} \right)^2 + \frac{t_1^2}{12} \right] + E_2 \alpha_2 t_2 \left[\left(h + \frac{t_2}{2} \right)^2 + \frac{t_2^2}{12} \right] + E_3 \alpha_3 h \left[\frac{h^2}{3} \right] \right\}}{\left\{ E_1 t_1 \left[\left(h + t_2 + \frac{t_1}{2} \right)^2 + \frac{t_1^2}{12} \right] + E_2 t_2 \left[\left(h + \frac{t_2}{2} \right)^2 + \frac{t_2^2}{12} \right] + E_3 h \left[\left(\frac{h}{2} \right)^2 + \frac{h^2}{12} \right] \right\}} \quad . \quad (6.38)$$

New constants are now introduced to simplify the previous equation. They are

$$\begin{aligned}
 K &= \frac{-bL^2}{16} \\
 A &= \alpha_1 t_1 \left[\left(h + t_2 + \frac{t_1}{2} \right)^2 + \frac{t_1^2}{12} \right] \\
 B &= E_2 \alpha_2 t_2 \left[\left(h + \frac{t_2}{2} \right)^2 + \frac{t_2^2}{12} \right] + E_3 \alpha_3 h \left[\left(\frac{h}{2} \right)^2 + \frac{h^2}{12} \right] \\
 C &= t_1 \left[\left(h + t_2 + \frac{t_1}{2} \right)^2 + \frac{t_1^2}{12} \right] \\
 D &= E_2 t_2 \left[\left(h + \frac{t_2}{2} \right)^2 + \frac{t_2^2}{12} \right] + E_3 h \left[\left(\frac{h}{2} \right)^2 + \frac{h^2}{12} \right]
 \end{aligned} \tag{6.39}$$

Using these, Equation 6.38 becomes

$$w_{tip} = K \left(\frac{E_1 A + B}{E_1 C + D} \right) \tag{6.40}$$

To apply the correspondence principle, the ratio $\frac{Q(s)}{P(s)}$ replaces E_1 in the transformed form of Equation 6.40. Like the mechanical load, the thermal gradient is considered to be a step function of time. (Transient heat conduction difficulties are being ignored.) Therefore, the general expression for the tip deflection in Laplace domain is

$$\bar{w}_{tip}(s) = \frac{K}{s} \frac{\left[\left(\frac{Q(s)}{P(s)} \right) A + B \right]}{\left[\left(\frac{Q(s)}{P(s)} \right) C + D \right]} \tag{6.41}$$

For a Maxwell fluid model, this becomes

$$\bar{w}_{tip}(s) = \frac{K}{s} \frac{\left[\left(\frac{q_1 s}{1 + p_1 s} \right) A + B \right]}{\left[\left(\frac{q_1 s}{1 + p_1 s} \right) C + D \right]} = \frac{K}{s} \left[\frac{s(Aq_1 + Bp_1) + B}{s(Cq_1 + Dp_1) + D} \right] \tag{6.42}$$

Once the Inverse Laplace transform has been performed, the previous expression becomes the time-dependent tip deflection. This is

$$w_{\text{tip}}(t) = \frac{K}{D} \left[B + q_1 \left(\frac{AD - BC}{Cq_1 + Dp_1} \right) e \left(\frac{-Dt}{Cq_1 + Dp_1} \right) \right] . \quad (6.43)$$

Unlike most of the previous viscoelastic studies, the tip deflection of a beam subjected to a thermal gradient is not a linear function of time. The time-dependent tip deflections for the two cases under consideration are shown in Figure 16. Upon inspection of this figure, it is apparent that, even though the tip deflection is actually an inverse exponential function of time, it appears to be an approximately linear function of time. The influence of time-dependent behavior of the face sheets on the tip deflection is slight; the percent increase of tip deflection in 20 years for the case of more time-dependent behavior is less than one percent.

Quasi-Elastic Approach

As was done for the three-layer beam model, the quasi-elastic approach can be used to study the five-layer beam. Here both the tip-loaded cantilever beam and the cantilever beam subjected to a linear through-the-thickness thermal gradient are considered. As before, the quasi-elastic increase in tip deflection is found by increasing the particular compliances by a certain factor. This increase in tip deflection is normalized with respect to the elastic tip deflection, as in Equation 4.77, and this ratio is reported in the third column of Table 12. As before, the first column indicates the material property that experiences a compliance increase and the second column presents the factor by which the compliance is increased. The fourth column shows the percent increase in tip deflection as computed by the viscoelastic approach and given by Equation 4.78. Like the quasi-elastic results for the three-layer model, the quasi-elastic results for the five-layer beam are nearly identical to the viscoelastic results

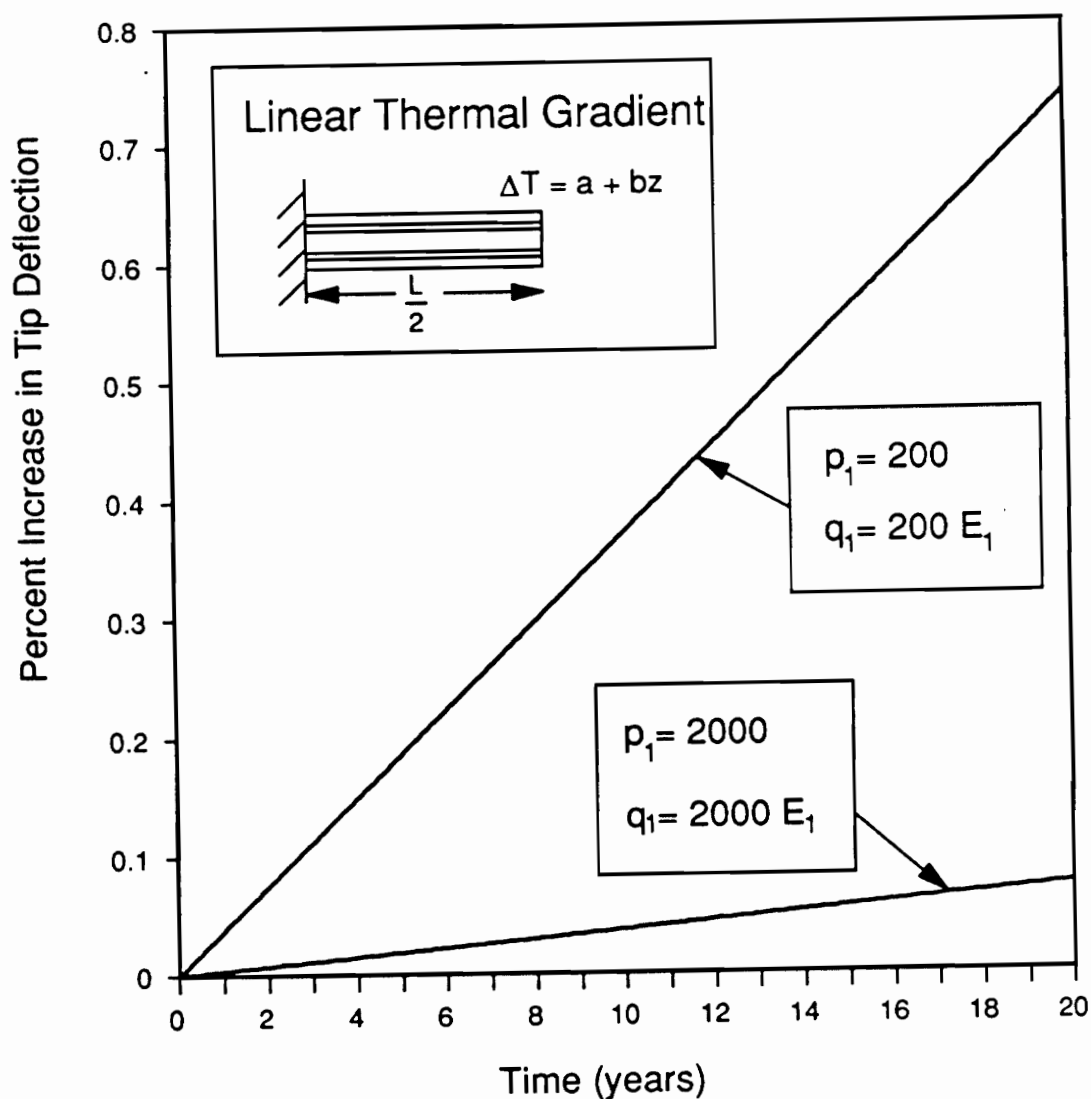


Figure 16. Percent Increase in Tip Deflection of Five-Layer Beam Model for $E_1(t)$ - Thermal Gradient

with only one exception; the quasi-elastic tip deflection for the case of an increased compliance which corresponds to G_3 (the shear modulus of the core) is slightly less than the viscoelastic tip deflection.

Table 12. Quasi-Elastic Tip Deflection of the Five-Layer Composite Beam

Tip-Loaded Cantilever Beam			
Material Property	Factor	Quasi-Elastic Result	Viscoelastic Result
G_1	10.0	0.2 %	0.2 %
G_2	10.0	0.4 %	0.4 %
G_3	10.0	123.5 %	127.3 %
Cantilever Beam Subjected to Thermal Gradient			
E_1	1.1	0.7 %	0.7 %

Summary

This completes the rather comprehensive treatment of the five-layer sandwich beam model. For the most part, the results are similar to the results found using the three-layer sandwich beam model. The single exception is the sensitivity of the beam to a thermal gradient when the modulus of elasticity of the composite face sheet is reduced. An explanation for this was presented based on the presence of an adhesive layer. Without using the five-layer model, this important physical effect would not have been revealed. As with the three-layer model, sufficient details have been presented so that the use of more complicated functions for the time-dependent behavior of the constituents can be considered.

The next chapter begins the discussion of the experimental aspects of this study. The apparatus used to measure the time-dependent response of various constituents are described, and the experimental procedure is discussed. There are inherent difficulties in measuring the time-dependent response of materials. Strain readings from electronic devices such as electrical strain gages can “drift” over time. Also, environmental changes such as

temperature, humidity and vibrations effect electrical resistance and mechanical measurement devices (e.g., dial gages). Even so, an attempt is made to observe the time-dependent behavior of the quartz-epoxy material in tension and the glass-imide honeycomb in shear. Based on the elastic sensitivity studies and the viscoelastic studies, the time-dependent behavior of these particular beam constituents have the most influence on the response of the sandwich beam. Simple viscoelastic models are then fit to the observed these behaviors and the three-layer sandwich beam model is used to predict the time-dependent response of a sandwich beam in three-point bending. This prediction is compared to experimental measurements of the response of a sandwich beam in three-point bending.

Chapter 7 - Experimental Apparatus and Procedure

The work presented in the previous chapters indicated that the time-dependent behavior of the sandwich beam constituents has an influence on the overall time-dependent behavior of the beam. The degree of influence depends on the particular constituent and the level of time-dependent behavior of that constituent. For demonstrative purposes, Maxwell fluid models with two levels of time-dependence were considered. Although the Maxwell fluid model might be considered an oversimplification, it does reflect one important aspect of polymer response, namely the tendency to continuously deform under stress. Although for purposes of demonstration a Maxwell fluid is a convenient model because of its simplicity, it does not necessarily accurately represent the behavior of any of the constituents, nor do the two levels of time-dependence studied accurately reflect the magnitude of time-dependence of the constituents. In this context, several important questions can be asked. First, do the quartz-epoxy face sheets loaded in tension or compression behave like a Maxwell fluid model? Can the behavior of the glass-imide honeycomb in shear be modelled as a Maxwell fluid? If so, what strain increases are observed with time? Second, if they do not behave as Maxwell fluids, which viscoelastic model can be used to more accurately reflect their behavior? Finally, once the viscoelastic behavior of the constituents is quantified and modelled, can these models be used in the three-layer or five-layer beam model to accurately predict the

response of an actual beam with time? These are important questions and constitute a study in their own right. However, to begin to answer these questions, some experimental work was conducted. The work focused on determining the time-dependent behavior of the quartz-epoxy face sheet material in extension, the time-dependent behavior of the glass-imide honeycomb core material in shear, and the time-dependent behavior of a sandwich beam subjected to three-point bending. The time-dependent shear behavior of the face sheets and the time-dependent behavior of the adhesive in both shear and extension were not studied. If the analytical predictions in the previous chapters are correct, then using the models which best fit the time-dependent behavior of the face sheets in extension and the core in shear in either beam model will result in predictions that should closely match the observed time-dependent beam deflection.

This chapter discusses the apparatus and procedure used to measure the time-dependent response of the quartz-epoxy face sheet material in extension, the glass-imide honeycomb in shear, and a sandwich beam in three-point bending.

Time-Dependent Behavior of the Quasi-Isotropic

Quartz-Epoxy Face Sheets

To observe the time-dependent behavior in tension of the quasi-isotropic Astroquartz-155 as a function of time, two coupons with nominal widths of 0.5" and thicknesses of 0.04" were cut. Two back-to-back strain gages were bonded to each specimen to measure axial strain. One sample was placed in a standard dead-weight loading creep frame and loaded. The other sample was in close physical proximity to the loaded specimen but remained unloaded. The four strain gages were used to complete a Wheatstone bridge circuit. Because the experiment was not performed in a controlled environment, the strain gages on the unloaded sample were

used to compensate for the effects of temperature or humidity changes on gage resistance. A load was applied in a step-wise fashion. For the first hour, the strain was recorded at intervals of less than ten minutes. Then, as the need for more frequent data readings declined, the interval increased gradually. The experiment continued for over 40 days. Compensation for electronic drift in the strain gages was not made. However, preliminary experiments with the same two specimens, both unloaded, indicated that drift was several orders of magnitude smaller than the readings for the loaded specimen.

Time-Dependent Behavior of the Glass-Imide Honeycomb Core

A special fixture to measure the time-dependent shear behavior of all three constituent materials (the quasi-isotropic quartz-epoxy face sheets, the film adhesive and the glass-imide honeycomb) was designed. A schematic of the fixture is shown in Figure 17. The fixture consists of two plates of steel, between which the material in question can be bonded. Two more pieces, the ends of the fixture, are removable. Each of the end pieces has three holes which allow the tensile load to be applied through the centerline of any of the three materials, each of which has a different thickness. In other words, the centerline of the material being tested coincides with the line of action of the applied tensile load. The relative displacement of the two steel plates is measured using a crack-opening-displacement (COD) gage. The initial opening of the COD gage can be adjusted by using a slider mechanism which is attached to the steel plates. This slider mechanism is shown in detail in Figure 18. The mechanism is composed of a slider which is set into a stationary block attached to one plate and controlled by a screw. The slider fits into a dove tail cut in the stationary block. Turning the screw either increases or decreases the distance between the slider and another block which is

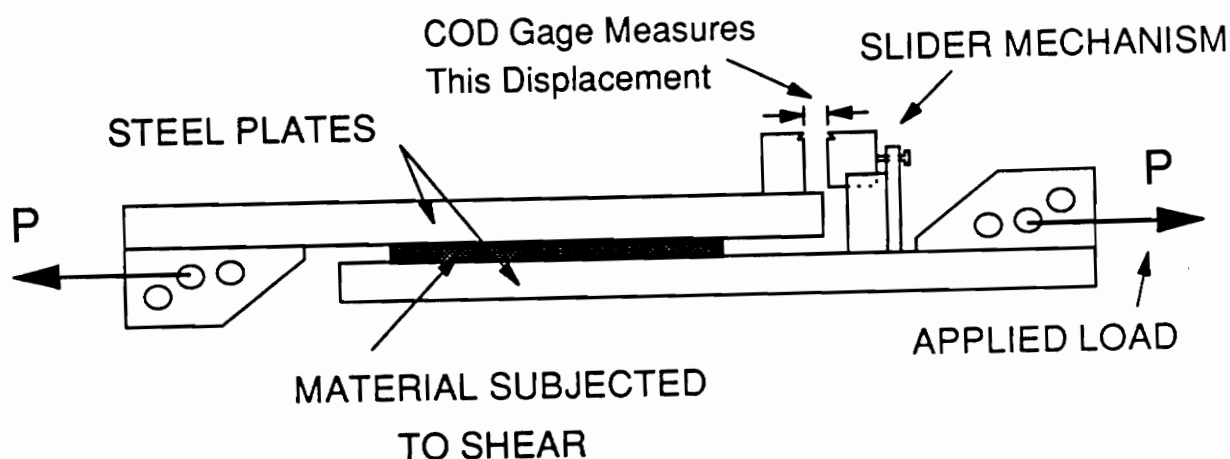


Figure 17. Shear Fixture

connected to the other steel plate. Both the slider and the second block have grooves into which the COD gage is set.

Although the fixture was designed to be used for all three constituent materials, the previous work indicates that the shear behavior of only the core is important. Therefore, for the second experiment, a sample of the glass-imide honeycomb was bonded to the fixture using the FM73 film adhesive. Thus, the data obtained from the fixture more accurately represent the core of the three-layer beam model, which is a combination of the honeycomb and adhesive layers. The specimen had a nominal width of 1.5" and length of 3.0". The fixture (complete with specimen) was placed in the creep frame. The COD gage was set in place. The slider mechanism was adjusted so that the initial, unloaded opening of the gage corresponded to a strain reading of zero. Like the previous experiment, the load was applied in a stepwise fashion, and the strain was recorded at intervals of less than ten minutes for the first hour.

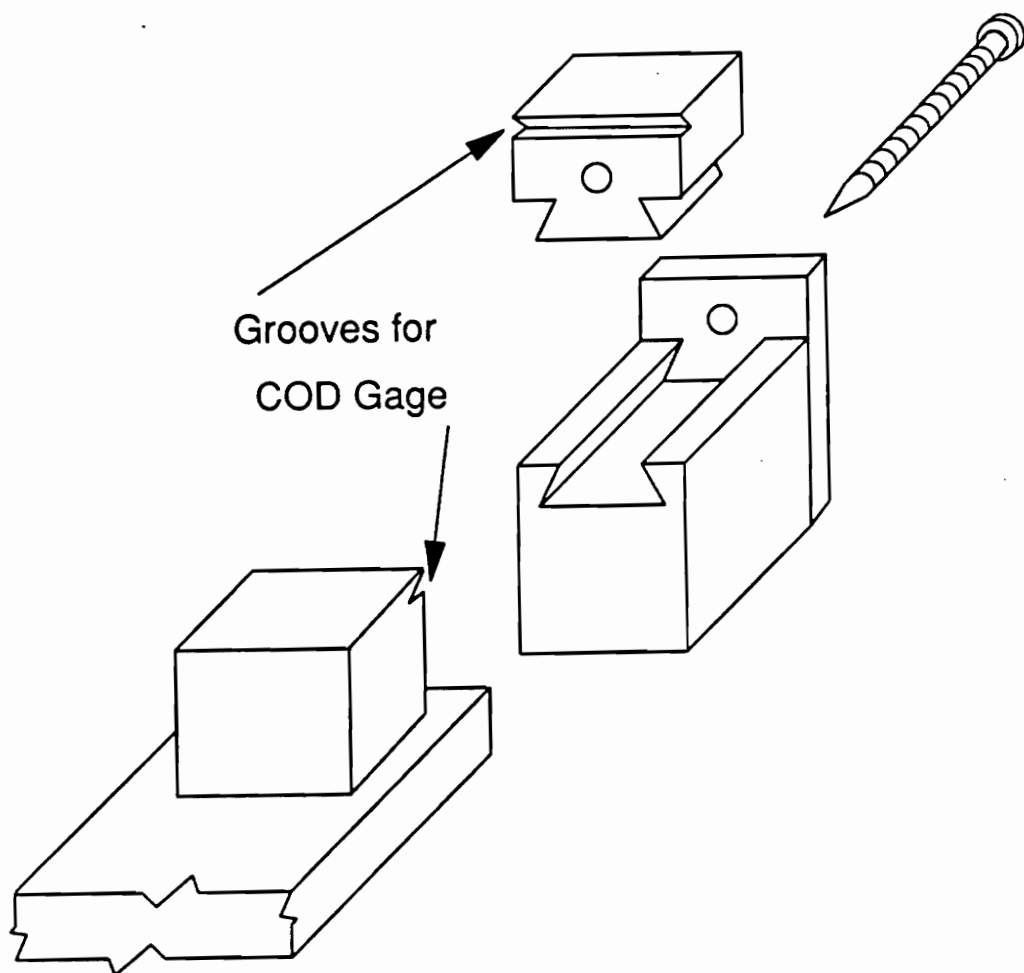


Figure 18. Slider Mechanism

Gradually, the intervals increased in length as the need for more frequent strain data decreased. This experiment was continued for about fourteen days.

Time-Dependent Behavior of the Sandwich Beam in Three-Point Bending

Another fixture was designed in order to examine the time-dependent behavior of a sandwich beam in three-point bending. This fixture is basically an elevated aluminum platform. Parallel grooves 8" apart in the aluminum plate constrain two dowel pins which act as simple supports for the beam. Midway between the simple supports are four posts, two on each side of the beam. The load is applied across the width of the beam at the midspan by a dowel pin which slides down between the four posts. Screws connect this dowel pin to a pan which holds weights. This apparatus is shown in Figure 19. In addition to the basic fixture, two posts were added at strategic locations to support the dial gages which were used to measure the beam's deflection.

A sandwich beam of Astroquartz-155 quasi-isotropic face sheets, FM 73 adhesive and HRH 327 glass-imide honeycomb core with a nominal width of 1" was placed in the fixture. A load was applied in a stepwise fashion by placing weights on the pan. The deflection of the beam at two points was measured using dial gages at a point 1" from the simple support and 1" from the center. The deflection of the beam at these two points was recorded, first for small intervals of time and then for gradually longer intervals. The experiment continued for 38 days. The measurement of the deflection at two points, as opposed to just one point, is used to check the consistency of the readings.

The results of the three experiments and the fitting of simple viscoelastic models to the data are presented in Chapter 8.

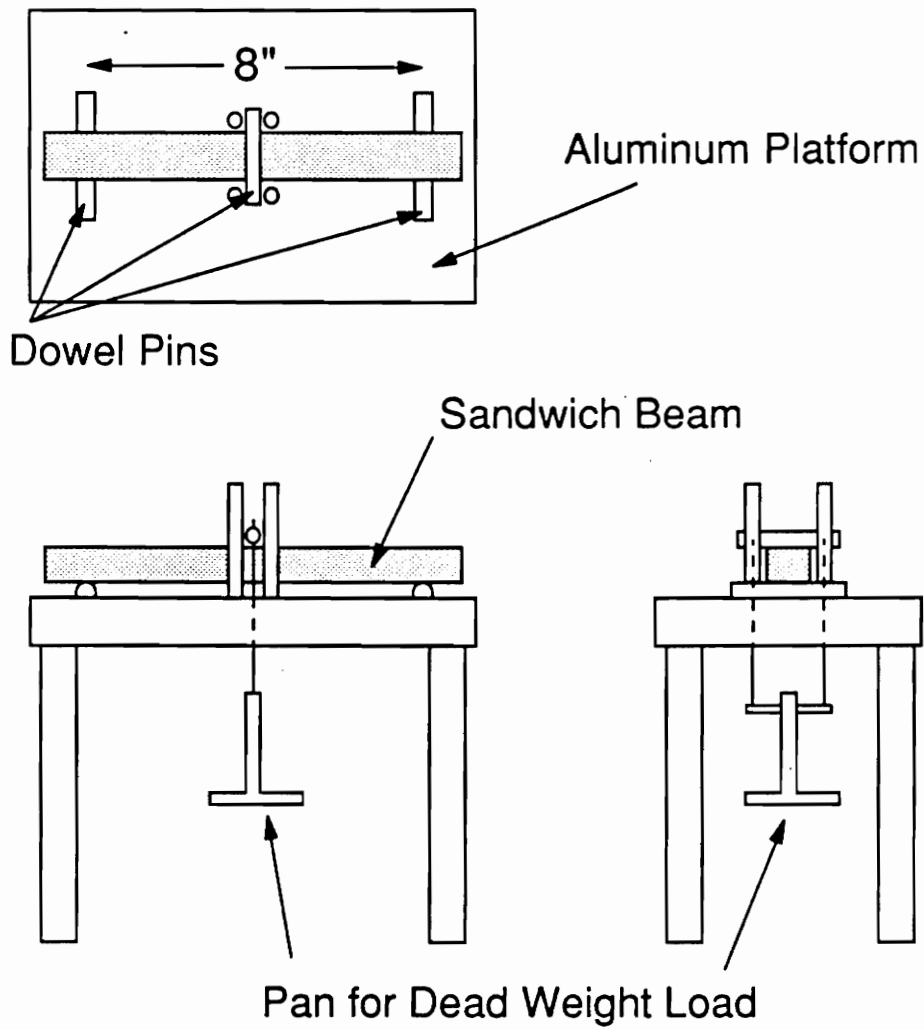


Figure 19. Three-Point Bending Fixture

Chapter 8 - Experimental Results and Viscoelastic Models

The results of measuring the time-dependent behavior of the quartz-epoxy face sheet material in extension and the glass-imide honeycomb material in shear are reported in this chapter. The results are reported as percent increase in strain as a function of time, or

$$\text{Percent Increase in Strain} = \frac{\epsilon(t) - \epsilon(0)}{\epsilon(0)} \times 100\% \quad (8.1)$$

Additionally, the initial value of strain, $\epsilon(0)$, is reported, as well as the stress level used for testing. Viscoelastic models are then chosen to represent the time-dependent behavior of these materials, and these models are used with the three-layer beam model to predict the percent increase of the deflection of the sandwich beam in three-point bending. This is then compared to the experimental results from the sandwich beam. Because the creep frame used magnifies the load using a lever arm and fulcrum, and because of the cross-sectional areas of the specimens, these stress levels are not "even" numbers (i.e., 50 psi), even though the dead weight loads were.

Time-Dependent Behavior of the Quasi-Isotropic Quartz-Epoxy Face Sheets

With an applied stress of 9,670 psi, the initial strain of the quasi-isotropic quartz-epoxy material was $3,650 \times 10^{-6}$. The percent increase in strain, Equation 8.1, is shown as a function of time in Figure 20. By definition, the percent increase in strain at time zero is zero. For the quartz-epoxy, the strain increased rapidly for approximately 10 days, after which the strain increased at a slower, nearly constant, rate.

One viscoelastic model which corresponds to this type of behavior is the four-parameter fluid. A four-parameter fluid consists of a free spring, Kelvin element, and free dashpot, all in series, as shown in Figure 21. The time-dependent percent increase in strain of a four-parameter fluid for a constant stress is also shown in that figure. The manner in which the parameters of a four-parameter fluid, E_0 , E_1 , η_1 and η_2 influence the time-dependent response is also noted in the figure. The free spring responds instantaneously to an applied stress, after which the Kelvin element and free dashpot contribute to the time-dependent portion of the strain. Eventually, the Kelvin element reaches a maximum amount of strain, after which the strain increases linearly for an indefinite period of time. The constitutive behavior of a four-parameter fluid is given by

$$\sigma + p_1 \dot{\sigma} + p_2 \ddot{\sigma} = q_1 \dot{\epsilon} + q_2 \ddot{\epsilon} \quad , \quad (8.2)$$

where

$$\begin{aligned} p_1 &= \frac{E_0 \eta_1 + E_0 \eta_2 + E_1 \eta_2}{E_0 E_1} \\ p_2 &= \frac{\eta_1 \eta_2}{E_0 E_1} \\ q_1 &= \eta_2 \\ q_2 &= \frac{\eta_1 \eta_2}{E_1} \end{aligned} \quad (8.3)$$

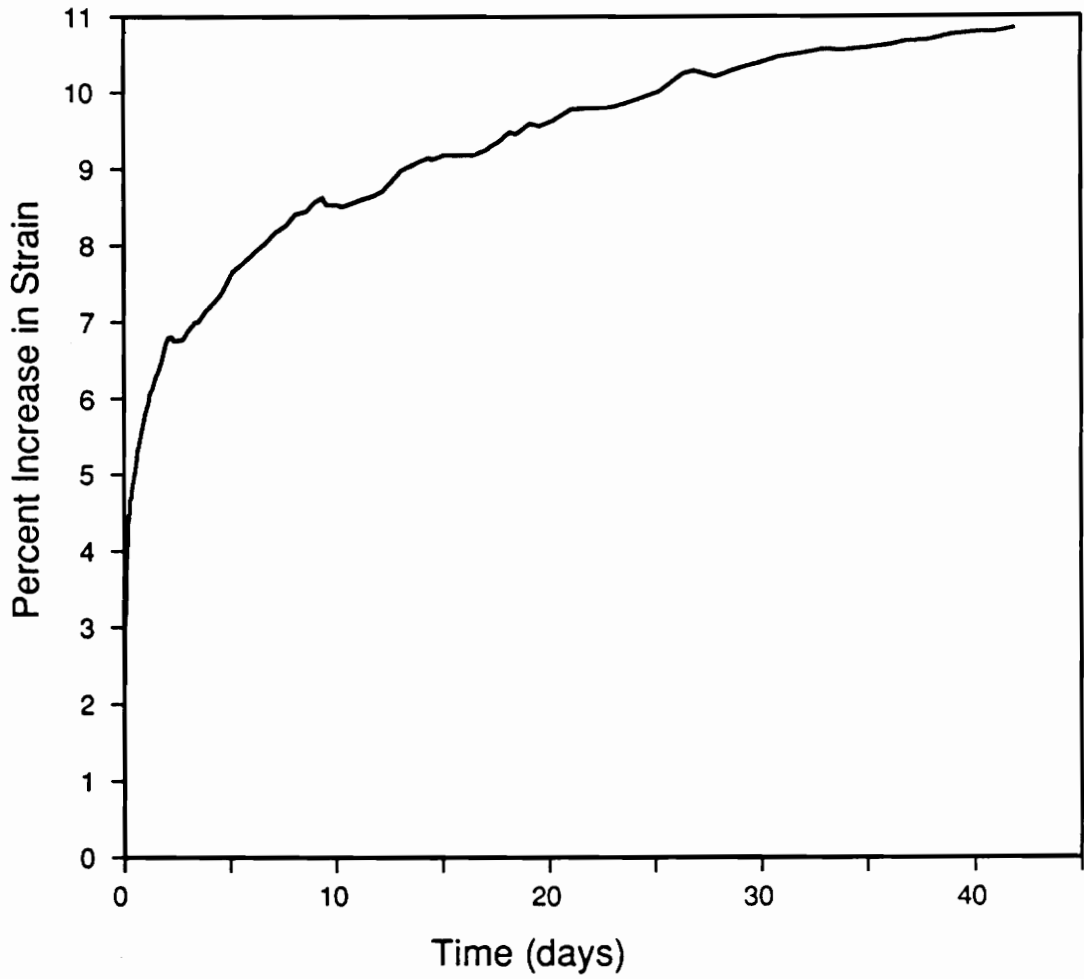


Figure 20. Percent Increase in Strain of Quartz-Epoxy Face Sheets

Equation 8.2 can be transformed to the Laplace domain:

$$\bar{\sigma}(s)(1 + p_1s + p_2s^2) = \bar{\epsilon}(s)(q_1s + q_2s^2) \quad (8.4)$$

For a stress that is applied as a step function, $\bar{\sigma}(s)$ is

$$\bar{\sigma}(s) = \frac{\hat{\sigma}}{s} \quad (8.5)$$

For this stress, the strain as a function of time can be found by substituting Equation 8.5 into Equation 8.4, solving for $\bar{\epsilon}(s)$, and performing the inverse Laplace transform. It is

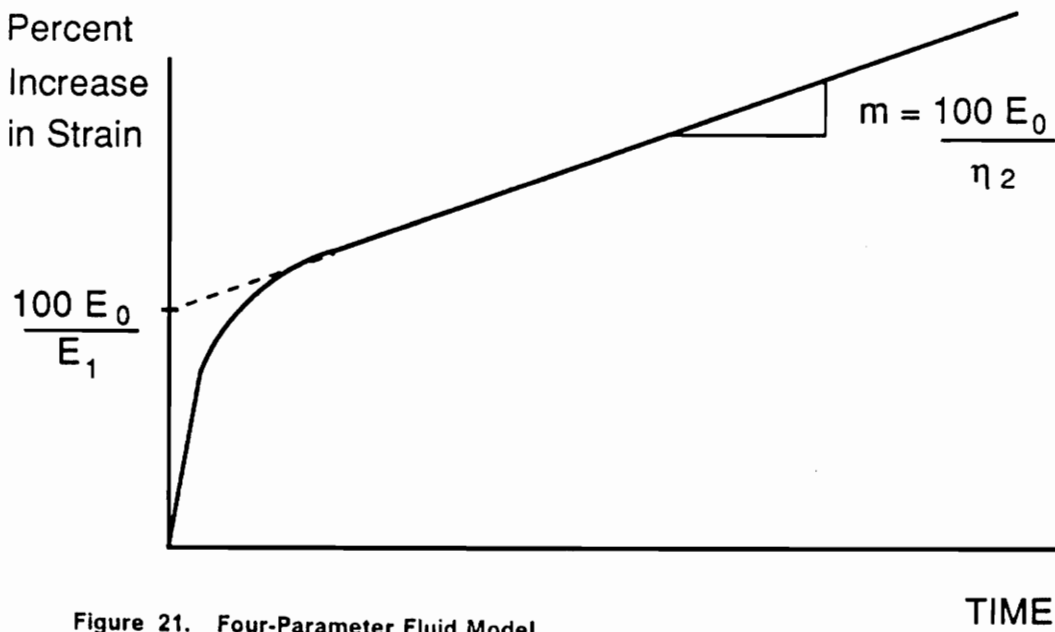
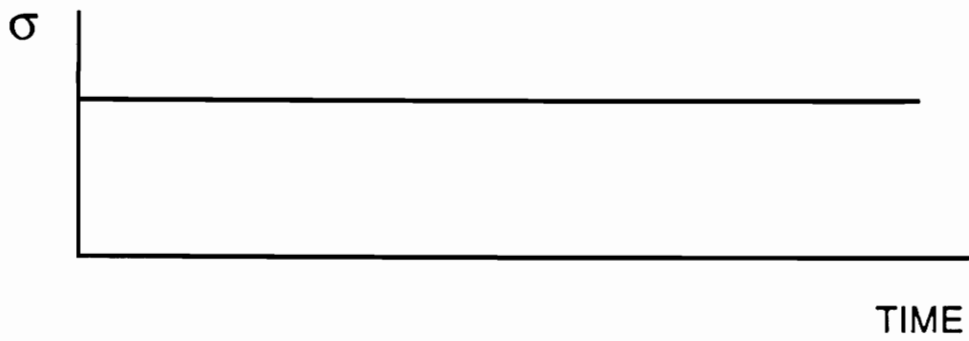
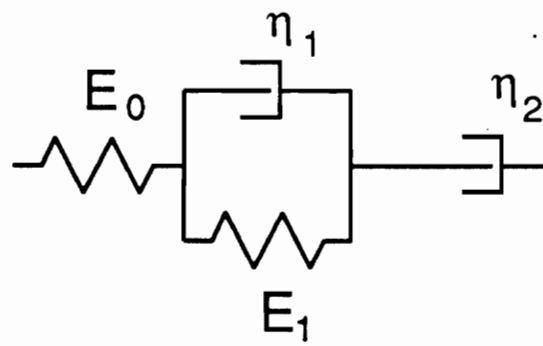


Figure 21. Four-Parameter Fluid Model

$$\varepsilon(t) = \hat{\sigma} \left(\frac{E_0 + E_1}{E_0 E_1} - \frac{1}{E_1} e^{\frac{-E_1 t}{\eta_1}} + \frac{t}{\eta_2} \right) . \quad (8.6)$$

The percent increase in strain of a four-parameter fluid can be written as a function of time as

$$\text{Percent Increase in Strain} = \left\{ \frac{E_0}{E_1} \left[1 - e^{\frac{-E_1 t}{\eta_1}} \right] + \left(\frac{E_0}{\eta_2} \right) t \right\} \times 100\% . \quad (8.7)$$

The constant E_0 can be determined from the initial strain. For the quasi-isotropic quartz-epoxy, it is

$$E_0 = \frac{\sigma}{\varepsilon(0)} = \frac{9670 \text{ psi}}{3650 \times 10^{-6}} = 2.65 \times 10^6 \text{ psi} , \quad (8.8)$$

which is, in fact, quite close to the elastic value used in Chapters 4 and 6, 2.5×10^6 psi. Once E_0 has been found, η_2 can be determined by examining the slope of the straight line portion of the percent increase in strain graph. The slope is

$$m = \frac{100 E_0}{\eta_2} . \quad (8.9)$$

For the quasi-isotropic quartz-epoxy, an hand-fit straight line through this latter portion of the data has a slope of approximately $0.0632 \frac{1}{\text{days}}$, thus

$$\eta_2 = \frac{100 E_0}{m} = \frac{100(2.65 \times 10^6 \text{ psi})}{0.0632 \frac{1}{\text{days}}} = 4.19 \times 10^9 \text{ psi-days} . \quad (8.10)$$

To find the other two constants, E_1 and η_1 , several different approaches can be used. One approach is a least-square error technique. For a range of E_1 and η_1 values, a cumulative error can be calculated by summing the squares of the difference between the computed

value of percent increase in strain from Equation 8.7 and the experimental value. In other words, for each E_1 and η_1 value, the error

$$ERR = \sum_i \left(\frac{\text{Experimental Percent Increase in Strain}}{\text{Computed Percent Increase in Strain}} - 1 \right)^2, \quad (8.11)$$

where i is the total number of data points, is calculated. The range of E_1 and η_1 can be refined to minimize this error. For the quasi-isotropic quartz-epoxy, the error is minimized when

$$\begin{aligned} E_1 &= 3.45 \times 10^7 \text{ psi} \\ \eta_1 &= 1.13 \times 10^7 \text{ psi-days} \end{aligned} \quad (8.12)$$

To compare this four-parameter fluid model to the experimental data, the percent increase in strain of both the model and the experiment are presented together in Figure 22. Although the agreement is not perfect, the four-parameter fluid model does capture the essential characteristics of the experimental behavior.

A different approach to finding E_1 and η_1 could yield better results. In this approach, the straight line that was used to find η_2 is extended to intercept the $t=0$ axis. This intercept is, as shown in Figure 21 by the dashed line,

$$\text{intercept} = \frac{100E_0}{E_1} \quad (8.13)$$

Thus, for this case, E_1 is

$$E_1 = \frac{100E_0}{\text{intercept}} = \frac{100(2.65 \times 10^6 \text{ psi})}{8.25} = 3.21 \times 10^7 \text{ psi} \quad (8.14)$$

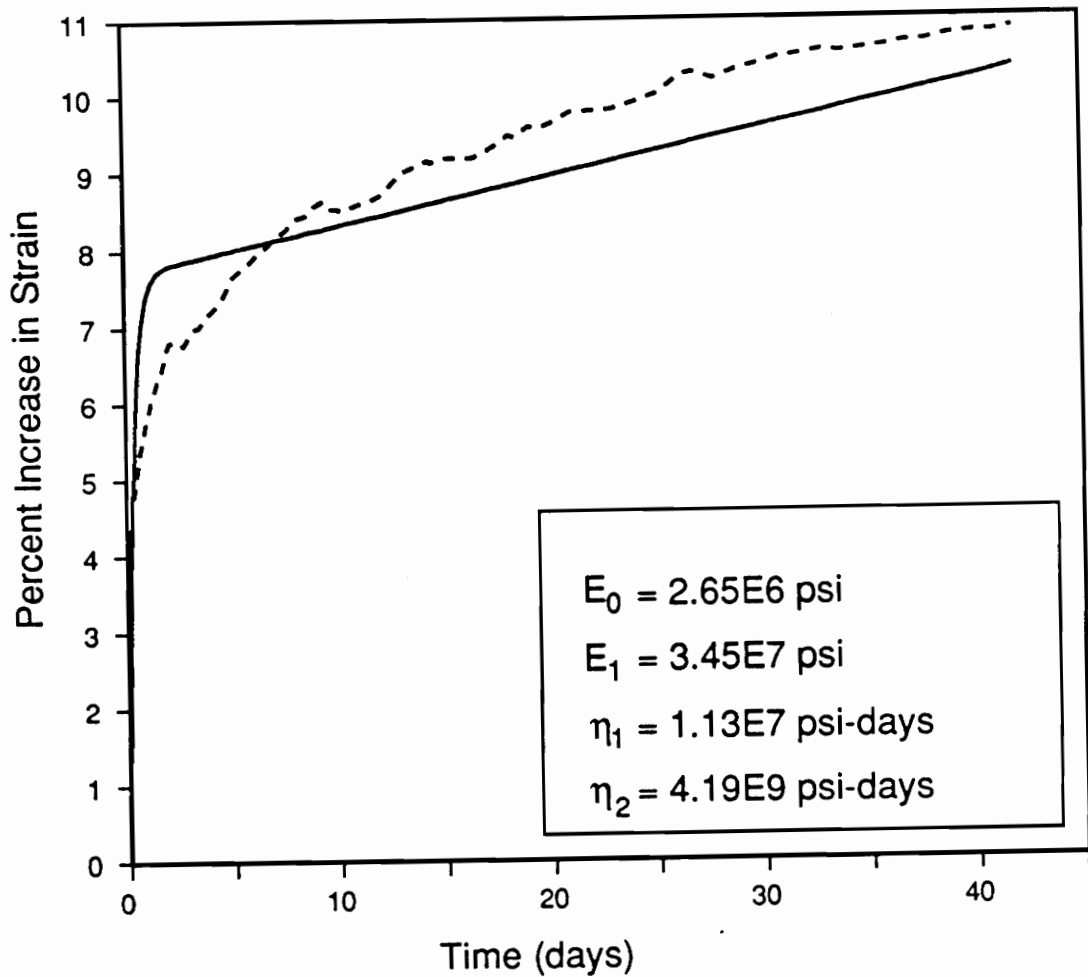


Figure 22. Percent Increase in Strain of Quartz-Epoxy Face Sheets - Experimental and Model (First Approach)

The value of η_1 can then be chosen, either by trial and error or by a least-squares approach, so that the four-parameter fluid model closely matches the experimental behavior. Using the former method resulted in

$$\eta_1 = 5.00 \times 10^7 \text{ psi-days} \quad . \quad (8.15)$$

The percent increase in strain of a four-parameter fluid model described by these constants and the ones in Equations 8.8 and 8.10 is shown in Figure 23, along with the experimental

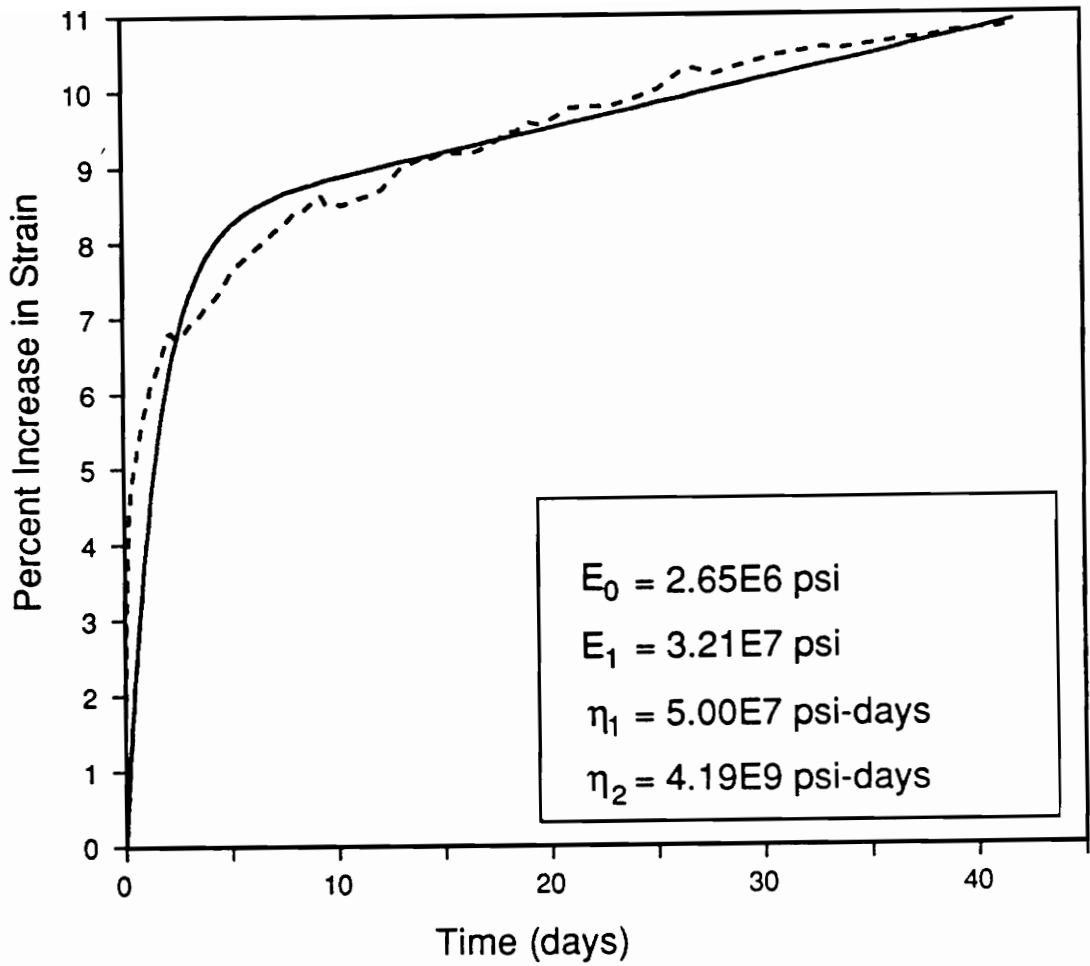


Figure 23. Percent Increase in Strain of Quartz-Epoxy Face Sheets - Experimental and Model (Second Approach)

data. The agreement between this model and experiment is much better than for the first approach and is used later.

Time-Dependent Behavior of the Glass-Imide Honeycomb Core

With a shear stress of 67 psi applied, the initial shear strain of the glass-imide honeycomb material was $15,100 \times 10^{-6}$. The percent increase in strain, Equation 8.1, is shown as a function of time in Figure 24. Like before, the time-dependent strain of the material behaves much like a four-parameter fluid, although the behavior is a bit more erratic. In order to avoid confusion between the four-parameter fluid models previously defined for the quartz-epoxy material in extension, the spring and dashpot constants are defined for this four-parameter fluid model as shown in Figure 25. As before, the spring constant of the free spring, now G_o , can be found using the initial strain and is

$$G_o = \frac{\tau}{\gamma(0)} = \frac{66.7 \text{ psi}}{15100 \times 10^{-6}} = 4.42 \times 10^3 \text{ psi} \quad (8.16)$$

Also like before, the dashpot constant of the free dashpot can be found by examining the slope of the straight line portion of Figure 24. An hand-fit straight line through the data has a slope of about $0.161 \frac{1}{\text{days}}$. Therefore, γ_2 is

$$\gamma_2 = \frac{100G_o}{m} = \frac{100(4.42 \times 10^3 \text{ psi})}{0.161 \frac{1}{\text{days}}} = 2.75 \times 10^6 \text{ psi-days} \quad (8.17)$$

The other two constants, G_1 and γ_1 , can be found using the same techniques as before. For ranges of these constants, the cumulative error is calculated using the least-squares approach in Equation 8.11. The ranges are refined until the error is minimized and the best values are found for G_1 and γ_1 . They are

$$\begin{aligned} G_1 &= 5.38 \times 10^4 \text{ psi} \\ \gamma_1 &= 8.33 \times 10^3 \text{ psi-days} \end{aligned} \quad (8.18)$$

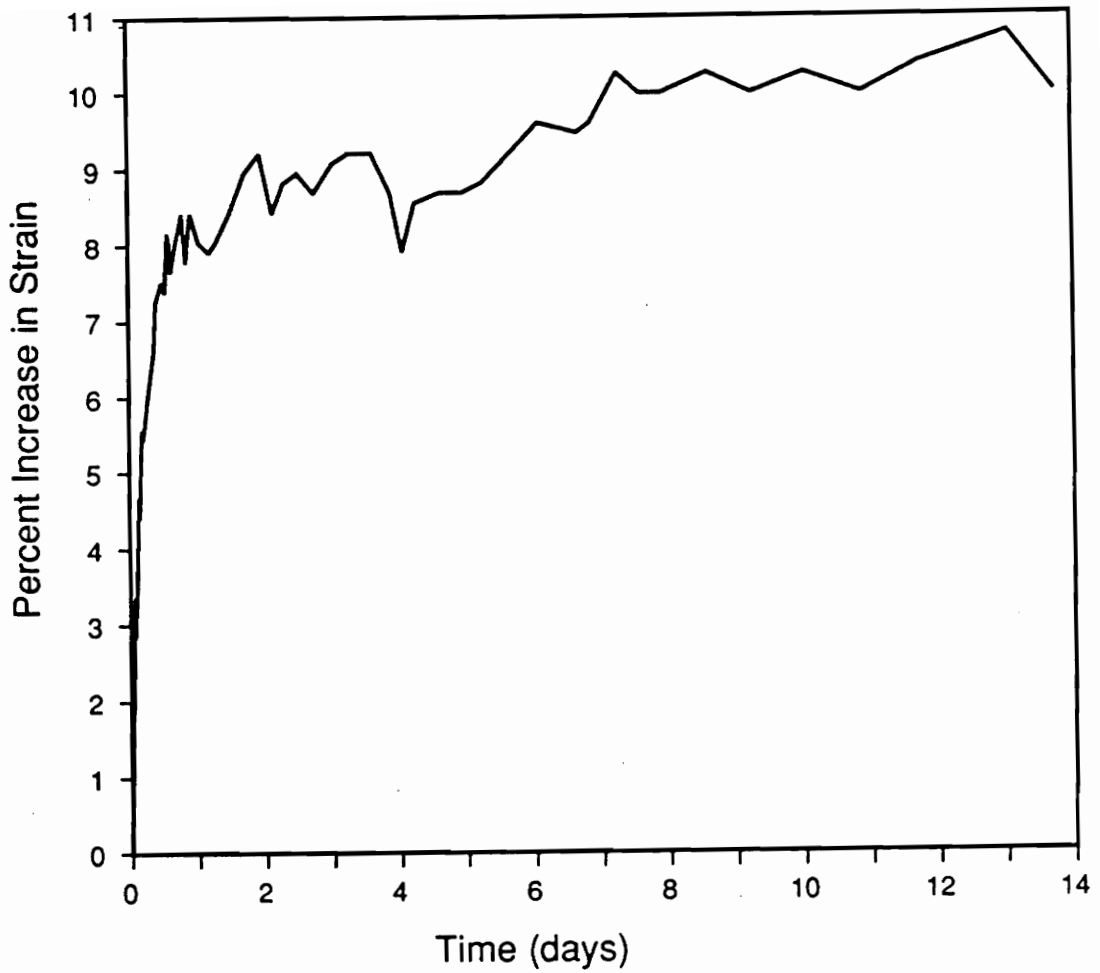


Figure 24. Percent Increase in Strain of Glass-Imide Honeycomb

Again, the percent increase in strain of the four-parameter fluid model which is described by Equations 8.16, 8.17 and 8.18 is presented with the experimental percent increase in strain in Figure 26. The time-dependent behavior of the glass-imide honeycomb in shear can be matched quite closely with this four-parameter fluid model.

For comparison, G_1 and γ_1 are also found using the second approach. As with Equation 8.10, G_1 is

$$G_1 = \frac{100G_0}{\text{intercept}} = \frac{100(4.42 \times 10^3 \text{ psi})}{8.25} = 5.36 \times 10^4 \text{ psi} \quad (8.19)$$

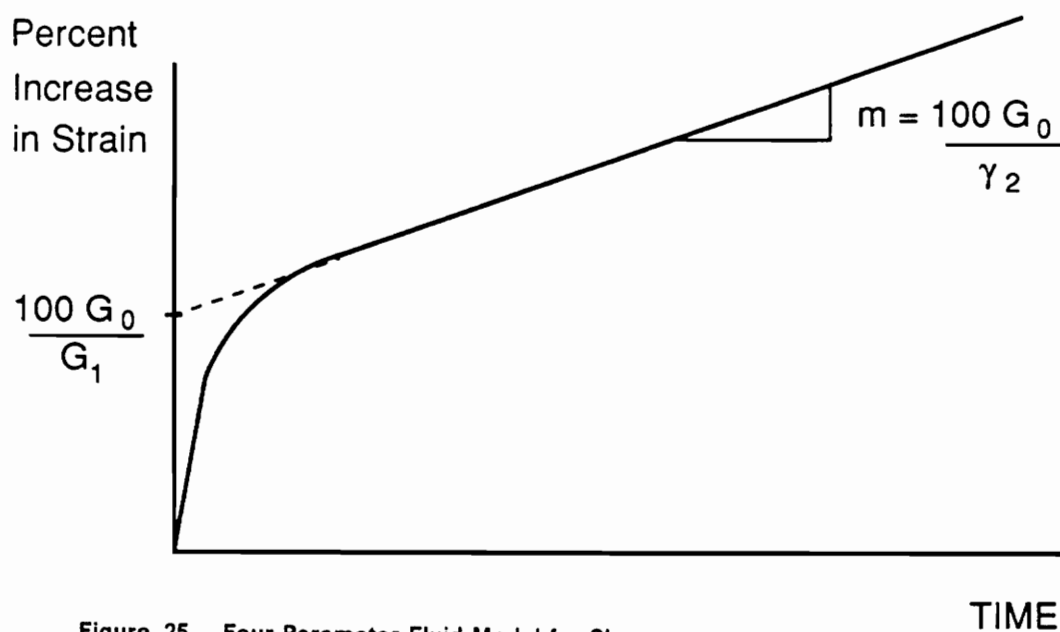
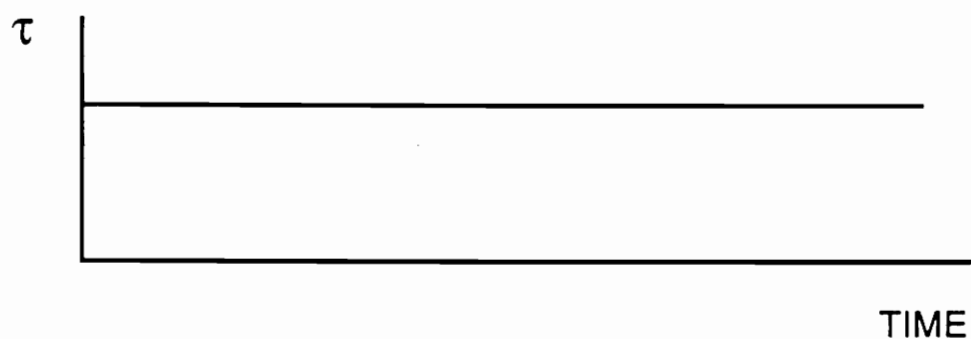
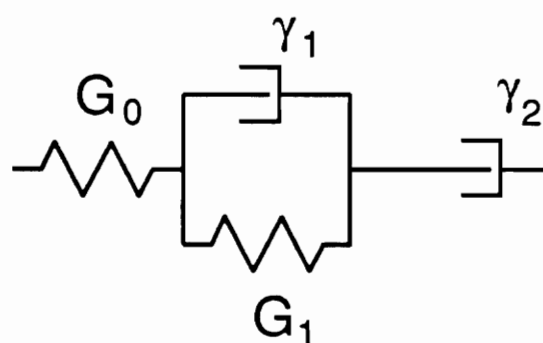


Figure 25. Four-Parameter Fluid Model for Shear

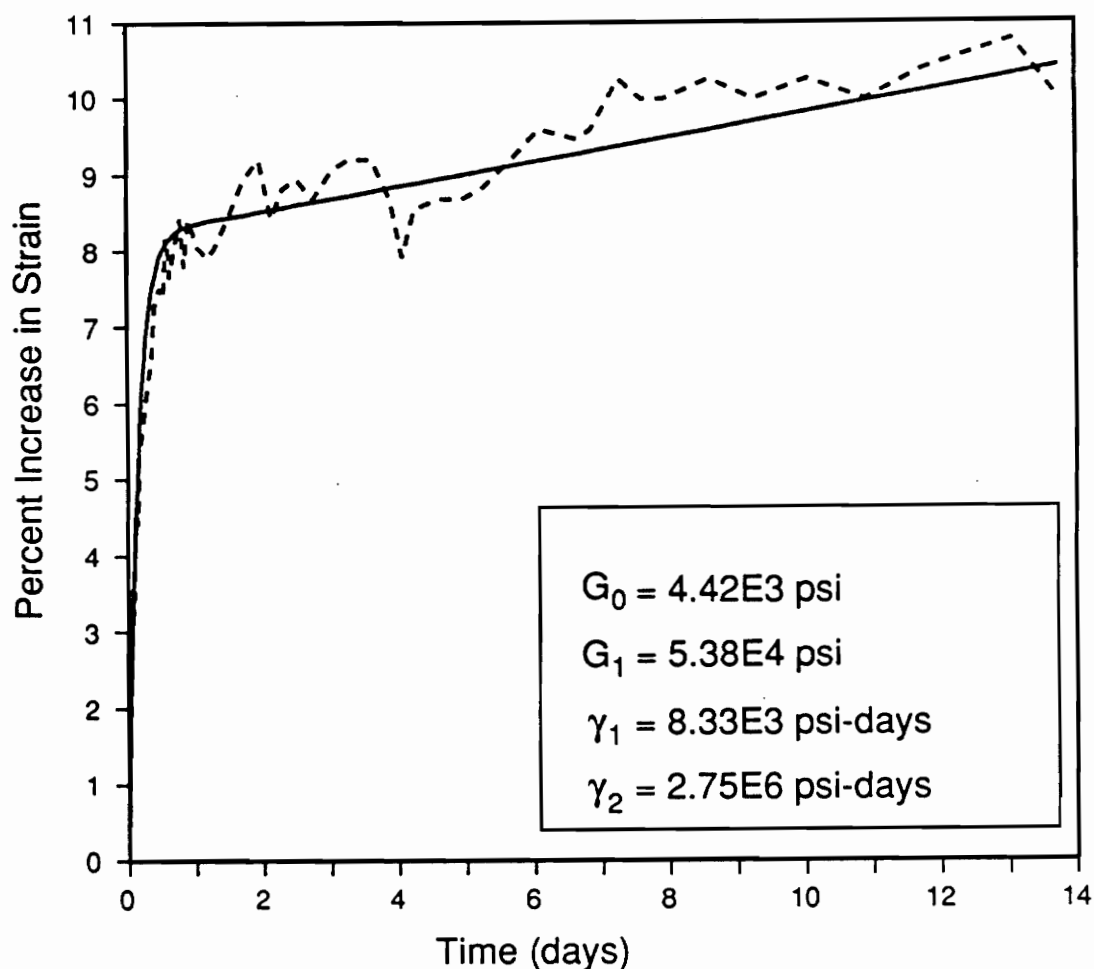


Figure 26. Percent Increase in Strain of Glass-Imide Honeycomb - Experimental and Model (First Approach)

This is within one percent of the previously determined G_1 . Therefore, because the least-squares approach yielded a model which so well represented the time-dependent behavior of the material in shear, and because G_1 is nearly identical, the value of γ_1 from before, namely,

$$\gamma_1 = 8.33 \times 10^3 \text{ psi-days} \quad , \quad (8.20)$$

is selected for the value of γ_1 for the second model. The percent strain increase of this model is presented along with the experimental data in Figure 27. As expected, the results from

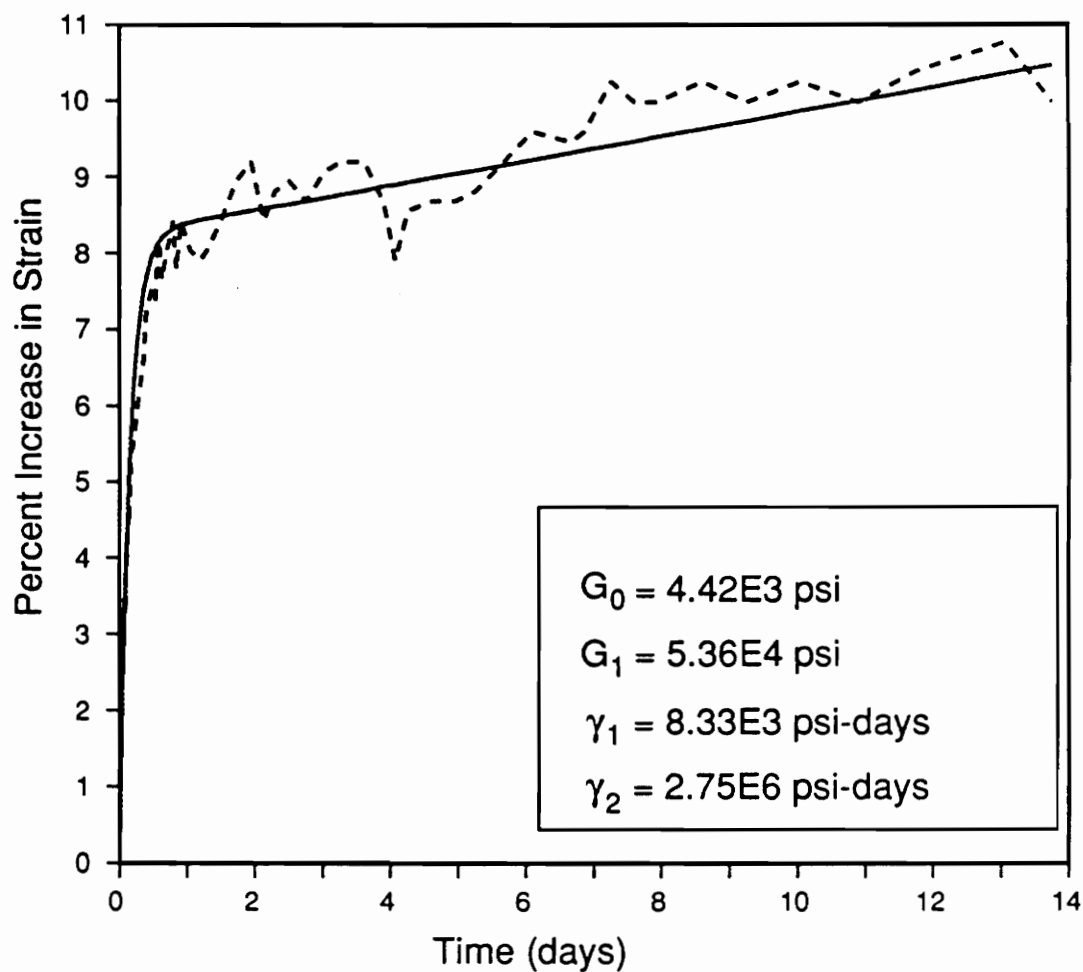


Figure 27. Percent Increase in Strain of Glass-Imide Honeycomb - Experimental and Model (Second Approach)

using the second approach for the reduction of the data are nearly identical to the results from using the first approach.

Time-Dependent Behavior of the Sandwich Beam in Three-Point Bending

The deflection of a sandwich beam subjected to three-point bending was measured at two points along the length of the beam over a period of about 38 days. Because the experimental work focuses on the agreement between the time-dependent portions of the analytical model and the experimental data, only the time-dependent portion of the data is reported here. Also, because the shape of the deflected beam does not change with time, the percent increase in deflection for the two points should, in theory, be the same. Figure 28 presents the average of the percent increase in deflection for the two points measured. For all intents and purposes, the results from measuring the deflection at the two points were identical.

As can be seen, the behavior is quite unlike what would be anticipated. The periodic oscillations were not expected. The period of the oscillations was about six or seven days, during which time period the deflection actually decreases as well as increases with constant load. Both dial gages registered this periodic characteristic. Despite the oscillatory behavior, the mean trend is for an increase in deflection. Because of this, it was felt that this trend could be predicted successfully using the four-parameter fluid models of the face sheets and the core in the three-layer sandwich beam model. First, the influence of the time-dependence of the quartz-epoxy face sheets is considered. For simplicity, the approximation tip deflection of Equation 4.71 is used. The tip deflection in Laplace domain is identical in form to Equation 4.72 and is repeated here for convenience:

$$\begin{aligned} \bar{w}_{tip}(s) = & \frac{P_o L^3}{96s \frac{Q(s)}{P(s)} t_1 (h^2 + ht_1 + \frac{1}{3} t_1^2)} \\ & + \frac{P_o L}{16s (h^2 + ht_1 + \frac{1}{3} t_1^2)^2} \left[\frac{(2h^2 + ht_1)^2}{c_9} + \frac{(ht_1 + \frac{2}{3} t_1^2)^2}{c_7} \right]. \end{aligned} \quad (8.21)$$

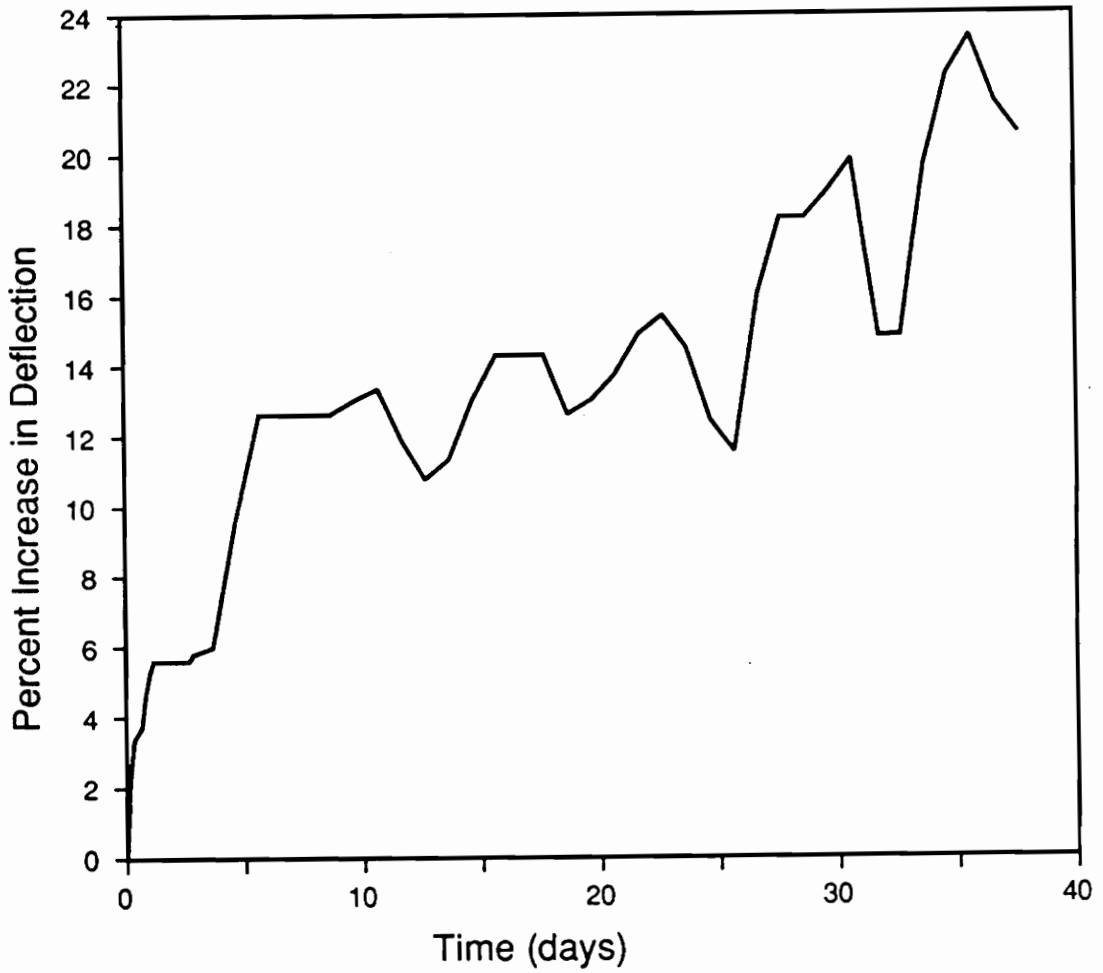


Figure 28. Percent Increase of Deflection of Sandwich Beam in Three-Point Bending

For a four-parameter fluid, the ratio of the polynomials $Q(s)$ and $P(s)$ is

$$\frac{Q(s)}{P(s)} = \frac{q_1 s + q_2 s^2}{1 + p_1 s + p_2 s^2} \quad (8.22)$$

where q_1 , q_2 , p_1 and p_2 are defined in Equation 8.3. When this ratio is substituted into Equation 8.18 and the inverse Laplace transform performed, the result is the time-dependent tip deflection. It is

$$w_{tip}(t) = w_{tip} + \frac{P_o L^3}{96t_1(h^2 + ht_1 + \frac{1}{3}t_1^2)} \left[\frac{t}{\eta_2} + \frac{1}{E_1} \left(1 - e^{-\frac{E_1 t}{\eta_1}} \right) \right] . \quad (8.23)$$

The response of the three-layer sandwich beam to the time-dependence of the honeycomb core in shear was studied in Chapter 4 also. The tip deflection in Laplace domain, Equation 4.49, is also repeated here:

$$\bar{w}_{tip}(s) = \frac{P_o}{s} \left[\frac{L^3}{48(R_1 + R_2)} + \frac{L}{4(R_1 + R_2)^2} \left(\frac{R_1^2}{2 \frac{Q(s)}{P(s)} h} + \frac{R_2^2}{c_7} \right) \right] . \quad (8.24)$$

The ratio $\frac{Q(s)}{P(s)}$ for a four-parameter fluid, Equation 8.19, is substituted into Equation 8.21. The time-dependent tip deflection is the inverse Laplace transform of the resulting equation, or

$$w_{tip}(t) = w_{tip} + \frac{P_o L}{4(R_1 + R_2)^2} \left(\frac{R_1^2}{2h} \right) \left[\frac{t}{\gamma_2} + \frac{1}{G_1} \left(1 - e^{-\frac{G_1 t}{\gamma_1}} \right) \right] . \quad (8.25)$$

The time-dependent response of the beam to both the time-dependent shear behavior of the core and the time-dependent extensional behavior of the face sheets can be found by combining the results in Equations 8.20 and 8.22. This does not mean that these equations are simply added; rather, the time-dependent portions are added, or

$$\begin{aligned} w_{tip}(t) = w_{tip} + \frac{P_o L^3}{96t_1(h^2 + ht_1 + \frac{1}{3}t_1^2)} & \left[\frac{t}{\eta_2} + \frac{1}{E_1} \left(1 - e^{-\frac{E_1 t}{\eta_1}} \right) \right] \\ + \frac{P_o L}{4(R_1 + R_2)^2} \left(\frac{R_1^2}{2h} \right) & \left[\frac{t}{\gamma_2} + \frac{1}{G_1} \left(1 - e^{-\frac{G_1 t}{\gamma_1}} \right) \right] . \end{aligned} \quad (8.26)$$

The percent increase in tip deflection should, as explained previously, be the same at any point along the length of the beam. Therefore, the percent increase in deflection as predicted by the three-layer beam model using the four parameter fluid models found in this chapter is

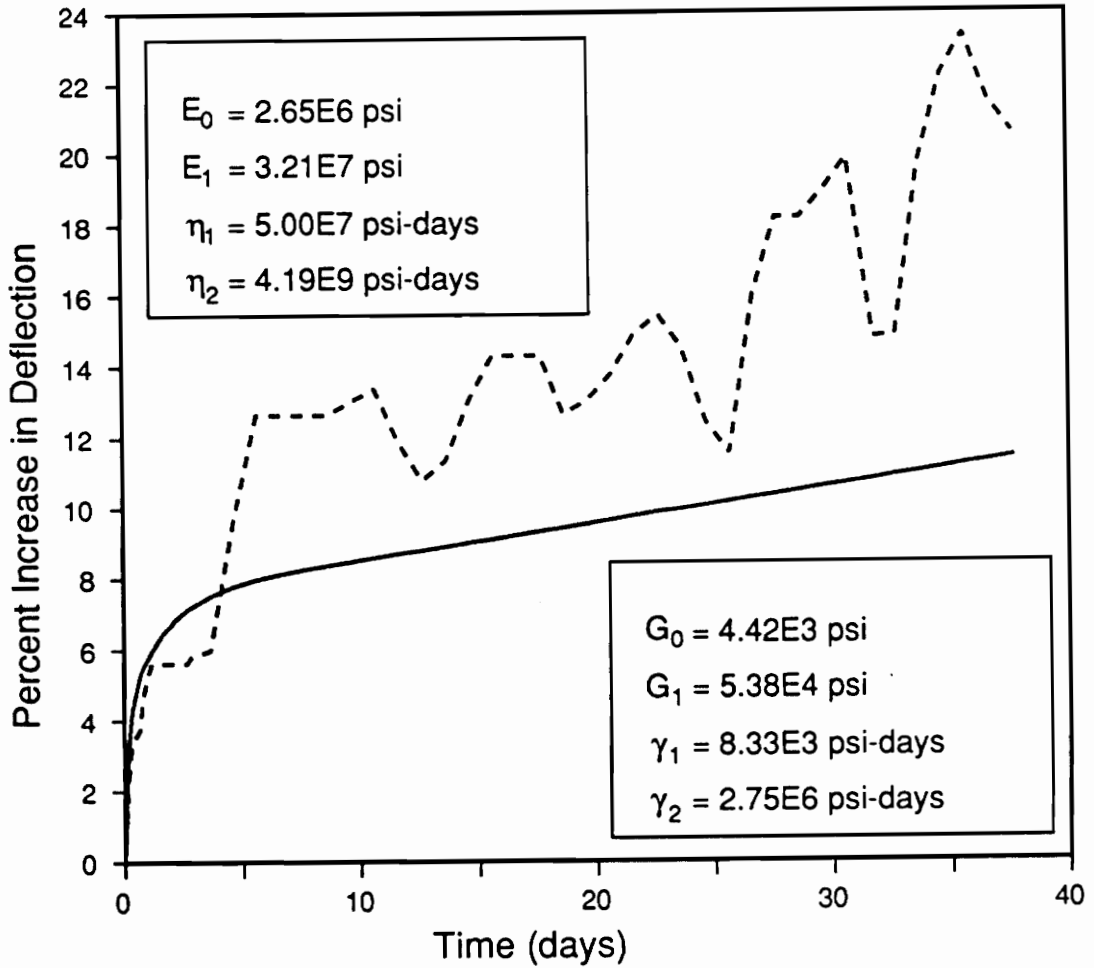


Figure 29. Percent Increase of Deflection of Sandwich Beam in Three-Point Bending - Experimental and Model

$$\text{Percent Increase in Deflection} = \frac{\frac{P_0 L^3}{96t_1(h^2 + ht_1 + \frac{1}{3}t_1^2)} \left[\frac{t}{\eta_2} + \frac{1}{E_1} \left(1 - e^{-\frac{E_1 t}{\eta_1}} \right) \right]}{w_{tip}} \times 100\% + \frac{\frac{P_0 L}{4(R_1 + R_2)^2} \left(\frac{R_1^2}{2h} \right) \left[\frac{t}{\gamma_2} + \frac{1}{G_1} \left(1 - e^{-\frac{G_1 t}{\gamma_1}} \right) \right]}{w_{tip}} \times 100\% \quad (8.27)$$

This is shown as a function of time in Figure 29 along with the experimentally-measured percent increase in deflection for comparison. For the first five days, this expression does a

marginally acceptable job of predicting the response of the beam. However, after the first five days, the experimental results are much higher than predicted by the model. There are several possible explanations for this. First, the time-dependent experiment on the honeycomb in shear was only conducted for fourteen days. Perhaps its behavior had not quite levelled off to a constant increase in strain, therefore making the four-parameter fluid a poor choice as a model. Also, none of these experiments were performed concurrently. Changes in weather, such as temperature and humidity, are known to effect polymer based materials, and unexpected vibration and motion of the experimental fixtures, such as that due to construction work in the building, may have adversely effected the results of the experiments. Because these experiments were not performed simultaneously, they may have been influenced by different environmental effects.

The periodic nature of the actual beam response remains an issue and certainly is a topic for future research. The periodic response, measured for over a month, raises suspicions of a periodically changing environment (e.g., air conditioning not run during weekends). Friction in the experimental apparatus would not cause the deflection to **decrease** with time. Friction would simply cause the deflection to remain constant for a period, then, as the friction is overcome, the deflection would increase again. Assuming the load is constant for a period, which in fact it should be, the only way for deflection to decrease with time is to have material properties which change with time. Specifically, the effective elastic moduli would have to increase with time! Another issue that can be considered is the response of quartz-epoxy material on the compression side of the beam. Experiments were conducted on the quartz-epoxy in tension. The time-dependent behavior was much greater than expected. This could be due to the time-dependent behavior of the matrix material, the time-dependent behavior of the fibers, or the time-dependent behavior of the interface between the matrix and the fibers. If the interface was losing bond integrity with time in tension, then the compression response could be quite different. Here, the time-dependent compressive response is assumed to be the same as the time-dependent tensile response. The time-dependent compressive behavior of the material is certainly a topic for further study.

Summary

Although the experimental results are less than comprehensive, they do demonstrate the potential of the sandwich beam models and the correspondence principle of viscoelasticity. If further experiments were performed in controlled environments, or at least concurrently, better agreement between the predictions for the deflection of the beam and the actual experimental data might be expected. However, the periodic nature of the actual beam response may involve other issues.

Chapter 9 - Observations, Conclusions and Recommendations for Further Study

In the course of this work, analytical elastic models in which the material properties appear explicitly were successfully developed for both the three-layer and five-layer symmetric sandwich beams. Knowledge of the form of the simpler three-layer beam model was used to predict the form of the more complicated five-layer model, and the predictions have been verified computationally. That the form of these models was similar supports the conclusion that a seven-layer (or even nine-layer) beam model can be developed by the same procedure. For a mechanical load, the response of the both models can be separated into two portions: the response of the beam as predicted by strength of materials, and an additional amount of response due to shear. The additional shear response is composed of several terms, many of which are so small as to be negligible.

Once the elastic models were developed, sensitivity studies were performed using representative material properties. From these sensitivity studies, several conclusions can be drawn. First, although they cannot predict the time-dependent response of the beam to a given loading condition, the elastic sensitivity studies are a useful tool which indicate which material properties most influence the response of the beam in both the elastic case and the

viscoelastic case. Thus, a material property which is important to the elastic response of the beam is likewise important to the viscoelastic response of the beam. Also, the elastic sensitivity studies of a beam in three-point bending yield similar results for both the three-layer and five-layer models. The single most important material property to the response of the beam in three-point bending is the modulus of elasticity of the face sheets. The second most important property is the shear modulus of the core. All other material properties have a smaller role in the response of the sandwich beam to three-point bending. For the elastic sensitivity studies of a beam subjected to a linear thermal gradient, the three-layer and five-layer models did not yield identical results. Specifically, because the three-layer model does not include the adhesive layers separately, the effect of these layers is overlooked. In the five-layer model, when the face sheet modulus of elasticity is reduced to the point where it is less than the adhesive extensional modulus, the thermal expansion properties of the adhesive, not the face sheets, control the response of the beam. One important conclusion that can be drawn based on this observation is that, although for most cases the five-layer model may not yield any unique information, it should not be overlooked. The effect of the adhesive layers are only manifested in the five-layer beam model. Also, if the material properties of the adhesive layer are in question (i.e., if a particular adhesive is to be chosen), the five layer model *must* be used.

After the models were studied for their elastic responses, the viscoelastic three-layer and five-layer models were developed using the correspondence principle of viscoelasticity. As already mentioned, the material properties which most influence the beam elastically also have the most influence on the time-dependent beam models. Specifically, time-dependence of the core in shear is much more important than time-dependence of either the adhesive or face sheets in shear. Also, the extensional time-dependent behavior of the face sheets has the most influence on the overall response of the beam, nearly a one-to-one relationship.

Once the analytical work, both elastic and viscoelastic, was complete, experiments to measure the time-dependent behavior of the constituent materials and the sandwich beam were designed and performed. The materials tested were representative of candidate mate-

rials for the precision segmented reflector construction. A quasi-isotropic quartz-epoxy face sheet material was tested in tension, and a glass-imide honeycomb was tested in shear. Both of these materials exhibited a much higher amount of time-dependent behavior than was expected, on the order of ten percent increase in strain in a matter of weeks.[4] Viscoelastic models were used to describe the behavior of these materials. For both, four-parameter fluid models captured the essential characteristics of their time-dependent behavior. These viscoelastic models were used in conjunction with the three-layer beam model to predict the time-dependent response of the beam to three-point bending. However, when this prediction was compared to actual observed behavior, the comparison was poor. The periodic nature of the observed response of the sandwich beam remains unexplained. In order to gain more insight into the actual time-dependent behavior of the sandwich beam and its constituents, further experimental work is strongly recommended. These experiments should be performed simultaneously and in close proximity to each other so that any aberrant weather conditions or other unexpected occurrences will similarly effect all of the experiments at the same time. The experiments performed for this study should be repeated. Additionally, the time-dependent behavior of the quartz-epoxy face sheet material in compression should be measured. Should it differ significantly from the time-dependent behavior in tension, serious consideration should be given to using a model which accounts for different tensile and compressive properties. Also, the time-dependent behavior of the adhesive in extension should be studied experimentally, and its influence on the response of the five-layer beam using the correspondence principle of viscoelasticity should be determined. The experimental results should then be used in conjunction with the five-layer beam model to more accurately reflect the behavior of the actual sandwich beam.

Appendix A. Coefficient of Thermal Expansion of Aluminum Honeycomb

A honeycomb material is, as the word honeycomb implies, composed of many hexagonal cells. The coefficient of thermal expansion of unsupported honeycomb material in two orthogonal directions can be defined. For a hexagonal cell, the increase in cell size can be measured from the center of one wall to the center of the opposite wall, or the increase in can be measured from one corner to the opposite corner. These two cases are depicted in Figure A.1, the two directions being referred to as the "w" direction and the "c" direction. With this notation, "w" denotes the wall-to-wall direction and "c" denotes the corner-to-corner direction.

By definition, the coefficient of thermal expansion of a material is the amount of strain caused by a one degree temperature increase. By using geometry and this basic definition of the coefficient of thermal expansion, the thermal expansion coefficient of the honeycomb in the "c" and "w" directions can be found.

If the lengths of each of the six walls of a cell are denoted by L, then the increase in length of each wall is

$$\Delta L = \alpha \Delta T L \quad , \quad (A.1)$$

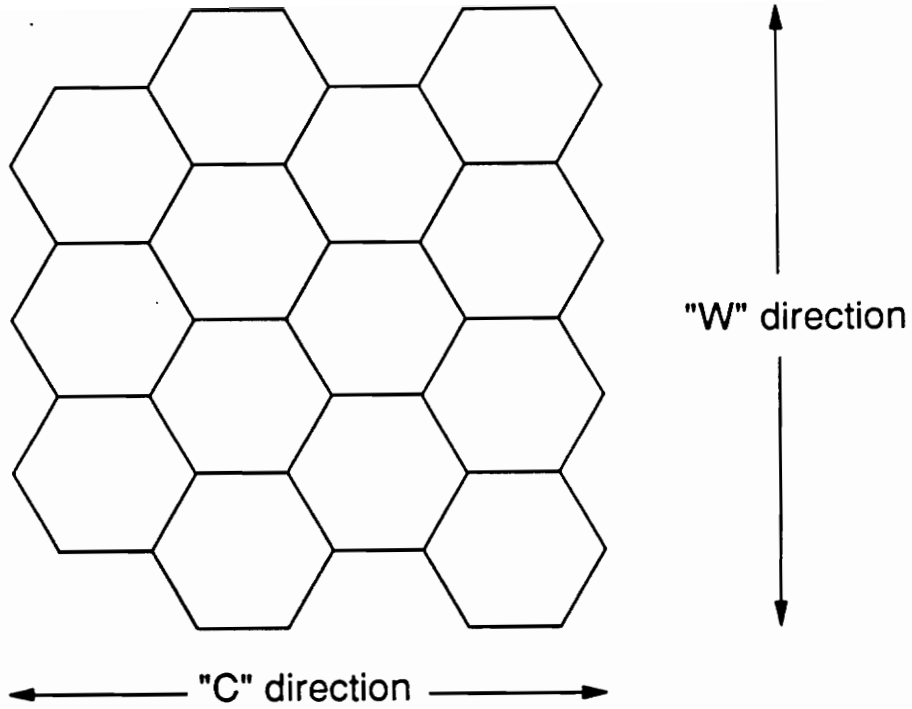


Figure A.1. Two Directions for Hexagonal Honeycomb Materials

where ΔT is the temperature change and α is the coefficient of thermal expansion of aluminum. The two coefficients of thermal expansion can be defined as, for the wall-to-wall direction,

$$\alpha_w = \frac{\left(\frac{\Delta W}{W} \right)}{\Delta T} , \quad (\text{A.2})$$

and for the corner-to-corner direction,

$$\alpha_c = \frac{\left(\frac{\Delta C}{C} \right)}{\Delta T} , \quad (\text{A.3})$$

where ΔW , W , ΔC and C are shown in Figure A.2. It is important to notice that with aluminum, thermal expansion results in similar hexagons, i.e. the original hexagon deforms simply into a larger hexagon. For the wall-to-wall case, using the geometry of a hexagon as shown in Figure A.2,

$$W = L \tan 60^\circ \text{ and } \Delta W = \Delta L \tan 60^\circ , \quad (\text{A.4})$$

which yields

$$\alpha_w = \frac{\left(\frac{\Delta L \tan 60^\circ}{L \tan 60^\circ} \right)}{\Delta T} = \alpha . \quad (\text{A.5})$$

For the corner to corner case,

$$C = 2L \text{ and } \Delta C = 2\Delta L , \quad (\text{A.6})$$

which yields

$$\alpha_c = \frac{\left(\frac{2\Delta L}{2L} \right)}{\Delta T} = \alpha . \quad (\text{A.7})$$

For both the "W" and "C" direction, the coefficient of thermal expansion of a honeycomb material is the same as the coefficient of thermal expansion of the material of which the honeycomb is composed. Thus, for the aluminum honeycomb core, the coefficient of thermal expansion is the same as the coefficient of thermal expansion for solid aluminum.

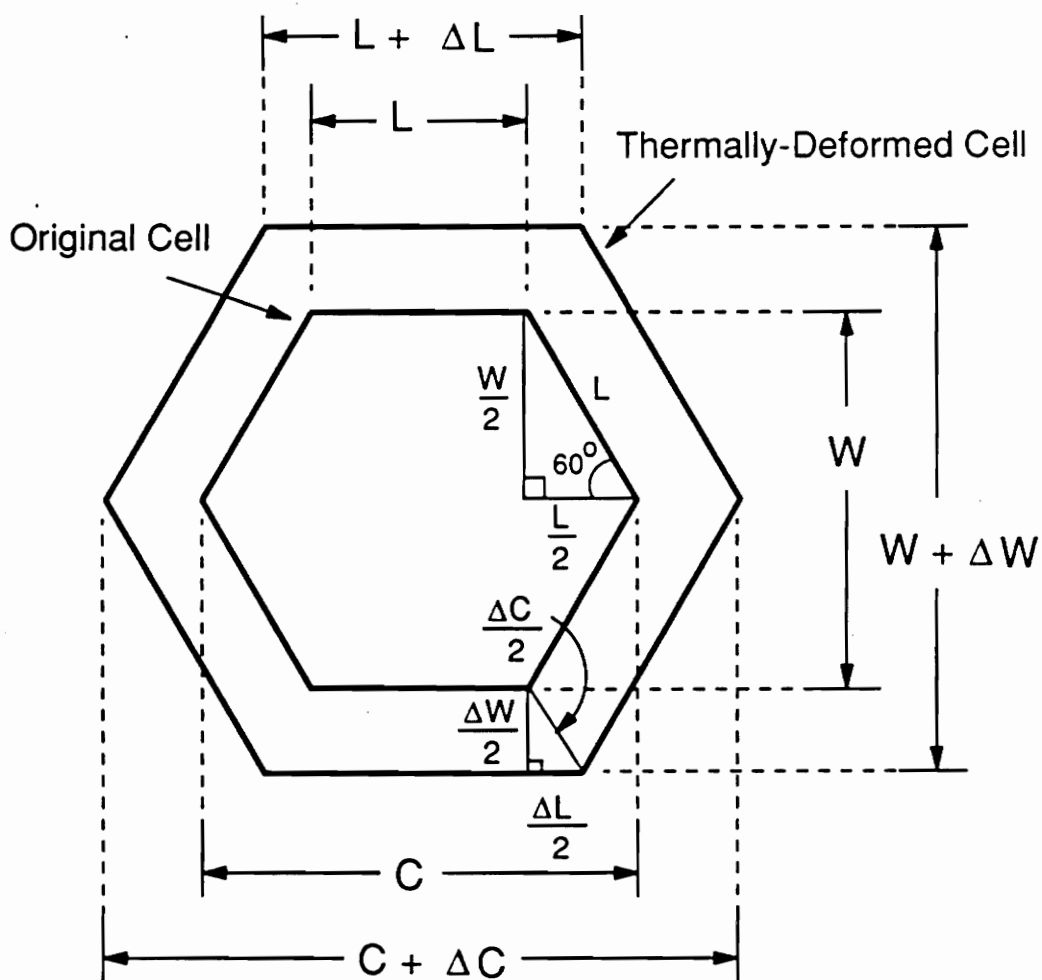


Figure A.2. Single Hexagonal Cell of Honeycomb - Unexpanded and Expanded

Appendix B. Approximations: Three-Layer Sandwich Beam Model

In Chapter 4, a few approximations were made to simplify the expression for the tip deflection based on the relative size of the terms of which it is composed. These approximations are justified in this appendix.

Approximation for Equation 4.12

The first of these approximations was used to simplify the tip deflection of the beam subjected to a linear through-the-thickness thermal gradient as it appeared in Equation 4.11. Equation 4.11 is repeated here for convenience:

$$W_{\text{tip}} = -\frac{(M_{\phi}^T + M_{\psi}^T)L^2}{8(R_1 + R_2)} - \frac{(M_{\psi}^T R_1 - M_{\phi}^T R_2)(c_7 R_1 - c_9 R_2)}{c_7 c_9 (R_1 + R_2)^2} \quad (\text{B.1})$$

The sensitivity studies were performed using the following approximate tip deflection:

$$w_{tip}^{apprx} = \frac{-(M_{\phi}^T + M_{\psi}^T)L^2}{8(R_1 + R_2)} \quad (B.2)$$

Notice that the omitted portion is exactly the expression for w_6 in Equation 4.6 multiplied by $\sinh \frac{\lambda L}{2}$, or

$$w_{tip}^{apprx} = w_{tip} - w_6 \sinh \frac{\lambda L}{2} \quad (B.3)$$

Another type of sensitivity study is now introduced. For this, the approximate tip deflection is compared to the actual tip deflection, Equation B.1, for all of the cases considered in the thermal sensitivity studies of Chapter 4. Two tables, Table B.1 and Table B.2 present in the left columns which material property or layer thickness is reduced from its nominal value as given in Table 1 on page 47 by a factor of ten. The right column is the value of the following:

$$\frac{w_{tip}^{apprx}}{w_{tip}} \quad (B.4)$$

Inspection of these tables reveals that the approximate tip deflection is at most 0.6% different than the actual tip deflection of Equation B.1.

Approximation for Equation 4.32

Another approximation was used in Chapter 4, this time to simplify the tip deflection of a cantilever beam in order to more easily apply the correspondence principle of viscoelasticity. The actual tip deflection was shown in Equation 4.4 and is repeated:

Table B.1. Approximation for Three-Layer Aluminum Beam - Thermal Gradient

Reduced Variable	$\frac{w_{tip}^{apprx}}{w_{tip}}$
NONE	1.000002
E_1	1.000002
G_1	1.000002
t_1	1.000000
α_1	0.999996
E_2	1.000000
G_2	1.000020
h	1.000000
α_2	1.000003
ALL	1.000000

$$w_{tip} = \frac{PL^3}{48(R_1 + R_2)} + \frac{PL}{4(R_1 + R_2)^2} \left(\frac{R_1^2}{c_9} + \frac{R_2^2}{c_7} \right) - \frac{P(c_7R_1 - c_9R_2)^2}{2c_7c_9\lambda(c_7 + c_9)(R_1 + R_2)^2} \left(1 - e^{-\frac{\lambda L}{2}} \right) \quad (B.5)$$

The approximate tip deflection includes only the first two terms, or

$$w_{tip}^{apprx} = \frac{PL^3}{48(R_1 + R_2)} + \frac{PL}{4(R_1 + R_2)^2} \left(\frac{R_1^2}{c_9} + \frac{R_2^2}{c_7} \right) \quad (B.6)$$

Again, the relative sizes of these expressions are compared for all of the cases considered in the Chapter 4 mechanical-load sensitivity studies. The results are presented in Table B.3 and Table B.4 for the aluminum and composite beams respectively. In these tables, the left columns indicate which material property or layer thickness is reduced by a factor of ten; the

right columns present the value of Equation B.4 for the tip and approximate tip deflections in Equations B.5 and B.6. It is apparent from these tables that the approximate tip deflection differs from the actual tip deflection by at most 3.1%.

Approximation for Equation 4.71

The final approximation in the three-layer model was used to simplify the expression for the tip deflection of a tip-loaded cantilever beam based on the relative values of the extensional moduli. Specifically, the modulus of elasticity of the core is so small in comparison to

Table B.2. Approximation for Three-Layer Composite Beam - Thermal Gradient

Reduced Variable	$\frac{W_{tip}^{approx}}{W_{tip}}$
NONE	1.000006
E_1	1.000006
G_1	1.000005
t_1	1.000001
α_1	1.000001
E_2	1.000001
G_2	1.000059
h	1.000000
α_2	1.000006
ALL	1.000000

Table B.3. Approximation for Three-Layer Aluminum Beam - Mechanical Load

Reduced Variable	$\frac{W_{tip}^{apprx}}{W_{tip}}$
NONE	1.003
E ₁	1.000
G ₁	1.002
t ₁	1.000
E ₂	1.003
G ₂	1.031
h	1.001
ALL	1.000

Table B.4. Approximation for Three-Layer Composite Beam - Mechanical Load

Reduced Variable	$\frac{W_{tip}^{apprx}}{W_{tip}}$
NONE	1.001
E ₁	1.000
G ₁	1.001
t ₁	1.000
E ₂	1.001
G ₂	1.020
h	1.000
ALL	1.000

that of the face sheets that it is approximated as zero. The approximate tip deflection, shown in Equation 4.71, is repeated:

$$w_{tip} = \frac{PL^3}{96E_1t_1(h^2 + ht_1 + \frac{1}{3}t_1^2)} + \frac{PL}{16(h^2 + ht_1 + \frac{1}{3}t_1^2)^2} \left[\frac{(2h^2 + ht_1)^2}{c_9} + \frac{(ht_1 + \frac{2}{3}t_1^2)^2}{c_7} \right] \quad (B.7)$$

This is compared to the value of the tip deflection as given by Equation B.6 for all of the cases considered previously. The left columns of Table B.5 and Table B.6 indicate which material property or layer thickness is reduced by a factor of ten. The right columns of these tables is the value of Equation B.4. The approximate tip deflection of Equation B.7 differs from that of Equation B.6 by less than one percent for all cases.

Table B.5. Approximation for Three-Layer Aluminum Beam ($E_2 = 0$) - Mechanical Load

Reduced Variable	$\frac{w_{tip}^{approx}}{w_{tip}}$
NONE	1.0001
E_1	1.0018
G_1	1.0001
t_1	1.0020
E_2	1.0000
G_2	1.0000
h	1.0000
ALL	1.0002

Table B.6. Approximation for Three-Layer Composite Beam ($E_2 = 0$) - Mechanical Load

Reduced Variable	$\frac{W_{tip}^{approx}}{W_{tip}}$
NONE	1.0006
E_1	1.0072
G_1	1.0006
t_1	1.0082
E_2	1.0001
G_2	1.0002
h	1.0000
ALL	1.0007

Appendix C. Approximations and Verifications:

Five-Layer Sandwich Beam Model

Verification of Equations 5.41 and 5.47

For the three-layer sandwich beam model, all of the constants w_i , $i = 0,1,2,3,5,6$ were found in closed form. In the five-layer sandwich beam model, all of the constants can be found in closed form; however, because of their complexity, not all of these constants are useful if left in the form in which they were found. The results of the three-layer beam model are used to simplify some of the constants of the five-layer beam model.

First, for the tip-loaded cantilever beam, the constant w_1 was found in closed form in Equation 5.38 and is

$$w_1 = \frac{P \left(\frac{R_1 BM}{c_9} + \frac{R_2 MA}{c_8} + \frac{R_3 AB}{c_7} \right)}{2(R_1 + R_2 + R_3)(AB + BM + MA)} \quad (C.1)$$

A form similar to that of w_1 for the three-layer model was assumed in Equation 5.41:

$$w_1^{(5)} = \frac{P}{2(R_1 + R_2 + R_3)^2} \left(\frac{R_1^2}{c_9} + \frac{R_2^2}{c_8} + \frac{R_3^2}{c_7} \right) . \quad (C.2)$$

For the expressions in Equation C.1 and C.2 to be equivalent, the following identities must be true:

$$\begin{aligned} \frac{BM}{(AB + BM + MA)} &\equiv \frac{R_1}{(R_1 + R_2 + R_3)} \\ \frac{MA}{(AB + BM + MA)} &\equiv \frac{R_2}{(R_1 + R_2 + R_3)} \\ \frac{AB}{(AB + BM + MA)} &\equiv \frac{R_3}{(R_1 + R_2 + R_3)} \end{aligned} \quad (C.3)$$

or

$$\frac{R_1(AB + BM + MA)}{BM(R_1 + R_2 + R_3)} \equiv \frac{R_2(AB + BM + MA)}{MA(R_1 + R_2 + R_3)} \equiv \frac{R_3(AB + BM + MA)}{AB(R_1 + R_2 + R_3)} \equiv 1 . \quad (C.4)$$

Also, for the cantilever beam subjected to a thermal gradient, w_2 was found in closed form in Equation 5.45. It is

$$\begin{aligned} w_2 = & \frac{M_\alpha^T [AB(c_2c_5 - 2c_3c_4) + BM(4c_4c_6 - c_5^2) + MA(c_3c_5 - 2c_2c_6)]}{2(8c_1c_4c_6 + 2c_2c_3c_5 - 2c_1c_5^2 - 2c_3^2c_4 - 2c_2^2c_6)(AB + BM + MA)} \\ & + \frac{M_\beta^T [AB(c_2c_3 - 2c_1c_5) + BM(c_3c_5 - 2c_2c_6) + MA(4c_1c_6 - c_3^2)]}{2(8c_1c_4c_6 + 2c_2c_3c_5 - 2c_1c_5^2 - 2c_3^2c_4 - 2c_2^2c_6)(AB + BM + MA)} \\ & + \frac{M_\gamma^T [AB(4c_1c_4 - c_2^2) + BM(c_2c_5 - 2c_3c_4) + MA(c_2c_3 - 2c_1c_5)]}{2(8c_1c_4c_6 + 2c_2c_3c_5 - 2c_1c_5^2 - 2c_3^2c_4 - 2c_2^2c_6)(AB + BM + MA)} \end{aligned} \quad (C.5)$$

A form similar to that of w_2 for the three-layer model was assumed in Equation 5.47 and is

$$w_2^{(5)} = \frac{-(M_\alpha^T + M_\beta^T + M_\gamma^T)}{2(R_1 + R_2 + R_3)} . \quad (C.6)$$

For Equations C.5 and C.6 to be equivalent, the following must be identities:

$$\begin{aligned}
\frac{AB(c_2c_5 - 2c_3c_4) + BM(4c_4c_6 - c_5^2) + MA(c_3c_5 - 2c_2c_6)}{(8c_1c_4c_6 + 2c_2c_3c_5 - 2c_1c_5^2 - 2c_3^2c_4 - 2c_2^2c_6)(AB + BM + MA)} &\equiv \frac{-1}{(R_1 + R_2 + R_3)} \\
\frac{AB(c_2c_3 - 2c_1c_5) + BM(c_3c_5 - 2c_2c_6) + MA(4c_1c_6 - c_3^2)}{(8c_1c_4c_6 + 2c_2c_3c_5 - 2c_1c_5^2 - 2c_3^2c_4 - 2c_2^2c_6)(AB + BM + MA)} &\equiv \frac{-1}{(R_1 + R_2 + R_3)} \\
\frac{AB(4c_1c_4 - c_2^2) + BM(c_2c_5 - 2c_3c_4) + MA(c_2c_3 - 2c_1c_5)}{(8c_1c_4c_6 + 2c_2c_3c_5 - 2c_1c_5^2 - 2c_3^2c_4 - 2c_2^2c_6)(AB + BM + MA)} &\equiv \frac{-1}{(R_1 + R_2 + R_3)} ,
\end{aligned} \tag{C.7}$$

or

$$\begin{aligned}
\frac{-[AB(c_2c_5 - 2c_3c_4) + BM(4c_4c_6 - c_5^2) + MA(c_3c_5 - 2c_2c_6)](R_1 + R_2 + R_3)}{(8c_1c_4c_6 + 2c_2c_3c_5 - 2c_1c_5^2 - 2c_3^2c_4 - 2c_2^2c_6)(AB + BM + MA)} &\equiv 1 \\
\frac{-[AB(c_2c_3 - 2c_1c_5) + BM(c_3c_5 - 2c_2c_6) + MA(4c_1c_6 - c_3^2)](R_1 + R_2 + R_3)}{(8c_1c_4c_6 + 2c_2c_3c_5 - 2c_1c_5^2 - 2c_3^2c_4 - 2c_2^2c_6)(AB + BM + MA)} &\equiv 1 \\
\frac{-[AB(4c_1c_4 - c_2^2) + BM(c_2c_5 - 2c_3c_4) + MA(c_2c_3 - 2c_1c_5)](R_1 + R_2 + R_3)}{(8c_1c_4c_6 + 2c_2c_3c_5 - 2c_1c_5^2 - 2c_3^2c_4 - 2c_2^2c_6)(AB + BM + MA)} &\equiv 1 .
\end{aligned} \tag{C.8}$$

If the six expressions of Equations C.4 and C.8 can be identically found to be exactly one for enough cases, then using the expressions for w_1 in Equation C.2 and w_2 in Equation C.6 is justified. The twelve material properties and layer thicknesses of the composite beam in Table 7 on page 103 are used as nominal values. Additionally, these material properties and layer thicknesses are both increased and reduced by a factor of ten. For every possible permutation of nominal, reduced and increased values, the six expressions are computed. This results in 3,188,646 (6×3^{12}) values, all of which must be exactly one to verify the assumptions. Out of 3,188,646 values, all but 132 fall within $\frac{1}{1000}$ % of one (greater than 0.99999 but less than 1.00001); all but three fall within $\frac{1}{100}$ % of one (greater than 0.9999 but less than 1.0001); and all 3,188,646 values are within one-tenth of one percent of being exactly one (greater than 0.999 but less than 1.001). Given the accuracy of real number computations on computers, it is safe to say that, at least for all 531,441 (3^{12}) cases considered, the six expressions are identically equal to one.

Approximation for Equation 5.42

The deflection of a tip-loaded cantilever beam was found in Chapter 5 and is completely described in Equations 5.35, 5.38 and 5.41. Like the three-layer beam, the tip deflection of the five-layer beam can be closely approximated by omitting terms which are much smaller than the rest. The tip deflection is given by

$$\begin{aligned}
 w_{\text{tip}} = & \frac{w_3 L^3}{8} + \frac{w_2 L^2}{4} + \frac{w_1 L}{2} + w_0 \\
 & + w_5 \cosh\left(\frac{\lambda_5 L}{2}\right) + w_6 \sinh\left(\frac{\lambda_5 L}{2}\right) \\
 & + w_7 \cosh\left(\frac{\lambda_7 L}{2}\right) + w_8 \sinh\left(\frac{\lambda_7 L}{2}\right) .
 \end{aligned} \tag{C.9}$$

Using Equation 5.38 and the definitions of the hyperbolic sine and cosine functions, the last five terms can be rearranged:

$$\begin{aligned}
 & w_0 + w_5 \cosh\left(\frac{\lambda_5 L}{2}\right) + w_6 \sinh\left(\frac{\lambda_5 L}{2}\right) + w_7 \cosh\left(\frac{\lambda_7 L}{2}\right) + w_8 \sinh\left(\frac{\lambda_7 L}{2}\right) \\
 & = w_6 \left[1 - e^{-\left(\frac{\lambda_5 L}{2}\right)}\right] + w_8 \left[1 - e^{-\left(\frac{\lambda_7 L}{2}\right)}\right] .
 \end{aligned} \tag{C.10}$$

Both exponents, $\frac{\lambda_5 L}{2}$ and $\frac{\lambda_7 L}{2}$, are sufficiently large for both the aluminum and composite beams that the following is true within the capabilities of most computers:

$$\begin{aligned}
 e^{-\left(\frac{\lambda_5 L}{2}\right)} &= 0 \\
 e^{-\left(\frac{\lambda_7 L}{2}\right)} &= 0 .
 \end{aligned} \tag{C.11}$$

If the approximate tip deflection consists of only the first three terms in Equation C.9, or

$$w_{\text{tip}}^{\text{apprx}} = \frac{w_3 L^3}{8} + \frac{w_2 L^2}{4} + \frac{w_1 L}{2} . \tag{C.12}$$

then the tip deflection can be written as

$$w_{\text{tip}} = w_{\text{tip}}^{\text{apprx}} + w_6 + w_8 \quad . \quad (\text{C.13})$$

As was done in Appendix B, the approximate tip deflection (Equation C.12) is compared to the actual tip deflection (Equation C.13) using the following ratio:

$$\frac{w_{\text{tip}}^{\text{apprx}}}{w_{\text{tip}}} \quad . \quad (\text{C.14})$$

This ratio is found for all of the cases considered in the sensitivity studies of Chapter 6. The left columns of Table C.1 and Table C.2 indicate which material property or layer thickness was reduced by a factor of ten; the right columns of these tables present the value of Equation C.14. Like the three-layer beam, the approximate tip deflection of the five-layer beam differs from the actual tip deflection by at most 3.1%.

Table C.1. Approximation of Five-Layer Aluminum Beam - Mechanical Load

Reduced Variable	w_{tip}^{approx}
NONE	1.0026
E_1	1.0001
G_1	1.0016
t_1	1.0000
E_2	1.0026
G_2	1.0028
t_2	1.0026
E_3	1.0026
G_3	1.0306
h	1.0006
ALL	1.0000

Table C.2. Approximation of Five-Layer Composite Beam - Mechanical Load

Reduced Variable	W_{tip}^{approx}
NONE	1.0013
E_1	1.0001
G_1	1.0006
t_1	1.0000
E_2	1.0012
G_2	1.0013
t_2	1.0012
E_3	1.0013
G_3	1.0203
h	1.0003
ALL	1.0000

References

1. Flugge, Wilhelm, 1975, *Viscoelasticity*, Springer-Verlag, Berlin.
2. Fung, Y. C., *Foundations of Solid Mechanics*, Prentice-Hall Inc., Englewood Cliffs, N.J., 1965, p.354.
3. Nixon, Floyd, 1960, *Handbook of Laplace Transformation*, Prentice Hall.
4. "Mechanical Properties of Hexcel Honeycomb Materials", TSB 120, 1988, Hexcel.
5. Personal communication with Dr. D. E. Bowles, NASA-Langley Research Center.

Vita

The author was born on the tenth day of August, 1966 in West Lafayette, Indiana (i.e. Purdue University - GO BOILERMAKERS!!) so she was destined to pursue some type of engineering career. She began her education in the Marlinton School system in Ohio where she graduated from high school in 1984. She then spent two years as a mechanical engineering student at the University of Akron. After transferring to the Engineering Science and Mechanics department at Virginia Polytechnic Institute and State University, she graduated magna cum laude in 1988. She is now pursuing her masters degree in that department. The author plays competitive volleyball and is a volunteer for the Humane Society of Montgomery County, which runs one of only a handful no-kill dog and cat shelters.

Lynda L. Olszewski